Fractionally charged anyons generated by topological path fusion of propagating electron in magnetic flux lattice

Tieyan Si[1]

[1]School of Physics, Harbin Institute of Technology, Harbin, 150080, China

(Dated: June 4, 2021)

Anyon is collective excitation of two dimensional electron gas subjected to strong magnetic field, carrying fractional charges and exotic statistical character beyond fermion and boson. So far, anyons with serial fractional charges only exist in fractional quantum Hall effect. It is still a challenge to find new serial of fractional charges in other physical system and develop an unified mathematical physics theory based on the same root. Here a topological path fusion theory of propagating electrons in magnetic flux lattice is proposed to explore the physical origin of fractional charges based on a generalization of Feynman's path integral theory and Thurston's train track theory. This mathematical physics theory generated the existed serial of fractional charges in fractional quantum Hall effect and predicted new serial of fractional charges. A serial of irrational charges are predicted in one dimensional lattice of magnetic fluxes. Fractionally charged anyons are also generated in two dimensional and three dimensional lattice of train tracks of electric currents, revealing an exact correspondence between knot lattice model and train track model. A new explanation for the modular symmetry of complex Hall conductance and composite fermion in fractional quantum Hall effect is also derived from this topological path fusion theory. Experimental observation of anyon in three dimensions can be realized by constructing three dimensional interlocking magnetic fluxes or mapping magnetic fluxes into forbidden zones in multi-connected space filled by solid state material. A photonic crystal with porous nano-structures is a promising system for detecting fractional charges and paved a new way for topological quantum computation.

PACS numbers: 73.43.Cd, 03.75.Ss, 05.30.Fk, 71.10.Fd

Contents

I. INTRODUCTION

The collective excitations of two dimensional electron gas in strong magnetic field carry a serial of fractional charges, which are measured by the fractional Hall conductance [1] and partly explained by Laughlin wavefunction [2] as well as composite fermion theory (i.e., one electron binding together with a pair of magnetic fluxes) [3]. Although the current physics theories offered an explanation for quantized Hall conductance from different perspectives, an unified mathematical physics theory based on the same root is still not achieved. Integral and fractional quantum Hall conductance remains one of the most famous unsolved problems in mathematical physics so far. Today, mathematicians still ask why the Hall conductance is quantized [4]. Topological order and fractionally charged quasiparticles inspired by fractional quantum Hall effect (FQHE) have attracted longstanding research interests of condensed matter physics [5][6][7][8]. Unlike the serial filling fractions in FQHE, only a few fractionally charged states are found in other many body physics theory, such as 0-charged spinon in resonance valence bond state [9], kinks with e/2 in Polyacetylene chain [10], fermions with e/2 in helical Luttinger liquid [11] and at the edge of quantum spin Hall insulator [12], 1/3 filling states in interacting boson system on Kagome lattice [13], irrational charge in quantum dimer model on hypercubic lattices [14], and fractional quasi-excitation states in one-dimensional optical superlattice [15]. Fractionally charged state is one of the most active research fields in quantum many body physics, revealing non-trivial topological order in topological matters [16] and potential application in topological quantum computation [7].

Here we proposed a topological path fusion theory for fractional charged states by generalizing Feynman's path integral theory [18] and Thurston's train track theory [19][20]. When an electron meets two magnetic fluxes, besides the two paths that keep both of the two fluxes to one side, there still exists one path that penetrates through the domain between the two fluxes (as showed in Fig. 1 (b)). According to Feynman's path integral theory [18], the scattering amplitude of an electron passing through this flux pair is the quantum interference of all possible paths. The quantum interference of the three paths leads to Aharonov-Bohm effect [17]. The conventional propagating paths are assumed to be well separated and propagate monotonically in one direction. The conventional assumption of monotonic propagation does not always meets physical reality when an electron scatters backward. Here we use a winding path to represent the backward scattering process, i.e., a path that winds back around fluxes in the opposite direction from input source to detector screen. There are two ways to count all possible winding paths. The first way is to fix the spatial ordering of magnetic fluxes, viewing each magnetic flux as a forbidden hole and the whole space as a multi-connected domain, and let the path wind around the magnetic fluxes. The other way is fixing the two endings of an open path to the input source and detector screen respectively and continuously braiding one flux around the other magnetic flux by keeping the initial path continuous and unbroken. These two operations are equivalent because the winding motion of an electron around a magnetic flux is the relative motion of a magnetic flux carrying an unbroken electric current around to exchange its position with the other magnetic flux.

Connecting the input point to the detecting point at infinity maps the open path into a closed curve. Each magnetic flux is equivalent to a genus in multi-connected space. Braiding magnetic fluxes that are enclosed by loop paths under the constraints that the paths must avoid self-crossing everywhere can be described by Thurston's train track theory [19][20], which is applied to design the optimal mixing strategy of two classical fluids with low Reynolds number [21][22], and study the topological fluid mechanics of point vortex [23] as well as topological chaos in dynamics systems [24][25]. It should be noted here that the self-avoiding rule is only well defined for a classical orbital. When one path segment gets too close to avoid its neighboring path segments, the quantum tunneling effect inevitably occurs to make the stacked path segments within the same neighboring domain indistinguishable. This so-called topological path fusion process is the quantum origin of fractional charges in this model. This fusion process generates topologically inequivalent path network which can not map into one other under continuous topological transformation. A promising experimental implementation of this model is topological mixing of two quantum fluids, one is charged superfluid which is experimentally realizable by charged superfluid helium [26] and the other is normal viscous fluid helium. The charged superfluid helium acts as conducting channel in which an electron can move around freely by keeping the total probability conserved simultaneously.

The paper is organized as follows: in section II, the topological path fusion of train tracks is introduced by quantum interference of three paths around a flux pair. Train tracks are described by Abelian Chern-Simons field theory and exactly mapped into knots on torus. Different serials of fractional charges are derived from the topological fusion of train tracks. Irrational charges are predicted by braiding three magnetic fluxes. In section III, the topological path fusion model are expanded into one dimensional lattice of magnetic fluxes. In section IV,

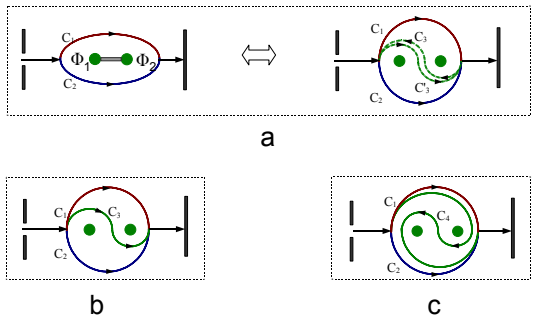

FIG. 1: (a) The two propagation paths (the red and the blue path) around a pair of magnetic fluxes (the two green discs) with a blockade in between (the gray bar) interferences each other to cause the Aharonov-Bohm effect. A path can not penetrate through the blockade. (b) The interference of three electron beams out of the same source is induced by the magnetic flux pair that is placed in between the source screen and detector screen. (c) Braiding the two fluxes once in clockwise direction generates one winding middle path that is sandwiched in between two boundary paths.

the winding train track pattern in two dimensional lattice of magnetic flux pairs are generated by translation operation as well as topological transformation of two dimensional knot lattice. In section V, the fractionally charged anyon is constructed in three dimensional lattice of magnetic fluxes. The last section is a brief summary and outlook.

II. FRACTIONAL CHARGES GENERATED BY TOPOLOGICAL PATH FUSION OF ELECTRON AROUND MAGNETIC FLUXES

A. The U(1) gauge symmetry of the train track of electron around the magnetic flux pair

There are only two topologically inequivalent paths for an electron going around one magnetic flux in the well-known Aharonov-Bohm effect [17]. Here we study the physical effect of an electron passing through two magnetic fluxes which are represented by the green disc labeled by Φ_1 and Φ_2 in Fig. 1 (a)). The two independent magnetic fluxes can be implemented by two independent solenoids. For the special case that there exists a blockade (the gray bar in Fig. 1 (a)) filling up the gap region between two fluxes, the flux pair is equivalent to one giant flux with $\Phi_1+\Phi_2$. The quantum interference between the two electron beams leads to the same Aharonov-Bohm effect as before. The two electron beams are represented by two wave function respectively,

$$|\psi_1\rangle = \psi_1 e^{\frac{ie}{\hbar c}\int_{C_1}\vec{A}(\vec{x})d\vec{x}}, \quad |\psi_2\rangle = \psi_2 e^{\frac{ie}{\hbar c}\int_{C_2}\vec{A}(\vec{x})d\vec{x}}, \quad (1)$$

where $\vec{A}$ is the electromagnetic potential in the surrounding region of the two magnetic fluxes. The phase difference between the two wave functions is proportional to the magnetic fluxes enclosed by the loop path, as illustrated by the superposition of the two wave functions, $|\Psi_c\rangle = |\psi_1\rangle + |\psi_2\rangle$,

$$\begin{aligned}
|\psi_c\rangle &= e^{\frac{ie}{\hbar c}\int_{C_2}\vec{A}(\vec{x})d\vec{x}}(\psi_1 e^{\frac{ie}{\hbar c}[\int_{C_1}\vec{A}(\vec{x})d\vec{x}-\int_{C_2}\vec{A}(\vec{x})d\vec{x}]}+\psi_2),\\
&= e^{\frac{ie}{\hbar c}\int_{C_2}\vec{A}(\vec{x})d\vec{x}}(\psi_1 e^{\frac{ie}{\hbar c}[\oint\vec{A}(\vec{x})d\vec{x}]}+\psi_2),\\
&= e^{\frac{ie}{\hbar c}\int_{C_2}\vec{A}(\vec{x})d\vec{x}}(\psi_1 e^{\frac{ie}{\hbar c}[\int\nabla\times\vec{A}d\sigma]}+\psi_2),\\
&= e^{\frac{ie}{\hbar c}\int_{C_2}\vec{A}(\vec{x})d\vec{x}}(\psi_1 e^{\frac{ie}{\hbar c}[\int Bd\sigma]}+\psi_2),\\
&= e^{\frac{ie}{\hbar c}\int_{C_2}\vec{A}(\vec{x})d\vec{x}}(\psi_1 e^{\frac{ie}{\hbar c}[\Phi_1+\Phi_2]}+\psi_2), \qquad (2)
\end{aligned}$$

where $\Phi_i = \int B_i d\sigma$ denotes the magnetic flux. The physical action of the blockade between two fluxes is equivalent to placing two oppositely propagating paths across the gap region between the two fluxes (C_3 and C_3' in Fig. 1 (a)). Since the vectorial integral of the two paths cancelled each other, the phase difference is still the sum of the two fluxes. It should be noted that the two paths (C_3 and C_3') are topologically equivalent because they can transform into each other continuously without passing any barrier.

For a general case of two free fluxes without the blockade, there are three topologically inequivalent paths travelling through the two fluxes, as labeled by C_1 (the red path), C_2 (the blue path) and C_3 (the green path) in Fig. 1 (b). In three dimensional space, any knotted curve is a possible configuration for a path. If we confine the paths exactly in two dimensional space, the knotted paths are forbidden to exist unless it intersects with itself. Any unknotted curve in the outer region far away from the flux pair is topologically equivalent either to path C_1 or C_2. When the three topologically inequivalent paths, labeled by C_1 (the red path), C_2 (the blue path) and C_3 (the green path) in Fig. 1 (b), travel through the two magnetic fluxes, the wave function of each path gains different phases,

$$\begin{aligned}
|\psi_1\rangle &= \psi_1 e^{\frac{ie}{\hbar c}\int_{C_1}\vec{A}(\vec{x})d\vec{x}}, \quad |\psi_2\rangle = \psi_2 e^{\frac{ie}{\hbar c}\int_{C_2}\vec{A}(\vec{x})d\vec{x}}.\\
|\psi_3\rangle &= \psi_3 e^{\frac{ie}{\hbar c}\int_{C_3}\vec{A}(\vec{x})d\vec{x}}. \qquad (3)
\end{aligned}$$

The initial state is the superposition of the three wave functions, $|\Psi_c\rangle = |\psi_1\rangle + |\psi_2\rangle + |\psi_3\rangle$. The probability density distribution on the detector screen is determined by the inner product of the incoming state $|\Psi_c\rangle$ and the final outgoing state $\langle\Psi_c|$,

$$\begin{aligned}
P_c &= \langle\Psi_c|\Psi_c\rangle = |\psi_1|^2+|\psi_2|^2+|\psi_3|^2\\
&+ 2Re[\psi_1^*\psi_3\exp(\frac{ie}{\hbar c}\Phi_2)] + 2Re[\psi_2^*\psi_3\exp(\frac{-ie}{\hbar c}\Phi_1)]\\
&+ 2Re[\psi_1^*\psi_2\exp(\frac{ie}{\hbar c}(\Phi_1+\Phi_2))]. \qquad (4)
\end{aligned}$$

The interference pattern indicates the resultant probability distribution on the final detector screen. A clockwise braiding operation on the two fluxes does not change the two boundary paths C_1 and C_2, but the path C_3 that passes the gap between the two fluxes is winded into C_4,

which is equivalent to a simple train track. Because the vectorial integration of electromagnetic potential along the new winding segments of C_4 cancelled each other, the interference pattern of C_1, C_2 and C_4 is the same as that of C_1, C_2 and C_3. This interference pattern is invariant for arbitrary number of braiding operations on C_3.

The invariant interference pattern under braiding operations upon the flux pair revealed an emergent U(1) gauge symmetry. We characterize the wave function by the locations of the two magnetic fluxes, $(z_1 = e^{i\theta_1}, z_2 = e^{i\theta_2})$, i.e., $\Psi_c = \Psi_c[\vec{z}]$ with $\vec{z} = (z_1, z_2)^T$. A continuous rotation around the middle point of the two fluxes without breaking the middle path C_3 keeps the wave function $|\Psi_c\rangle$ invariant,

$$\Psi_c[\vec{z}] = \Psi_c[U(\theta)\vec{z}], \tag{5}$$

where $U(\theta)$ is a group element of the proper rotation group SO(2), which is isomorphic to one dimensional unitary transformation group $U(1)$. The rotation of two fluxes is equivalent to introducing a phase factor into the resultant wave function Ψ_c under the action of U(1) group $U(\theta) = \exp[i\theta]$. This rotation operation revealed the invariance of the resultant probability distribution P_c, which is also illustrated by the exchange of two fluxes, $\Phi_1 + \Phi_2 = \Phi_2 + \Phi_1$. The generator of this U(1) group is the z-component of angular momentum operator,

$$\hat{L}_z = -i\frac{\partial}{\partial\theta}, \quad \hat{L}_z\Psi_m = m\Psi_m, \quad \Psi_m = e^{im\theta}. \tag{6}$$

The resultant wave function after transformation can be simplified as, $\Psi_c' = U(\theta)\Psi_c = e^{im\theta}\Psi_c$. The eigenvalue of angular momentum $\hat{L}_z$ is an integer, $(m = \pm1, \pm2, \pm3, \cdots)$, that counts how many periods the two fluxes are exchanged either in clockwise or in counterclockwise direction, which is also the winding number in topology theory. This number is exactly the eigenvalue of braiding operator that results in fractional charges in knot lattice model [27].

B. The Abelian Chern-Simons field theory of winding train tracks around magnetic flux pair

In order to construct a topological field theory of train tracks, we utilize the U(1) gauge field as revealed by braiding the two fluxes to construct the Abelian Chern-Simons field theory which is proved a topological invariant for knots in three dimensional space [28]. It will be shown a train track in two dimensional plane is the equivalent projection of a knot in three dimensional space. Therefore, Chern-Simons field theory is also a topological invariant of train tracks.

To keep the topology of the knot invariant during the projection, it is required that one arbitrary curve on the projection plane must avoid crossing with another curve. This self-avoidance rule puts a strong mathematical constraints on the projection angle and knot conformation in

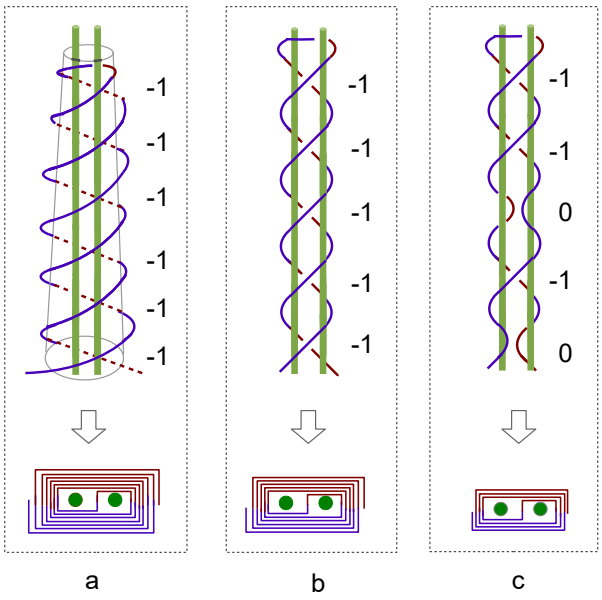

FIG. 2: (a) The double helix path of an propagating electron around an asymmetric distribution of magnetic field strength projects a winding train track around two fluxes. (b) The asymmetric base manifold is transformed into a symmetric manifold to map the helical path into a normal lattice of many knots. (c) An exemplar state of one dimensional knot lattice around two fluxes with vertical vacuum states, $|O_{\pi/2}\rangle = \rangle\langle$.

space. For the simplest case of Fig. 2, the projection of a spiral curve around two magnetic flux tubes into the two dimensional plane in bottom produces exactly its corresponding train track, that passes the border gap region between the two fluxes to wind around the outer region of two fluxes (Fig. 2). The double helix track in Fig. 2 is equivalently an one dimensional knot lattice [27]. The two ending points of the double helix are fixed to a source point and a drain point respectively, which is assumed to merge into one point at infinity to form a close curve in train track theory. The total mass of electron flowing in this closed curve obeys the conservation law of mass. Because the radius of the circular path for an electron in magnetic field is proportional to the inverse of magnetic field strength. A decreasing magnetic field is applied from top to down to continuously expand the circle orbital (Fig. 2), which generates a double helical track on an conic surface (Fig. 2 (a)).

The asymmetric magnetic field is replaced by an uniform magnetic field distribution for simplicity without changing the topology of the helical curve (Fig. 2 (b)). The train track in bottom plane depicts a vortex path with the two fluxes as its double core. Thus the topological linking number of the knot lattice is also a topological characterization of vortex with double core. The linking number equals to the number difference between the total number of positive crossings N_+ and the number of negative crossings N_-, $L_{link} = (N_+ - N_-)/2$. By mapping the over crossing to $+1$ and under crossing to -1,

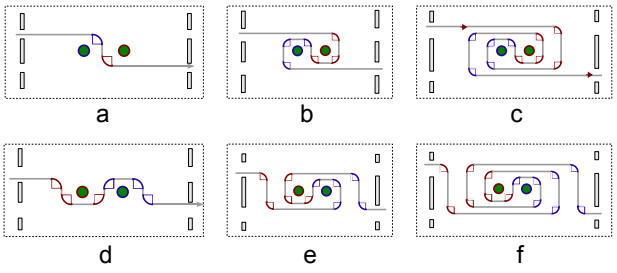

FIG. 3: (a) The initial path that penetrates through the border region between two fluxes. (b) The path generated by one clockwise braiding and (c) by two clockwise braiding. (d) The path generated by one counterclockwise braiding, (e) two counterclockwise braiding and (f) three counterclockwise braiding.

each double helix path is represented by a collective state of Ising spin along the flux tube. For the knot lattice in Fig. 2 (c), the knot state $|\psi\rangle = (-1,-1,0,-1,0)$ project the same train track curve to two dimensional boundary as $|\psi\rangle = (-1,-1,-1,0,0)$ and $|\psi\rangle = (-1,0,-1,0,-1)$, and so on. Therefore, this projection smeared out the spatial distribution of magnetic field strength along the longitudinal axis of the flux tube. However the topology of the knot curve in three dimensions are preserved in the two dimensional boundary. The non-crossing state does not contribute to the linking number. Here we use the vacuum state, $|O_{\pi/2}\rangle = \rangle\langle$, to represent the non-crossing state (Fig. 2 (c)). The non-crossing state does not increase the number of winding train tracks around the two fluxes. Since the linking number of train tracks can be directly computed by Abelian Chern-Simons field theory, it is a natural route to apply train tracks for studying fractional quantum Hall effect.

The Abelian Chern-Simons field theory provided a hierarchy construction for fractional quantum Hall effect [8]. The fractional filling factor ν in the Hall conductance coefficient,

$$\sigma_{xy} = \frac{e^2}{h}\nu, \tag{7}$$

is constructed from the hierarchy Lagrangian of Abelian Chern-Simons field theory [8],

$$\mathcal{L}_{CS} = -\frac{1}{4\pi}K_{IJ}\epsilon^{\mu\nu\lambda}a_{I\mu}\partial_\nu a_{J\lambda} + \frac{e}{2\pi}q_I\epsilon^{\mu\nu\lambda}A_\mu\partial_\nu a_{I\lambda}, \tag{8}$$

Where K_{IJ} is a matrix with its diagonal terms assigned with the integer of filling factors, i.e., $K_{11} = m = 3$, $K_{ii} = m_{i-1} = 2 = m_{i-1} = 2, K_{i,i-1} = K_{i-1,i} = -1; i = 2,3,\cdots$. Here A is electromagnetic potential, and a_μ is the gauge potential introduced by the U(1) gauge symmetry of electron wavefunction due to braiding two fluxes. This hierarchy filling fraction reads

$$\nu = \frac{1}{m - \frac{1}{m_1 - \frac{1}{m_2 - \cdots}}}. \tag{9}$$

The hierarchy Lagrangian of Abelian Chern-Simons field theory can be exactly expressed by topological splitting process of train tracks around two fluxes. These train track represents the trajectory of a moving electron. When the external magnetic field is oriented in z-direction, an electron moves along a helical path under the propulsion of Lorentz force. The projection of the helical path into x-y plane suggest that the action of magnetic field is to bend the electric current from x-axis to y-axis or vice versa. Therefore the turning arcs in Fig. 3 quantifies the Hall current,

$$J^\mu = \frac{\delta S_{CS}}{\delta A} = \sigma_{xy}\epsilon^{\mu\nu\lambda}\partial_\nu a_\lambda, \tag{10}$$

where $S_{CS} = \int \mathcal{L}_{CS}$ is the action of the Chern-Simons Lagrangian. Notice here the external electromagnetic potential A and U(1) gauge potential a_μ acts together to determine the motion of electrons.

Fig. 3 constructed the serial train tracks for the hierarchy structure of fractional filling factors ν in fractional quantum Hall effect. Fig. 3 (a-d) and (b-e) are governed by the basic Lagrangian $\mathcal{L}_m$ with $m = 1$ and $m = 3$ respectively,

$$\mathcal{L}_m = -\frac{m}{4\pi}\epsilon^{\mu\nu\lambda}a_\mu\partial_\nu a_\lambda + \frac{e}{2\pi}\epsilon^{\mu\nu\lambda}A_\mu\partial_\nu a_\lambda. \tag{11}$$

The filling factor is defined as $\nu = 1/m$. The first term on the right hand side of Eq. (11) is the coupling between gauge potential and gauge field tensor, while the second term couples the external electromagnetic potential to gauge field tensor. The train track in Fig. 3 (a) and 3 (d) draw the trajectory of an electron with integral charge. Fig. 3 (b) is the trajectory of a fractional charge $Q = e/m = e/3$, its dynamic equation of motion can be derived from the Lagrangian $\mathcal{L}_{m=3}$. Fig. 3 (e) corresponds to the fractional charge $Q = 2e/3$. In Abelian Chern-Simons field theory, the integer m is introduced by hand. Here the integer m can be directly read out by counting number of the turning arcs (represented by the quarter fan) around one of the two fluxes in Fig. 3. For example, there is one turning arc in Fig. 3 (a), three turning arcs in Fig. 3 (b) and five turning arcs in Fig. 3 (c) going around Φ_1. The same number of turning arcs are confirmed for Fig. 3 (d-f) by taking into account of the cancellation of oppositely oriented turning arcs. The integer m counts the total number of crossings in the knot lattice with respect to the train tracks it projected. As Fig. 2 (b) shows, each crossing is associated by half of the four turning arcs located at the four corners. Since each crossing is attached by two turning arcs, which are shared by two fluxes. The total number of turning arcs around one flux counts the total number of crossings.

The integer m in Lagrangian Eq. (11) can also be computed by a hybrid symmetric gauge, i.e., the symmetric gauge potential vector field around the left flux is oriented into the opposite direction as that around the right

flux,

$$\begin{aligned}\vec{a}_l &= -\frac{y}{2}b\mathbf{e}_x + \frac{x}{2}b\mathbf{e}_y, \quad x<0,\\ \vec{a}_r &= \frac{y}{2}b\mathbf{e}_x - \frac{x}{2}b\mathbf{e}_y, \quad x>0,\\ \vec{a}_l &= \vec{a}_r = \frac{|y|}{2}b\mathbf{e}_y, \quad x=0. \end{aligned} \tag{12}$$

A mono-directional gauge potential vector is introduced at $x=0$ on the borderline interface between the two domains to ensure the continuity of gauge potential vector field. These gauge potential vectors together form convective flow that ejects out of the north pole ($y>0$) and sinks into the south pole ($y<0$). The complete gauge potential vector is defined on two domains, $\vec{a}=\vec{a}_l+\vec{a}_r$. $\vec{a}_l$ generates gauge field current J_l in the left half-plane, $x<0$. $\vec{a}_r$ generates J_r in the right half-plane, $x>0$,

$$\vec{J}_l H_s(-x) = \nabla\times\vec{a}_l, \quad -\vec{J}_r H_s(x) = \nabla\times\vec{a}_r, \tag{13}$$

where $H_s(x)$ is the Heaviside function. $[H_s(x)=1, x>0;\ \ H_s(x)=0, x<0]$. The integer m defines the vorticity of gauge potential vectors $\vec{a}$,

$$m = \frac{1}{\pi}\nabla\times\vec{a}. \tag{14}$$

The train tracks in Fig. 3 (d-f) is generated by counterclockwise braiding, which yields negative m but equal absolute value as that of clockwise braiding after the same periods of braiding operations. In that case, the vorticity of gauge potential vectors is negative m.

The whole serial of filling fractions is spontaneously generated by sequent braiding operation on train track with respect to $\mathcal{L}_{m=1}$. Take the train track of fractional charge $Q=e/3$ as the mother pattern (Fig. 3 (b)), one more clockwise breading generates two more turning arcs in the same direction as before (Fig. 3 (c)). The two new turning arcs carry new gauge potential field $\bar{a}_\mu$ which generate new gauge field current $\bar{J}^\mu=\epsilon^{\mu\nu\lambda}\partial_\nu\bar{a}_\lambda$. Besides the coupling between the new gauge potential $\bar{a}_\mu$ and new gauge field current $\bar{J}^\mu$, the new gauge potential $\bar{a}_\mu$ also couples to the old gauge field current J^μ in the mean time. The complete Lagrangian for this train track reads

$$\begin{aligned}\mathcal{L}_{m,m_1} &= \frac{e}{2\pi}\epsilon^{\mu\nu\lambda}A_\mu\partial_\nu a_\lambda - \frac{m}{4\pi}\epsilon^{\mu\nu\lambda}a_\mu\partial_\nu a_\lambda\\ &- \frac{m_1}{4\pi}\epsilon^{\mu\nu\lambda}\bar{a}_\mu\partial_\nu\bar{a}_\lambda + \frac{1}{2\pi}\epsilon^{\mu\nu\lambda}a_\mu\partial_\nu\bar{a}_\lambda. \end{aligned} \tag{15}$$

This Lagrangian governs the motion of fractional charge $Q=e2/5$. The hierarchy filling fraction derived from this Lagrangian is

$$\nu = \frac{1}{m-\frac{1}{m_1}}, \tag{16}$$

where $m=3$, $m_1=2$. It naturally yields $\nu=2/5$. The train tracks with respect to other filling fractions can be constructed by braiding the mother state of $\nu=1/3$. These train tracks spontaneously matches the hierarchy Abelian Chern-Simons field theory. For instance, Fig. 3 (f) is the train track pattern with respect to $\nu=3/5$. Therefore, Thurston's train track theory [19][20] can be exactly applied to visualize the fractional charges in the hierarchy construction of Abelian Chern-Simons field theory for fractional quantum Hall effect. Note that Abelian Chern-Simons field theory only holds for fractions with odd denominator. The corresponding train tracks are also simple track patterns which can be viewed as projection of knots in three dimensional space. It is still unknown if an arbitrary knot can be projected into train track without self-crossing. The combination of knot theory and train track theory would shed new light on fractional quantum Hall states.

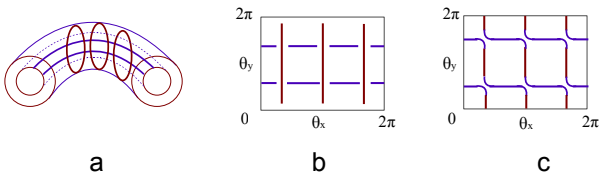

FIG. 4: (a) The x- and y-loop are placed on two separated torus surface respectively to construct a link. (b) The knot lattice of crossing loop segments in $\theta_x-\theta_y$ coordinate system. (c) The knot lattice fused into one knot on torus by vacuum states.

C. A theoretical explanation of fractional quantum Hall effect based on train track and chaotic path

Fractional quantum Hall effect is an exotic phenomena of strongly correlated electrons confined in two dimensions. Abelian Chern-Simons field theory was proved an effective field theory for fractional quantum Hall conductance with odd denominators and topological invariant of knot as well. However it is still unclear so far how knots are applied to quantify fractional quantum Hall effect. As we know, a knot is rigorously defined as a closed curve in three dimensions. One systematic way of generating knots in two dimensions is to construct closed curve on torus surface. In physics theory, a torus surface is realized by setting up periodical boundary conditions for both of the two dimensions of a 2D open lattice (Fig. 4 (a)). Here we view the knot as the propagating path of electrons, which locate the density peak of probability distribution of electron waves. The interlocked knots on the torus of Fig. 4 (a) is expressed as a knot lattice in $\theta_x-\theta_y$ plane (Fig. 4 (b)), where θ_x is the angle of the circular track. Each horizontal track is represented by a wave function $|\psi_x\rangle=\psi_x|x\rangle$, and each vertical path is expressed by $|\psi_y\rangle=\psi_y|y\rangle$. The wave function of an electron in this knot lattice is

$$\begin{aligned}|\psi\rangle &= \psi_x|x\rangle + \psi_y|y\rangle,\\ \psi_\alpha(t) &= \sqrt{\rho_\alpha(t)}\,e^{-i\theta_\alpha(t)}, \quad \alpha=x,y. \end{aligned} \tag{17}$$

with a normalized probability density, $|\psi_x|^2 + |\psi_y|^2 = 1$, i.e., $\rho_x + \rho_y = 1$. This wave function evolves under the action of a hopping Hamiltonian, $\hat{H} = H_{\alpha\beta}|\alpha\rangle\langle\beta|$,

$$H = \begin{pmatrix} eV_x & t_{xy} \\ t_{yx} & eV_y \end{pmatrix}. \tag{18}$$

where V_α is electric voltage along the path oriented in α-direction. e is the elementary electric charges. $t_{yx} = -t_{xy}$ is the hopping amplitude from x-path to y-path, or vice versa. Substituting the complex wave function Eq.(17) into the Schrödinger equation,

$$\frac{d}{dt}\begin{pmatrix} \psi_x \\ \psi_y \end{pmatrix} = -\frac{i}{\hbar}\begin{pmatrix} eV_x & t_{xy} \\ t_{yx} & eV_y \end{pmatrix}\begin{pmatrix} \psi_x \\ \psi_y \end{pmatrix}, \tag{19}$$

yields a pair of nonlinear equations for the two phases,

$$\begin{aligned} \frac{d\theta_x}{dt} &= \frac{e}{\hbar}V_x + \frac{t_{xy}}{\hbar}\sqrt{\frac{\rho_y}{\rho_x}}\cos(\theta_y - \theta_x), \\ \frac{d\theta_y}{dt} &= \frac{e}{\hbar}V_y + \frac{t_{xy}}{\hbar}\sqrt{\frac{\rho_x}{\rho_y}}\cos(\theta_x - \theta_y). \end{aligned} \tag{20}$$

When $t_{xy} = t_{yx} = 0$, there is no tunnelling current between x-loops and y-loops, thus they construct a knot lattice in Fig. 4 (b). In this case, the nonlinear Eq. (20) reduces to a brief formulation,

$$\frac{d\theta_\alpha}{dt} = \frac{e}{\hbar}V_\alpha, \quad \alpha = x, y. \tag{21}$$

The separated loops are united into one complete closed curve by periodical boundary condition, i.e., a knot on torus (Fig. 4 (b) (c)). This knotted path generates the fractional Hall conductance. The fractionally quantized Hall conductance is protected by the topology of knot path, which is governed by the dynamic Eq. (21) of the two phases. If the electric voltage matches the value of the inverse of fractional charges,

$$\frac{V_x}{\hbar} = (\frac{e}{a_x})^{-1}, \quad \frac{V_y}{\hbar} = (\frac{e}{a_y})^{-1}, \tag{22}$$

the dynamic equation of the two phases reduces to a pair of nonlinear equations,

$$\frac{d\theta_\alpha}{dt} = a_\alpha, \quad , \alpha = x, y; \tag{23}$$

where a_α is the winding number of the knot path winding around the α-axis. For example, the trefoil knot path in Fig. 4 (c) admits ($a_x = 3, a_y = 2$). The elementary charge splits into 3 equal parts in x-direction and 2 equal parts in y-direction. In a general case, the elementary charge splits into fractional charges,

$$Q_x = \frac{a_x}{a_x + a_y}, \quad Q_y = \frac{a_y}{a_x + a_y}. \tag{24}$$

These fractional charges result in the quantized fractional Hall conductance. According to nonlinear dynamics and chaos theory[29], only if the ratio of a_x to a_y is a rational number, the trajectory of the electron on torus is a knot curve. In that case, the particle flow out of the path in one direction completely joined in another direction without any loss, indicating a conservation law of the total number of particles, $\rho_x + \rho_y = 1$.

If the ratio of a_x to a_y is an irrational number, the solution of the nonlinear Eq. (23) is a quasi-periodical curve on torus [29], which is not a closed curve instead it draws an endless open curve that never intersect with itself. This quasi-periodical curve is a chaotic path for propagating electron. It exists only in the transition state from one fractional conductance to another one, leading to both the diagonal current and the off-diagonal Hall current. The chaotic path leads to the classical behavior of Hall resistance $R_{_H}$ and diagonal resistance $R_{_D}$,

$$R_{_H} = V_y/vQ_x, \quad R_{_D} = V_\alpha/vQ_\alpha, \tag{25}$$

where v is the velocity of electron, Q_α is the local electric charge in the α-axis. For any given point on torus, there always exists a chaotic path that can approach to that point as close as possible, but never intersect with that point. This means an electron inputting from the left slit of Fig. 3 (a) can approach to any one of the two output sites on the right hand site (Fig. 3 (a)). Therefore both the Hall resistance and diagonal resistance admits a finite value.

When the tunneling rate is finite, $t_{xy} = t_{yx} \neq 0$, the separated loops in Fig. 4 (b) intersects with one another due to the nonzero tunneling current, constructing a grid of electric current in Fig. 6 (a)-II. The tunneling current obeys the dynamic equation,

$$\begin{aligned} \frac{d\rho_y}{dt} &= \frac{it_{xy}}{\hbar}(\psi_x^*\psi_y - \psi_y^*\psi_x) \\ &= \frac{2t_{xy}}{\hbar}\sqrt{(1-\rho_y)\rho_y}\sin(\theta_x - \theta_y). \end{aligned} \tag{26}$$

The particle flow oscillates following the solution of the tunneling current Eq. (26),

$$\rho_y = \cos^2[-\frac{t_{xy}}{\hbar}\sin(a_x - a_y)t], \quad \rho_x = 1 - \rho_y. \tag{27}$$

Therefore the particle moves around as a wave package by turning its direction constantly from one path segment to another path segment (as showed in Fig. 4 (c) where $a_x/a_y = 1.5$).

It was showed in last section that the knot in three dimensions can be equivalently projected into train tracks in two dimensions. Here we further prove that the knot on two dimensional torus surface is also equivalent to train tracks around two magnetic fluxes. As all know, a torus is expanded by sweeping one generating circle along another generating circle. The forbidden holes of the two generating circles are equivalent to two magnetic fluxes. Since both the knot and train track are closed curves, they should be able to transform into each other under topological transformation. For example, the 1/3 filling

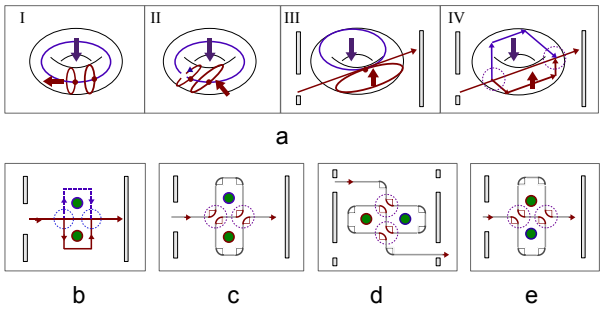

FIG. 5: (a) I-IV, The scheme to show the mapping procedure of three electron path loops on torus into path loops around two magnetic fluxes. One loop is cut to create an open path. (b) The final pattern of the path on torus in Fig. (a) IV is projected into plane and reformed into two square loops surrounding two fluxes with an open path in between. (c) The crossings split into a pair of self-avoiding vacuum arcs, $|O_{\pi/4}\rangle$=(⌟⌜). (d) Rotation of two fluxes by an angle of $\pi/2$ in clockwise direction. (e) The left splitting of crossing currents is realized by the left vacuum state, $|O_{3\pi/4}\rangle$=(¬⌞).

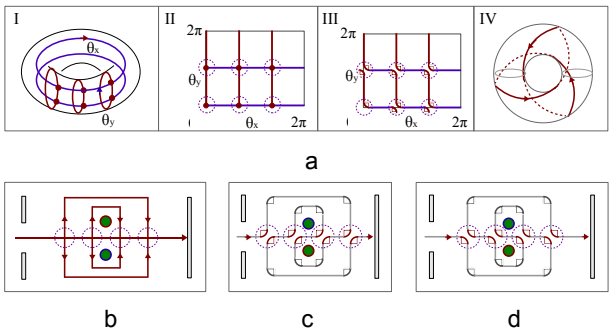

FIG. 6: (a) I-IV, The mapping procedure of five loops on torus into trefoil knot on torus with track splitting operation using vacuum state. (b) The double layered square loops, as a reformed representation of two x-loop and three y-loop on torus, have four crossings. (c) The splitting action of right vacuum state $|O_{\pi/4}\rangle$=(⌟⌜) maps out a winding train track around two fluxes, which matches the fractional charge state 2/5. (d) The left splitting by left vacuum state $|O_{3\pi/4}\rangle$=(¬⌞) generates the fractional charge state 3/5.

state is generated by three loop paths on torus (Fig. 5 (a)), i.e., two vertical loops around the horizontal hole (red loops in Fig. 5 (a)) intersect with the horizontal loop wrapping around the vertical hole (blue loop in Fig. 5 (a)). Replacing the two intersecting points (labeled by the two red dots in Fig. 5 (a)) by the non-crossing configuration of topological vacuum state[27] (as showed in the dashed circle of Fig. 5 (c)) generates a knot on torus, which winds around two perpendicular forbidden holes. The normal orientation of the two forbidden holes are labeled by the blue and red vectors in Fig. 5 (a). In order to rotate the two perpendicular forbidden holes into two parallel ones for simulating the two parallel flux tubes, the two vertical loops are continuously tilted into the same plane of the horizontal loop by keeping the topology of the curves invariant (Fig. 5 (a)-II). One of the two vertical loops is cut to create two open ending points that are connected to the input slit and the output detector (Fig. 5 (a)-III). Then the three loops are transformed into an open channel that is sandwiched in between the two closed loops (Fig. 5 (a)-IV). The irregular path pattern of Fig. 5 (a)-IV is reshaped into rectangular loops around two parallel fluxes oriented in the vertical direction (Fig. 5 (b)). The loop path in Fig. 5 (b) is mapped into train track curve by replacing every crossing point (enclosed by the dashed circle in Fig. 5 (b)) with a right vacuum state $|O_{\pi/4}\rangle$=(⌟⌜) or a left vacuum state $|O_{3\pi/4}\rangle$=(¬⌞), which matches exactly the vacuum state of the knot lattice model [27]. Two right vacuum states lead to the train track curve in Fig. 5 (c), which is equivalent to rotate the two fluxes in clockwise direction over an angle of $\pi/2$. A further rotation of the flux pair by an angle of $\pi/2$ in clockwise direction produces a train track curve in Fig. 5 (d) that is exactly the same as the winding path of electron beam in Fig. 3 (b). Connecting the two open ending points at infinity generates exactly the closed curve in train track theory [19][20]. Therefore, the topological transformation maps the knot on torus into the train track in Fig. 5 (d) with respect to the same fractional charges $e/3$. The dual fractional charge state $e2/3$ is generated by replacing the two crossing points by two left vacuum states under one more counterclockwise rotation upon the flux pair in Fig. 5 (e).

The topological transformation protocol above offers a new systematic method for constructing train tracks for fractional charges. For example, adding a vertical loop and a horizontal loop upon the initial loop pattern of 1/3 filling state generates the initial loop pattern of 2/5 filling state (Fig. 6 (a)-I). In the phase coordinates system $\theta_x - \theta_y$, every loop is represented by a straight line under periodical boundary condition (the three red vertical lines Fig. 6 (a)-II correspond to the three vertical loop in Fig. 6 (a)-I, the two horizontal blue lines indicate the two horizontal loops in Fig. 6 (a)-I). Replacing the six crossing point (enclosed by the dashed circle) by the left vacuum state $|O_{3\pi/4}\rangle$=(¬⌞) fuses the five initial loops into a trefoil knot on torus (Fig. 6 (a)-III,IV). The same trefoil knot is also obtained by performing the same topological transformation procedure on the non-intersecting loops on the double layer torus (Fig. 4 (a)), which projects out a knot lattice in two dimensions [27]. When the loop paths on torus is mapped into loop patterns around two parallel flux tubes (Fig. 6 (b)) following the same rotation procedure as that of 1/3 state above, splitting the four crossing points by four right vacuum states $|O_{\pi/4}\rangle$ = (⌟⌜) leads to the train tracks for the 2/5 charge state under one more $\pi/2$ rotation over the flux pair (Fig. 6 (c)). While the 3/5 charge state is derived by splitting the crossings by four left vacuum states $|O_{3\pi/4}\rangle$ = (¬⌞) (Fig. 6 (d)). The train tracks for other serial fractional charges can be derived by the same topological transforation protocol as above.

The topological transformation protocol does not change the topology of the propagating path of electron. Therefore fractional quantum Hall conductance is protected by the topology of knot as well as train track. The chaotic path results in classical Hall is not completely disordered, instead it has quasi-periodical structures. Integral Hall resistance exists in the two dimensional material with more disorders, while fractional quantum Hall effect only exist in clean material with low disorders [1]. From the point of view of physics, more disorder results in more chaotic paths, which in turn drives the electron into classical behavior of transportation. Less disorder results in less chaotic path and more closed paths (i.e., train tracks and knots), which leads to fractional Hall conductance.

D. The geometric quantification of effective magnetic field for train tracks

Fractional quantum Hall effect only exist in strong magnetic field [1]. The Hall resistance is in an approximate linear relationship with the strength of magnetic field. In order to predict the exact train track pattern with respect to a given magnetic field strength. The magnetic field strength must be extracted from the geometric parameters of the classical orbital of electron in the domain of magnetic fields. In classical electromagnetic field theory, the effective magnetic field strength B is proportional to the number of magnetic fluxes in unit area, i.e., $B = N(\Phi)/S$, where S is the area of cross section surface, $N(\Phi)$ is the number of magnetic fluxes. If the distance between two nearest neighboring fluxes is denoted as d, then the unit area is $S = d$ for one dimensional lattice of fluxes and is $S = d^2$ for two dimensional square lattice. If there are only two magnetic flux tubes in space, the corresponding magnetic field strength is

$$B = \Phi_0/d, \tag{28}$$

where $\Phi_0 = h/2e = 2.07\times10^{-15}$ Weber is the flux quanta, h is Planck's constant and e is the electron charge. A large separation distance d indicates a weak magnetic field strength.

In classical physics, a moving electron in magnetic field moves along an isolated circular track. The magnetic field strength is inversely proportional to the radius of the circular track,

$$B = \frac{m_e v}{e\, r_e}, \tag{29}$$

where m_e is the mass of electron, and v is the initial velocity. Strong (weak) magnetic field confines an electron to a small (large) circle. For a fixed value of magnetic field strength, every flux is surrounded by a fixed number of concentric circles with respect to the distribution window of kinetic energy. Small kinetic energy results in circular tracks with large radius. The minimum circle is limited by the zero point energy due to quantum fluctuation. The flux tube in weak magnetic field is surrounded by more concentric orbital circles than that in strong magnetic field. Increasing the magnetic field strength shortens the distance between two fluxes, then two far separated fluxes draw close to each other, as a result, the orbital circles began to meet and fuse into a single track. Stronger magnetic field fuses more layers of orbital circles. We assume that the electron moves at the same speed in the fused spiral tracks (as shown in Fig. 2). In Fig. 2, the train track in Fig. 2 (a) is formed by the fusion of seven concentric circles. Fig. 2 (b) fused six circles and Fig. 2 (c) fuses four circles. When the distance between two fluxes continuous to be shortened with respect to an increasing strength of magnetic field, the radius of circular track is further reduced according to Eq. (29), then the train tracks around the two fluxes are strongly bind together to form single bundle, winding around the flux pair with a small radius. This track fusion keep operating until there is only one track left to pack all of the other tracks. We call this fusion process as topological path fusion. The ultimate track pattern is that of fractional charge 1/3 (as showed in Fig. 3 (b)). This geometrically quantified magnetic field strength explained why fractional charge 1/3 is only observed in the strongest magnetic field region [1].

Every winding current track contributes an additional magnetic filed upon the external magnetic field. Each circular electric current is effectively a magnetic dipole. The total magnetic field is strengthened if the magnetic dipole points in the same direction as external magnetic field, otherwise, the total magnetic field strength is reduced. The orientation of the magnetic dipole is determined by the winding number m of the spiral track, which is exactly the number of braiding operations over the flux pair. m also counts the number of concentric loops before the track fusion, and is proportional to the radius of the outmost orbital circle around a flux. m is also the same integer index in Abelian Chern-Simons field theory. In this train track model, the effective magnetic field strength B^* is defined as,

$$B^* = \frac{B}{1 - 2p\, m}, \tag{30}$$

where B is the external magnetic field. $2p$ counts the number of flux quanta absorbed by the electron path. This effective magnetic field strength agrees with the effective magnetic field in the composite fermion theory of FQHE [3]. For the exemplar winding paths in Fig. 2, there are six braiding periods in Fig. 2 (a), five in Fig. 2 (b) and three in Fig. 2 (c). The corresponding effective magnetic field strength with respect to the train track in Fig. 2 (a) is quantified by $B^* = B/(1 - 2p6)$, $B^* = B/(1 - 2p5)$ in Fig. 2 (b) and $B^* = B/(1 - 2p3)$ in Fig. 2 (c). The winding number for the cases above is positive because the two fluxes are braided in counterclockwise direction. If the two fluxes are braided in clockwise direction, the winding number m is a nega-

tive integer, leading to an increasing term upon the external magnetic field. The effective magnetic field Eq. (30) holds for arbitrary number of braiding periods. This train track model offers a topological explanation on the effective magnetic field in the composite fermion theory of FQHE [3].

E. The train tracks for the fractional conductance with odd denominator

The fractional conductance with odd denominator is effectively constructed by Abelian Chern-Simons field theory [8], which is a topological invariant of knots. In fact, projecting the knot lattice of double helical electric current into train tracks around two fluxes is not only a mathematical projection, but also provide a physical mechanism of track fusion. When there exist two flux tubes oriented in opposite direction, the chirality of the circling track of electron around one flux is exactly in the opposite direction of that around the other one. The two circling electric currents meet in the border region between two fluxes and naturally fused into one, because their local electric current segments along the borderline flows in the same direction. If the initial velocity of electron is tilted out of the x-y plane, the electron moves along a helical trajectory in three dimensions. The physical constraints of two dimensional electron gas pressed the double helical electric current into a two dimensional plane. Then the strong magnetic field binds many layers of electric current tracks into one electric current bundle. This strong binding reduced the thickness of the electric current bundle until it is smaller than the de Broglie wavelength of electron. In that case, the electric current bundle is covered by one electron wave and can be viewed as one effective track. This physical phenomena is the so-called topological path fusion.

The topological path fusion provides a physical mechanism for fractional Hall conductance with odd denominator and extends out of the scope of quantum field theory. Because fractional Hall conductance is measured by using quantum contacting points[1], we place the flux pair in between two screens with double slits in Fig. 7. The slits No. 1 and No. 3 are at the back of the flux, and the slits No. 2 and No. 4 are in the front of the flux. Because the currents in front of flux run in the perpendicular direction of that in the back (Fig. 2), whenever a current runs from No. 1 to No. 4 (or from No. 2 to No. 3), the electric current switched its propagating direction from x-axis to y-axis, or vice versa, contributing one unit of fractional Hall resistance (or termed as off-diagonal resistance). Every continuous current must first spirals up to the edge and then turns back to form a double helix current. This theoretical conclusion is coincide with the observation in FQHE experiment that the Hall resistance is not detectable unless the edge is connected [1].

We draw a vertical line passing through the center of the ith flux in the flux pair of Fig. 7 (a) to count how

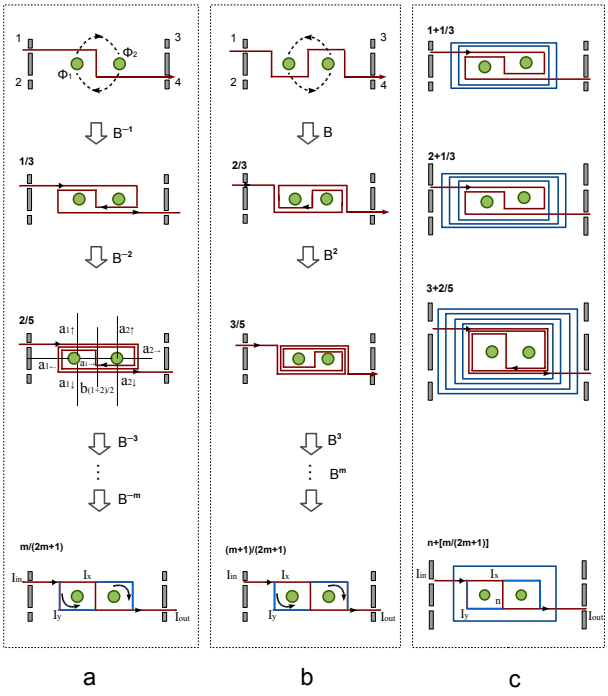

FIG. 7: (a) The flux pair (represented by the two green discs) is placed in between two screens with double slits (represented by the gray bars) and braided in clockwise direction. (b) A serial of braiding operations in counter-clockwise direction on the flux pair generates the dual stacks as Fig (a). (c) The train track pattern of fractional charges accompanied by the integral filling states which are represented by concentric loops.

many layers of track segments in front of the flux pair and that in the back of the flux pair intersect the vertical line, as denoted by $a_{i\uparrow}$ and $a_{i\downarrow}$. Another vertical line is place in between the two fluxes to count the total number of horizontal tracks, $b_{(i+j)/2}$. These weight factors obey the equation,

$$b_{(i+j)/2} = a_{i\uparrow} + a_{i\downarrow}, \tag{31}$$

which is in fact the conservation equation of charge. The train tracks on one side of the flux shows an alternating orientation when the track segments stacks. The electric current in the nearest neighboring tracks flow in opposite direction. However, a physical implementation of electrons propagating along these train tracks inevitably meets a physical limit when two nearest neighboring tracks get too close to distinguish from each other due to quantum tunneling effect. In that case, the electric current segments switched to the same direction after topological path fusion. This fusion process reduced the electromagnetic energy of the electric current bundle, because electric current segments flowing in opposite orientation repel each other, while those flowing in the same direction attract each other. The topological path fusion mechanism generates fractional charges and fractional Hall conductance. The number of stacked track layers is preserved during the fusion process, indicating

an incompressible fluid of electron gas in quantum Hall effect. Inputting one elementary charges from the slit No. 1 splits the charges into two fractional charges, as quantified by the weight of the track bundle above and below the flux pair in Fig. 7 (a),

$$Q_{i\uparrow} = \frac{a_{i\uparrow}}{b_{(i+j)/2}}, \quad Q_{i\downarrow} = \frac{a_{i\downarrow}}{b_{(i+j)/2}}. \tag{32}$$

The fractional charges run in the fused track bundles, leading to Hall resistance in quantum Hall effect,

$$R_{xy} = V_x/I_y = V_x/v_e Q_y, \tag{33}$$

where V is the applied voltage, v_e is the velocity of the charge. A more clear visualization of Hall resistance is tracing a helical path back upward from the entrance at the bottom in Fig. 2, it shows that a current in the front side of the flux (represented by the solid blue lines) switches its direction on the edge and flows into the perpendicular tracks in the back (represented by the dashed red lines).

For the simplest case of single track that directly runs from the slit No. 1 to No. 4 by passing the border region between the two fluxes (Fig. 7 (a)), a clockwise braiding on the flux pair $\hat{B}^{-1}$ folds the initial single track into asymmetric laminar tracks around the two fluxes (Fig. 7 (a) 1/3), where the number of track layers above and below the two fluxes are listed as following:

$$\begin{aligned} a_{1,\uparrow} &= 2, \quad a_{1,\downarrow} = 1, \quad a_{2,\uparrow} = 1, \quad a_{2,\downarrow} = 2. \\ a_{1,\leftarrow} &= 1, \quad a_{1,\rightarrow} = 1, \quad a_{2,\leftarrow} = 1, \quad a_{2,\rightarrow} = 1. \end{aligned} \tag{34}$$

Each track represents one unit of passing probability of electron. The total number of track layers on the cross section of each side of flux represents the passing probability of one electron. When an electron with an elementary charge e is injected into the track from slits No. 1, a fractional charge $2e/3$ goes into the track $a_{1,\uparrow}$ and a fractional charge $e/3$ runs into $a_{1,\leftarrow}$ to fulfill the conservation law of charges. The fractional charge $2e/3$ splits into two tracks across the border region of two flues, one $e/3$ winds around the flux Φ_2 from above, the other $e/3$ runs along the border line. The fractional quantum Hall resistance is formulated as

$$R_{xy} = R_0 \frac{1}{Q_y}, \quad Q_y = \frac{a_{1,\leftarrow}}{a_{1,\leftarrow} + a_{1,\uparrow}} = \frac{a_{1,\downarrow}}{a_{1,\downarrow} + a_{1,\uparrow}}, \tag{35}$$

here $R_0 = h/e^2$ is the quantum of resistivity in quantum Hall systems. The train track pattern in Fig. 7 (a) (1/3) corresponds to the fractional filling state with $\nu = 1/3$.

Other serial fractional charges are generated by systematic braiding on the flux pair. For instance, one more braiding in clockwise direction on the train track pattern in Fig. 7 (a) (1/3) leads to the fractional charges of $2e/5$ and $3e/5$ (Fig. 7 (a) (2/5)). Note here the number of track layers on the left side $a_{1,\leftarrow}$ of flux Φ_1 is always equal to that below $a_{1,\downarrow}$. While its dual flux Φ_2 shows the opposite case, $a_{2,\rightarrow} = a_{2,\uparrow}$. After m round of braiding, the weight of tracks around the flux pair counts as follows:

$$\begin{aligned} a_{1,\uparrow} &= m+1, \quad a_{1,\downarrow} = m, \quad a_{2,\uparrow} = m, \quad a_{2,\downarrow} = m+1. \\ a_{1,\leftarrow} &= m, \quad\quad a_{1,\rightarrow} = 1, \quad a_{2,\leftarrow} = 1, \quad a_{2,\rightarrow} = m, \end{aligned} \tag{36}$$

Here we used one thick track to summarize the stacked tracks around each flux in Fig. 7 (a) (m). The total number of track layers is labeled by m. The conservation equation holds for arbitrary number of braiding, $a_{i,\uparrow} + a_{j,\uparrow} = b_{(i+j)/2} = 2m+1$. These train track patterns correspond to the fractional quantum Hall states with fractional charges,

$$\begin{aligned} Q_{1,\leftarrow} &= Q_{2,\rightarrow} = \frac{m}{2m+1}, \quad Q_{1,\rightarrow} = Q_{2,\leftarrow} = \frac{1}{2m+1}, \\ Q_{1,\uparrow} &= Q_{2,\downarrow} = \frac{m+1}{2m+1}, \quad Q_{1,\downarrow} = Q_{2,\uparrow} = \frac{m}{2m+1}, \end{aligned} \tag{37}$$

The fractional charge serial above converges to a half charge $e/2$ under infinite times of braiding, and obeys a special linear group transformation, $SL(2,m)$,

$$\begin{aligned} Q_{2,\uparrow}(m) &= \frac{m}{2m+1} = \begin{pmatrix} 1 & 0 \\ 2 & 1 \end{pmatrix}(m) = U_{2,\uparrow}(m), \\ Q_{1,\downarrow}(m) &= \frac{m+1}{2m+1} = \begin{pmatrix} 1 & 1 \\ 2 & 1 \end{pmatrix}(m) = U_{1,\downarrow}(m). \end{aligned} \tag{38}$$

The group elements of $SL(2,m)$ is denoted by matrix $U_{i,\uparrow}$ and $U_{i,\downarrow}$, which maps an integer m into a fractional number. The limit of this fractional serial is 1/2 when m approximates to infinity. Note the fractional charge $1/(2m+1)$ always runs along the border line between the two fluxes. The clockwise braiding only generates the fractional Hall resistance serial,

$$R_{xy} = R_0 \frac{1}{Q_y} = R_0 \frac{2m+1}{m}. \tag{39}$$

In order to reach the other fractional Hall resistance serial,

$$R_{xy} = R_0 \frac{1}{Q_y} = R_0 \frac{2m+1}{m+1}. \tag{40}$$

a counterclockwise braiding must be performed on the initial track, as showed in Fig. 7 (b). In that case, the fractional charge $Q = \frac{m+1}{2m+1}$ turns into its perpendicular direction without losing charge.

A serial of fractional charges near other integral filling state is also observed in FQHE experiment [1]. Here the integral filling state is represented by concentric circles around the flux pair outside the fractional train tracks. Because integral filling state only exist in weak magnetic field , which allows the electron to move along a circle with large radius. The total number of layers of concentric circles equals to the number of electrons. Then the fractional filling serial around integer n is generated by

the train tracks of braiding two fluxes, enveloped by $n+1$ layers of concentric circles. Fig. 7 (c) shows the typical train tracks for filling states of $1+(1/3)$, $2+(1/3)$, and $3+(2/5)$. The train tracks of a general fractional charges,

$$\begin{aligned} Q_{1,\leftarrow} &= Q_{2,\rightarrow} = Q_{1,\downarrow} = Q_{2,\uparrow} = n + \frac{m}{2m+1}, \\ Q_{1,\uparrow} &= Q_{2,\downarrow} = n + \frac{m+1}{2m+1}, \\ Q_{1,\rightarrow} &= Q_{2,\leftarrow} = \frac{1}{2m+1}, \end{aligned} \tag{41}$$

are represented by fused track rectangles around each flux with its four edges assigned with different weight. The brown edges represent a current that switch its direction into its perpendicular direction without losing or gaining any charges (Fig. 7 (c)). The blue circle outside around the flux pair in Fig. 7 (c) is assigned with a number $n+1$ that tells how many electrons filled in the flux pair. The Hall resistance of these fractional charged states obeys similar equations as Eq. (39)

$$R_{xy} = R_0 \frac{1}{Q_y} = R_0 \frac{1}{n + \frac{m}{2m+1}}, \quad n = 0, 1, 2, 3 \cdots \tag{42}$$

and $m = 1, 2, 3, \cdots$. The dual serial of fractional resistance reads

$$R_{xy} = R_0 \frac{1}{Q_y} = R_0 \frac{1}{n + \frac{m+1}{2m+1}}, \quad n = 0, 1, 2, 3 \cdots \tag{43}$$

which is generated by the braiding operations in counterclockwise direction.

The measured Hall resistivity increases almost linearly with respect to an increasing magnetic field [1][5]. This experimental measurement agrees with the Hall resistance Eq. (42) and the effective magnetic field strength Eq. (30). Here the effective magnetic field strength for the fractional charges around other integral filling states is quantified by

$$B^* = \frac{B - \frac{1}{n}}{(1 - 2pm)}, \quad n = 1, 2, 3 \cdots \tag{44}$$

where m is winding number of train tracks and the total number of braiding operations as well. n is total number of layers of concentric circles around the outer region of the flux pair. The maximal magnetic field strength generates fractional charge of $e/3$ with $m = -1$ and $n = 0$, here all layers of train tracks fused into an ultimate single track bundle in strong magnetic field. A reduction of magnetic field strength result in track splitting. Because the electron is confined by weaker Lorentz force to wind around the flux pair along a circular track with larger radius. For instance, when the distance between two fluxes grows by one step, the electron would be able to wind around the center of flux pair over one more period, it drives $e/3$ state into $2e/5$ state. For a more general weight distribution of stacked tracks around the flux, one period of track splitting modifies the local weights as following,

$$\begin{aligned} \delta a_{1,\uparrow} &= 1, \ \ \delta a_{1,\downarrow} = 1, \ \ \delta a_{2,\uparrow} = 1, \ \ \delta a_{2,\downarrow} = 1; \\ \delta a_{1,\leftarrow} &= 1, \ \ \delta a_{1,\rightarrow} = 0, \ \ \delta a_{2,\leftarrow} = 0, \ \ \delta a_{2,\rightarrow} = 1. \end{aligned} \tag{45}$$

When the external magnetic field reaches $1/n$, the effective magnetic field reduces to zero. The strongly confined track bundle is completely released from the core region of the flux pair, because the distance between the two fluxes reaches infinity. Since there exist both a large number of layers of train track segments above and below the flux pair, the elementary charge splits evenly into half charge $e/2$ when it passes the flux pair. Thus the half filling states is the limit case of fractional charge serial for a vanished effective magnetic field. However there always exist an infinitely small fractional charge, $e/(2m+1)$, along the borderline between the two fluxes. When the external magnetic field continuous to decrease, the two dimensional electron gas system steps into the fractional filling state around another integral filling state. More isolated circles began to enclose the flux pairs without penetrating through the border region, approaching to another limit charge $e(n + (1/2))$. However, the integer n for this case is far larger than the fractions,

$$n \gg \frac{m}{2m+1}, \tag{46}$$

the tiny plateau of fractional Hall resistance is almost invisible by experimental measurement in this case. As a result, only integral Hall effect are detected. This topological conclusion also agrees with experimental fact that integral Hall effect is observed in a relatively weak magnetic field [1].

F. The Hamiltonian theory of topological path fusion of train tracks around flux pair

Braiding the flux pair generates many stacks of electric current segments. The nearest neighboring current segments always run in antiparallel direction before topological paths fusion, as showed by the train track of $1/3$ in Fig. 8 (a) and that of $2/5$ in Fig. 8 (d), which share the same track stack distribution with three independent paths in Fig. 8 (c) and five independent paths in Fig. 8 (f) after topological path fusion, i.e., Fig. 8 (b) and Fig. 8 (e). Each independent path represents one part of the elementary charge. The topological fusion of the propagating paths on the same side of the flux indicates a condensation of electric currents. The condensed electric currents flows in the same direction along the fused tracks. Because antiparallel electric currents repel one another and parallel electric currents attract one another. The condensation of electric currents reduced the total energy of the train track stacks. The potential energy between two parallel electric currents is proportional to their current strength $\ln[r] I_1 I_2$, where r is the perpendicular distance between the two currents. In the most

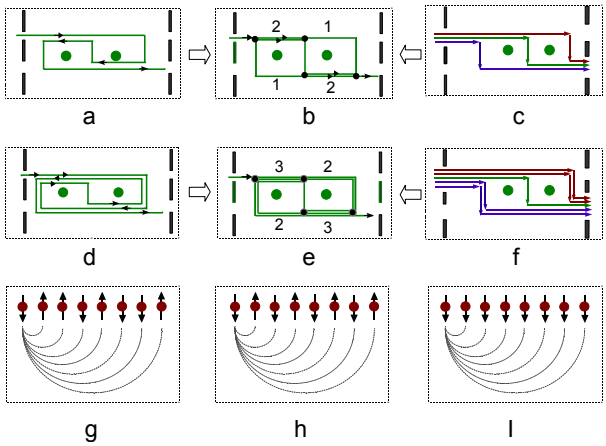

FIG. 8: (a) The train track after one braiding operation and (c) The three independent paths lead to the same weight distribution after topological path fusion in (b). (d) The train track after two braiding operations and (f) the five independent paths result in the same track stack distribution in (e). (g) The one dimensional lattice of randomly oriented current segments with long range coupling interaction. (h) The antiferromagnetic phase and (I) the ferromagnetic phase of electric current segments with long range coupling interaction.

general case that quantum paths are not fully fused, the orientation of current segments are randomly oriented, the total electromagnetic energy is counted by the generalized Ising model of electric currents with long range coupling interaction (Fig. 8 (g)),

$$H_I = \frac{\mu_0 l_i}{2\pi} \sum_{j>i=1}^{N} \ln[(j-i)d] I_i I_j, \quad I_i = \pm 1, \tag{47}$$

Here $I_i = \pm 1$ is the classical Ising spin. $\mu_0 = 1.26 * 10^{-6}(Tm/A)$ is dielectric coefficient. l_i is the horizontal length of the current track at the ith site. d is the perpendicular distance between the nearest neighboring electric currents. Since the distance between two moving electrons in one dimensional electronic system usually falls in micro/nanometer scale, it is reasonable to set $d << 1$ to make sure the repulsive energy increases when two antiparallel currents get closer.

In the antiferromagnetic phase of electric current stack (Fig. 8 (h)), the total electromagnetic energy of these antiparallel currents is summarized as

$$E_{af} = -\frac{\mu_0 l}{2\pi} \sum_{j>i=1}^{N} (-1)^{j-i} \ln[(j-i)d]. \tag{48}$$

Here we have set the value of current operators as $I_i = 1$ and incorporate the sign of $I_i = -1$ into the coefficient terms $(-1)^{r-l}$. The numerical computation of the total energy E_{af} is showed in Fig. 9. The energy curve of odd number of currents is always below that of even number of current stack. Two antiparallel currents bear the maximal initial energy. Therefore fractional charges

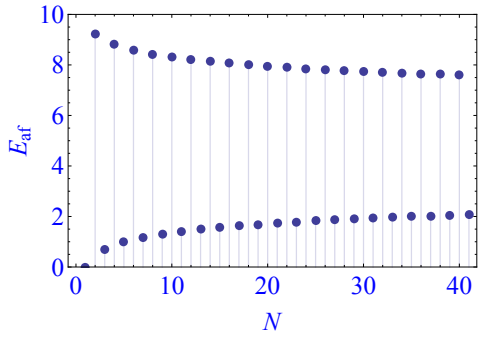

FIG. 9: The total electromagnetic energy for 41 layers of antparallel currents, E_{af}. Here the distance d = 0.0001.

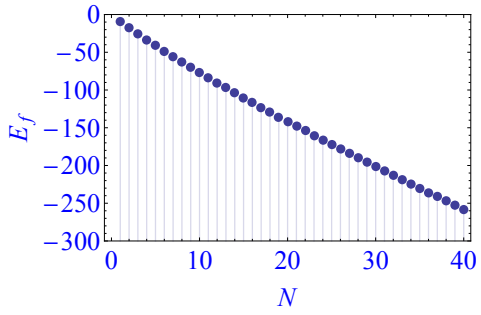

FIG. 10: The total electromagnetic energy for 41 layers of parallel currents, E_f. Here the distance d = 0.0001.

prefer to stay on the current stack composed of odd number of currents due to its lower electromagnetic energy. Even number of stacked currents always has higher energy than odd number of currents. The energy of even number of currents decreases as the total number of stack layers grows. While on the opposite side, odd number of currents shows an increasing energy curve (Fig. 9). The energy curve of odd stack and even stack finally converges to a fixed point when the total number of stacked currents approaches to infinity under infinite number of braiding. That fixed point energy is the eigenenergy of the half-charged states in the limit of $m \to \infty$, which is 4.95174 for the numerical setting above. The electromagnetic energy for finite fractional charges are listed as the discrete points in Fig. 9. The integral filling states $\nu = n$ is realized by the stack of $(n+1)$ layers of concentric circles, in which electrons circling around the flux pair with the same chirality. These circular electric currents attract one other, because the electric current flows in the same direction in these orbital circles.

The ferromagnetic phase of current stacks is composed of many parallel currents (Fig. 8 (I)) that attract one another. The total electromagnetic energy of the ferromagnetic phase is

$$E_f = \frac{\mu_0 l}{2\pi} \sum_{j>i=1}^{N} \ln[(j-i)d], \tag{49}$$

which is far lower than that of the antiferromagnetic

phase, $E_f < E_{af}$. The total energy E_f decreases as the total number of layers of currents grows (Fig. 10). While the total energy of the antiferromagnetic phase shows the opposite behavior. Therefore fractional charge prefer to exist in the ferromagnetic phase of current stacks.

Topological path fusion drive the train tracks into the ferromagnetic phase. Low temperature plays a key role in topological path fusion. The de Broglie wavelength is enlarged to cover more neighboring train tracks when the temperature is dropped to absolute zero degree. In the mean time, the mean free path of electron grows to 1/5 mm at low temperature around 1K [1]. The longer winding track can be braided over more periods, carrying lower electromagnetic energy and higher probability to exist at ground state. A rising temperature reduces the maximal length of the winding path, preventing the generation of fractional charges near the half charge state which only exist for the maximal mean free path. When the temperature grows above the critical value, the mean free path of electron is not long enough to complete the minimal winding operation around a flux pair. As a result, the electron falls into the range of ballistic transportation, demonstrating a classical transportation behavior. The existence probability of a given train track with energy $H(c)$ obeys the Boltzmann-Maxwell distribution,

$$P(c) = \frac{1}{Z}\exp[-E(c)/k_bT], \tag{50}$$

where k_b is Boltzmann constant, T is temperature and H(c) is the Hamiltonian for the train track pattern c. Z is partition function,

$$Z = \sum_c \exp[-E(c)/k_bT]. \tag{51}$$

Suppose there are only two possible states, fully fused or unfused, with respect to the ferromagnetic phase or antiferromagnetic phase. Then the partition function is directly read out by substituting the energy Eq. (48) and Eq. (49) into the partition function Eq. (51),

$$\begin{aligned} Z &= \exp[\frac{\mu_0 l}{2\pi k_bT}] \prod_{j>i=1}^{N} [(j-i)d]^{(-1)^{j-i}} \\ &+ \exp[-\frac{\mu_0 l}{2\pi k_bT}] \prod_{j>i=1}^{N} [(j-i)d]. \end{aligned} \tag{52}$$

The denominator and numerator of the fractional charges is the upper limit of the product equation in partition function terms above. Yang-Lee zeros of phase transition [30] suggest that the critical temperature can be derived by the zero point of partition function, i.e., $Z(T) = 0$. Note here the distance between neighboring current d should be smaller than $10^{-6}m$ to meet the spatial limit of de Broglie wavelength.

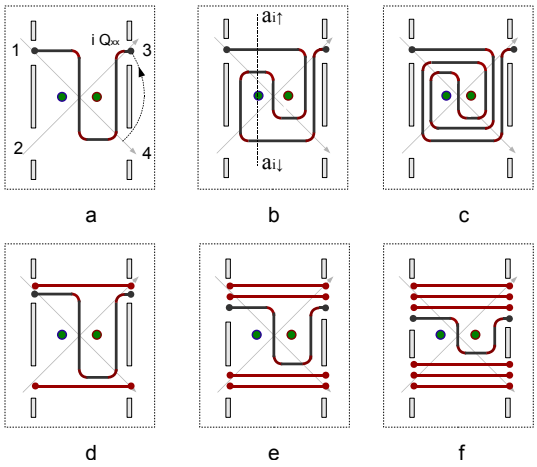

FIG. 11: (a) The initial path connects the slit No. 1 with slit No. 3 for generating diagonal charge. (b) The two fluxes are braided once in clockwise direction. (c) The two fluxes are braided twice in clockwise direction. (d) The three independent paths that generate the same diagonal charge after topological fusion of the train track in (b). (e) The five independent paths generate the same diagonal charge after topological fusion of the train track in (c). (f) Three pairs of independent paths are added upon the initial path in (a) to generate the same effect as the train track for fractional charge 3/7 after track fusion.

G. The modular symmetry of complex Hall conductance

The measured serial plateau of fractional quantum Hall conductance is partly explained by effective quantum field theory [31][32] and investigated by modular group transformation [33][34][35][36]. From the point view of modular group transformation [33][34], the modular group transformation for the complex Hall conductance $\sigma = \sigma_{xy} + i\sigma_{xx}$,

$$\sigma \to \Gamma(\sigma) = \frac{a\sigma + b}{c\sigma + d}, \tag{53}$$

generates an invariant scaling flow diagram of conductance with respect to temperature [37][38][39]. The measured scaling flow of Hall conductance in $GaAs/Al_xGa_{1-x}As$ heterostructures [40] is in agreement with the theoretical result[41], which supports the modular symmetry conjecture of Hall conductance in spite of its unclear physical origin. Here we proposed a different physical explanation for this emergent symmetry based on topological path fusion theory of train tracks in magnetic flux lattice.

According to *Ohm*'s law in electromagnetic theory, the Hall conductance is defined as electric current divided by Hall voltage by

$$\sigma_{xy} = I_x/V_y, \quad \sigma_{xx} = I_x/V_x. \tag{54}$$

The electric current is proportional to the electric charge Q and its moving velocity v, $I = Qv$. We set the voltage

V_x as equal to V_y for simplicity. The complex Hall conductance $\sigma = \sigma_{xy} + i\sigma_{xx}$ is proportional to the complex electric charge,

$$Q = Q_{xy} + iQ_{xx}. \tag{55}$$

The complex charge is consists of two fractional charges, the diagonal charge Q_{xx} and off-diagonal charge Q_{xy}. The diagonal charges is measured by the track stack from the slit No. 1 to No. 3 and from No. 2 to No. 4 in Fig. 11. While the off-diagonal charge is governed by the track stack from the slit No. 1 to No. 4 and from No. 2 to No. 3 in Fig. 11. The track stack redistributes under braiding operations upon the two fluxes (Fig. 11). The topological fusion of these track stacks determines local probability distribution of electron cloud, which further determines how the elementary charge is redistributed into the train track stacks on different sides of the two fluxes. Therefore the local probability distribution $\rho = \rho_{xy} + i\rho_{xx}$ is proportional to the local charge distribution,

$$\begin{aligned} \rho^{\uparrow}_{xy} &= Q^{\uparrow}_{xy} = \frac{a_{i\uparrow}}{a_{i\uparrow} + a_{i\downarrow}}, \\ \rho^{\downarrow}_{xy} &= Q^{\downarrow}_{xy} = \frac{a_{i\downarrow}}{a_{i\uparrow} + a_{i\downarrow}}, \end{aligned} \tag{56}$$

where $\rho^{\uparrow}_{xy} + \rho^{\downarrow}_{xy} = 1$. In order to show fractional charge in complex plane in Fig. 11, the slits No. 1 and No. 3 are located on the real axis with their position coordinates $z_1 = 1$ and $z_4 = -1$. The slits No. 2 and No. 3 are located on the imaginary axis, $z_2 = e^{-i\pi/2}$ and $z_3 = e^{i\pi/2}$.

The braiding operation upon the two fluxes can be equivalently realized by rotating the two ending points of the path that connects two slits. We denote the location of two ending by a vector $\vec{z} = (z_a, z_b)^T$, rotation of the two endings is realized by a 2 by 2 matrix,

$$U\ \vec{z} = \begin{bmatrix} e^{i\theta_a} & 0 \\ 0 & e^{i\theta_b} \end{bmatrix} \begin{bmatrix} z_a \\ z_b \end{bmatrix} = \begin{bmatrix} e^{i\theta_a} z_a \\ e^{i\theta_b} z_b \end{bmatrix} \tag{57}$$

The train track for off-diagonal charge is generated by placing the two endings at the slit No. 1 to No. 4 and rotating the two ending points, $z_a = 1$ and $z_b = -1$, by the rotation matrix

$$U_{R} = \begin{bmatrix} e^{im\pi} & 0 \\ 0 & e^{im\pi} \end{bmatrix}. \tag{58}$$

The propagating path is kept continuous and unbroken during this rotation. While the train track stack for diagonal charge is generated by rotation matrix,

$$U_{I} = \begin{bmatrix} \exp[im\frac{3\pi}{2}] & 0 \\ 0 & \exp[im\pi] \end{bmatrix}. \tag{59}$$

The diagonal paths in Fig. 11 carry an $\exp[i\pi/2]$ phase factor, contributing to the imaginary part of the complex charge. Neither braiding of two fluxes nor the rotation of two ending points changes the two boundary paths in the outer region of two fluxes. Only the path that goes through the middle gap between the two fluxes is winded into nontrivial train track pattern (Fig. 11). The local probability distribution of fusing two boundary paths with the middle path is the same as that generated by fusing the middle path alone after one more braiding operation, as Fig. 11 (b) and (d) showed as well as Fig. 11 (c) and (e). The fractional charge runs in closed path that is only well constructed by rotating the two endings of path synchronously around the central point over a phase of $\theta = m\pi, (m = \pm 1, \pm 2, \cdots)$ (Fig. 11). When the train track breaks out of the phase locking mode under an arbitrary rotation angle $\theta \neq m\pi$, it lead to an endless chaotic path that carries both the diagonal charge and off-diagonal charge, $Q = Q_{xy} + iQ_{xx}$. In that case, a path with one ending fixed fixed at slit No. 1 has a probability to extend its other ending point into both the slit No. 3 and No. 4 in Fig. 11, resulting in nonzero complex density function, $\rho = \rho_{xy} + i\rho_{xx}$.

The braiding operation only redistributes the local charges but keeps the total charge of the elementary charge invariant. Different fractional charges are caused by different local density functions of electron cloud. Modular group transformation provides an effective description for the linear transformation between different fractions. The modular transformation maps one fractional density function into another

$$\rho \to \Gamma(\rho) = \frac{a\rho + b}{c\rho + d}. \tag{60}$$

and one fractional charge into another complex charge, $Q = Q_{xy} + iQ_{xx}$,

$$Q \to \Gamma(Q) = \frac{aQ + b}{cQ + d}. \tag{61}$$

For the special case of fractional charge with odd denominator, the hopping from fractional charge $Q_{xy}(m) = \frac{m}{(2m+1)}$ to $Q_{xy}(m+1) = \frac{(m+1)}{2(m+1)+1}$ is governed by the modular group transformation,

$$\Gamma(Q_{xy}(m)) = \frac{-Q_{xy}(m) + 1}{-4Q_{xy}(m) + 3} = Q_{xy}(m+1), \tag{62}$$

where the diagonal charge is not a fraction but an integer $Q_{xx}(m) = 1$. Because the paths that directly connect the two slits from the outer region form a short circuit (as showed in Fig. 11 (d)(e)(f)). The complete elementary charge $Q_{xx}(m) = e$ passes through the track stacks above the two fluxes without splitting. This offers a possible explain for the zero diagonal Hall resistance in the parameter zone of Hall plateau [1]. The modular group transformation matrix,

$$\Gamma = \begin{pmatrix} -1 & 1 \\ -4 & 3 \end{pmatrix}, \tag{63}$$

leads to the hopping sequence from one Hall plateau to another one,

$$\frac{1}{3} \to \frac{2}{5} \to \frac{3}{7} \to \frac{4}{9} \cdots. \tag{64}$$

here $det(\Gamma) = 1$. The modular symmetry is deeply rooted in the conservation law of charge and describes the local density redistribution when strong magnetic field drives the two dimensional electron gas from one fractional charge state into another one.

H. The train tracks for the fractional conductance with even denominator

The fractional Hall resistance with even denominators was observed in quantum Hall effect [1][5]. The Abelian Chern-Simons field theory cannot effectively describe the fractional Hall resistance with even denominators. It is generally believed $5e/2$ state is non-Abelian state but is still not confirmed so far. Here we provide a systematic construction of fractional charges with even denominators by topological path fusion theory.

In the train track for fractional charge with odd denominator, there always exists an edge current along the borderline carrying a fractional charge,

$$Q_e = \frac{a_\uparrow - a_\downarrow}{a_\uparrow + a_\downarrow}. \tag{65}$$

When the two fluxes are oriented in opposite directions, the edge current is the sum of two current segments flowing in the same direction, one comes from the left flux and the other one is from the right flux. When the two fluxes are oriented in the same direction, the interface current around the left flux runs exactly in the opposite direction of that around from the right flux, resulting in cancellation of the two current segments. Then the two fluxes form a dimer, around which only the loop currents in the outer region survive. The loop current around the flux dimer is the track unit for constructing fractional charge with even denominators.

It takes at least two flux dimers to construct fractional charges with even denominators. In Fig. 12, the first dimer is composed of flux No. 1 and No. 2, which is separated from the second flux dimer of No. 3 and No. 4. Braiding the fluxes No. 1 and No. 2, or No. 3 and No. 4, does not generate fractional charges because the fluxes are enveloped in the same domain. The two tracks that bridge the fluxes No. 1 and No. 2 are squeezed into the front slit of the left double slits, while the bridge track between flux No. 3 and No. 4 is squeezed into the back slit of the right double slits. We fix the flux No. 1 and No. 4, because they falls outside of the double slits wall. One counterclockwise braiding on flux No. 2 and No. 3 results in the track stack distribution as follows,

$$\begin{aligned} a_{2,\uparrow} &= 1, \quad a_{2,\downarrow} = 3, \quad a_{3,\uparrow} = 3, \quad a_{3,\downarrow} = 1. \\ a_{2,\leftarrow} &= 1, \quad a_{2,\rightarrow} = 2, \quad a_{3,\leftarrow} = 2, \quad a_{3,\rightarrow} = 1. \end{aligned} \tag{66}$$

The elementary charge splits into fractional charges along the edges around flux No. 2 and No. 3 after topological path fusion,

$$\begin{aligned} Q_{2,\leftarrow} &= Q_{3,\rightarrow} = \frac{1}{4}, \quad Q_{2,\rightarrow} = Q_{3,\leftarrow} = \frac{2}{4}, \\ Q_{2,\uparrow} &= Q_{3,\downarrow} = \frac{1}{4}, \quad Q_{2,\downarrow} = Q_{3,\uparrow} = \frac{3}{4}. \end{aligned} \tag{67}$$

Two counterclockwise braiding results in the fractional charge serial around the flux pair of No. 2 and No. 3,

$$\begin{aligned} Q_{2,\leftarrow} &= Q_{3,\rightarrow} = \frac{3}{8}, \quad Q_{2,\rightarrow} = Q_{3,\leftarrow} = \frac{2}{8}, \\ Q_{2,\uparrow} &= Q_{3,\downarrow} = \frac{3}{8}, \quad Q_{2,\downarrow} = Q_{3,\uparrow} = \frac{5}{8}. \end{aligned} \tag{68}$$

Fractional charge $5e/12$ is generated by three counterclockwise braiding on flux No. 2 and No. 3 (Fig. 12 (a)). The fractional charge generated by m rounds of braiding are list as follows,

$$\begin{aligned} Q_{2,\leftarrow} &= Q_{3,\rightarrow} = \frac{m-1}{2m}, \quad Q_{2,\rightarrow} = Q_{3,\leftarrow} = \frac{2}{2m}, \\ Q_{2,\uparrow} &= Q_{3,\downarrow} = \frac{m-1}{2m}, \quad Q_{2,\downarrow} = Q_{3,\uparrow} = \frac{m+1}{2m}. \end{aligned} \tag{69}$$

Note there is a fractional charge $1/m$ running along the borderline between flux No. 2 and No. 3. Similar to the fractional charges with odd denominator, a clockwise braiding on the fluxes No. 2 and No. 3 results in the dual charge distribution,

$$\begin{aligned} Q_{2,\leftarrow} &= Q_{3,\rightarrow} = \frac{m+1}{2m}, \quad Q_{2,\rightarrow} = Q_{3,\leftarrow} = \frac{2}{2m}, \\ Q_{2,\uparrow} &= Q_{3,\downarrow} = \frac{m+1}{2m}, \quad Q_{2,\downarrow} = Q_{3,\uparrow} = \frac{m-1}{2m}. \end{aligned} \tag{70}$$

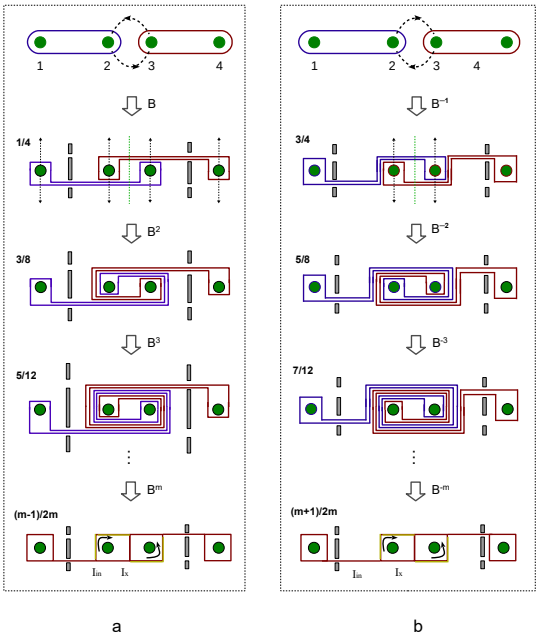

FIG. 12: (a) Counterclockwise braiding over the nearest neighboring fluxes that belong to different loop dimer generates the fractional charges with even denominator, $\frac{m-1}{2m}$. (b). Clockwise braiding over the nearest neighboring fluxes leads to the fractional charge serial, $\frac{m+1}{2m}$.

This fractional serial above is not the only serial that can be generated by braiding the four fluxes. Fixing No. 1 and No. 3 and braiding No. 2 and No. 4 generates a different serial of fractional charges with even denominator. There exists many different fractional serials with respect to different braiding operations. The winding number of braiding operations is inversely proportional to the strength of effective magnetic field. Therefore these fractional charges can be observed by well-designed spatial distribution of magnetic field.

I. The topological surgery theory for the correspondence between integral Hall conductance and fractional Hall conductance

The composite fermion theory of FQHE suggested an accurate correspondence between fractional quantum Hall effect and integral quantum Hall effect [3], which matches the experimental observation of fractional Hall resistance with odd denominator. This correspondence is still not proved by a rigours physical theory so far. Here we proposed a topological surgery theory of train tracks to reveal the exact correspondence between integral Hall resistance and fractional Hall resistance that holds for both odd denominator and even denominator.

The integral filling states of integral quantum Hall effect are represented by a stack of concentric loop currents that envelope two fluxes without penetrating through their border region (Fig. 13 (b)). The zero filling state $\nu = 0$ is represented by one loop current around the flux pair (Fig. 13 (b) - 0). The filling state $\nu = 1$ corresponds to two loop currents around the flux pair (Fig. 13 (b) - 1). Three loop currents represent the filling state of $\nu = 2$ (Fig. 13 (b) - 2). In general, the $\nu = m$ filling state is represented by $m + 1$ concentric loop currents enveloping a flux pair.

In order to construct train track for fractional charges, the concentric loop currents are cut along the borderline of two fluxes into two groups of current arcs (Fig. 13 (b)). The upper (lower) group is a stack of concentric red (blue) arcs (Fig. 13 (b)). Then the arc stack together with the flux they surrounded is translated along the cutting line by finite steps. The red arcs are docked with the blue arcs on the opposite side of the cutting line at the new locations. Finally the separated arcs are unified into one closed curve of train tracks with respect to different fractional charges. Translating the upper arc stack to the left hand side by one step and docking them with the lower arc stack generates the fractional filling states with $\nu = m/(2m + 1)$ (Fig. 13 (a)). While the opposite translation to the right hand side generates the fractional filling states with $\nu = (m + 1)/(2m + 1)$ (Fig. 13 (c)). The translation direction determines the chirality of braiding operations. Translating to the left (right) hand side induces a counterclockwise (clockwise) braiding over the flux pair. The number of braiding operations exactly equals to the integral filling factor $\nu = m$. Therefore, the correspondence between integral Hall effect and fractional Hall effect is a rigorous mathematical relation in this topological surgery theory.

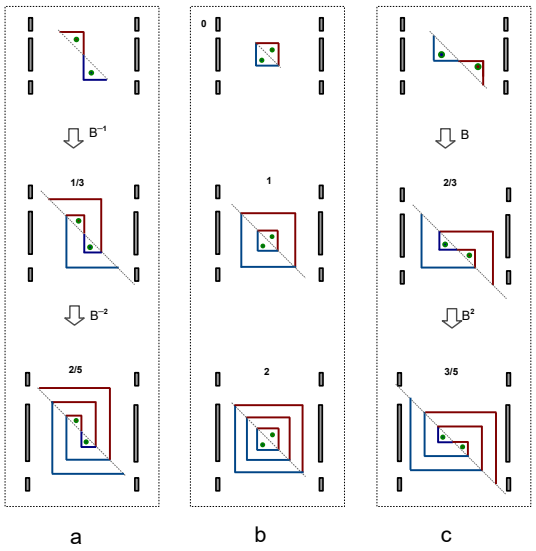

FIG. 13: (a) The train tracks generated by translating the upper arcs to the left hand side and docking them with the bottom arcs. (b) The concentric loop tracks represent the integral filling states. (c) The train tracks generated by translating the upper red arcs to the right hand side and docking them with the bottom arcs.

The topological surgery theory not only generates fractional charges with odd denominator, but also generated fractional charges with even denominators. An even number of translation steps results in fractional charges with even denominator. In Fig. 14 (a), the two-step translation to the left hand side generates the fractional charges $(m - 1)/2m$. Two-step translation to the right hand side leads to the fractional charges $(m+1)/2m$ (Fig. 14 (c)). An effective 1/3 filling state also exist as 2/6 in this fractional serial with the even denominator, but it is different from the 1/3 in the fractional serial with odd denominator which corresponds to the integral filling $\nu = 1$ (Fig. 13 (b)). The 2/6 state here corresponds to the integral filling factor $\nu = 3$ (Fig. 14 (b)). A general translation operation of p (p>2) steps generates other 1/3 state with respect to higher integral filling factor. Higher integral filling factor indicates a weaker magnetic field. Therefore, the 1/3 state is a highly degenerated state that exists for different magnetic field strength.

An odd number of translation steps generates fractional charge serial with odd denominators. Fig. 15 shows the train tracks generated by three-step translation. The minimal integral filling state for the three-step translation is $\nu = 3$. Three-step translation to the left hand side

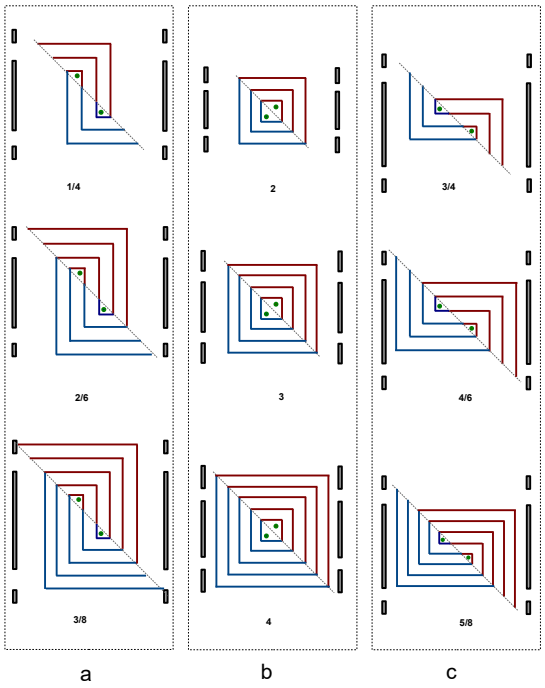

FIG. 14: (a) The upper semi-circles are translated by two steps to the left hand side and glued together with the bottom semi-circles at the new contacting point. (b) The electric current loops around a pair of fluxes represented by the two small green discs. (c) The upper semi-circles arcs translated to the right hand side by two steps and reunite with bottom semi-circles.

generates the fractional serial (Fig. 15 (a))

$$\begin{aligned} Q_{1,\leftarrow} &= Q_{2,\rightarrow} = Q_{1,\downarrow} = Q_{2,\uparrow} = \frac{m-2}{2m-1}, \\ Q_{1,\uparrow} &= Q_{2,\downarrow} = \frac{m+2}{2m-1}, \\ Q_{1,\rightarrow} &= Q_{2,\leftarrow} = \frac{3}{2m-1}. \end{aligned} \tag{71}$$

While three-step translation to the right hand side leads to the dual serial of fractional charges (Fig. 15 (c)),

$$\begin{aligned} Q_{1,\leftarrow} &= Q_{2,\rightarrow} = Q_{1,\downarrow} = Q_{2,\uparrow} = \frac{m+2}{2m-1}, \\ Q_{1,\uparrow} &= Q_{2,\downarrow} = \frac{m-2}{2m-1}, \\ Q_{1,\rightarrow} &= Q_{2,\leftarrow} = \frac{3}{2m-1}. \end{aligned} \tag{72}$$

Note an open track is sandwiched in between the loop currents around two separate flux dimers. This hybrid train track can be viewed as the combination of the one-step translation with the two-step translation. The $1/3$ state is equivalently represented by $3/9$ which corresponds to the integral filling $\nu = 5$.

In the most general case of p-step of translations, the fractional charges generated by topological surgery theory are list as following,

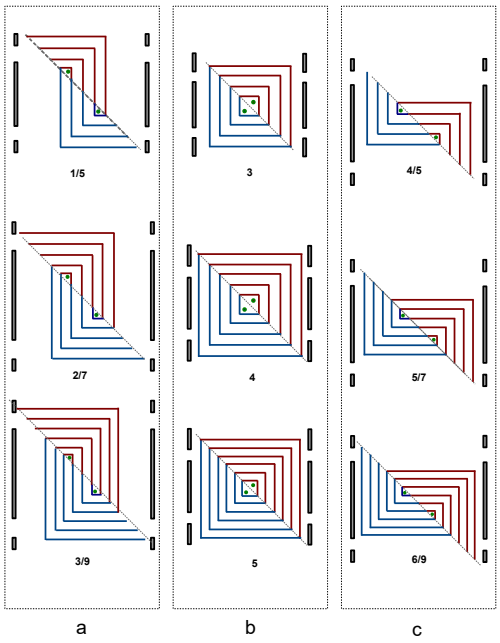

FIG. 15: (a) The upper semi-circles are translated to the left hand side by three steps and reunite with the bottom arcs. (b) The electric current loops around a pair of fluxes represented by the two small green discs. (c) The upper semi-circles are translated to the right hand side by three steps and reunite with bottom arcs.

$$\begin{aligned} Q_{1,\leftarrow} &= Q_{2,\rightarrow} = Q_{1,\downarrow} = Q_{2,\uparrow} = \frac{m-(p-1)}{2m+1-(p-1)}, \\ Q_{1,\uparrow} &= Q_{2,\downarrow} = \frac{m+(p-1)}{2m+1-(p-1)}, \\ Q_{1,\rightarrow} &= Q_{2,\leftarrow} = \frac{p}{2m+1-(p-1)}, \end{aligned} \tag{73}$$

here $p \geqq 2$. There are $(p-2)$ open tracks sandwiched in between the two loop tracks around flux dimer. Whenever the number of braiding operations m and the number of translation steps p obey the equation $m+1 = 2p$, the fractional charge $1/3$ is generated by p-step translations with respect to different integral filling state. Because the number of translation steps cannot outnumber the integral filling factor, the maximal degeneracy degree of one fractional filling state is limited by the integral filling factor.

When the translation operation increases the distance between the two fluxes, the magnetic field strength is reduced following $1/d$ with d the separation distance. Weakening magnetic field strength induced track splitting, resulting in the generation of increasingly lager fractional charges until it reaches half-charge $1/2$. On the contrary case, when the translation operation shortens the distance between the two fluxes, the increasingly stronger magnetic field confines more tracks into small-

er radius to fuse with the inner arcs of the arc stack, driving the fractional charges into low filling state. This topological surgery theory provides a rigorous protocol for topological path fusion process.

J. The correspondence between the fractional charge in knot lattice model and that of train track model

The fractional filling state also exist in the anyon model of knotted electric currents [27], where the fractional filling factor is defined as the ratio of the number of Majorana fermion operators $N(\psi)$ to the number of braiding operations $N(B)$,

$$\nu = \frac{L_{link}}{N(B)} = \frac{N(\psi)}{N(B)}, \tag{74}$$

with L_{link} the linking number, which counts how many flipping operations it takes to map a multi-crossing knot to the minimal crossing state. $N(B)$ counts the total number of braiding operations for generating the multi-crossing knot from an uncrossing circle [27]. As we have already proved that the spiral train track around magnetic flux tube is topologically equivalent to its two dimensional projection in the bottom plane. Event though the definition of filling factor in knot lattice model is different from the train track model, we would further prove the fractional charge in train track model has an rigorous one-to-one correspondence with the knot lattice model [27].

1. *Mapping the knot lattice into fractional charge with odd denominators in train track model*

The knot lattice of a typical fractional charge $e/3$ is taken as the first example to explain the correspondence theory between train tracks and knot lattice. Fig. 16 (a) shows the knot lattice of $e/3$ with three crossings, which are generated by flipping one of the two fluxes three times on the initial current loop around two fluxes. A flipping operation is performed on the middle crossing by the Majorana fermion operators ψ which flips a positive crossing state to a negative crossing state, or vice versa. The back line behind the two fluxes is brought forward to the front, and fuse with the other two segments in the front. This fusion reduced the multi-crossing knot to the single crossing knot (Fig. 16 (a)) by keeping the topology of knot invariant. The exactly same single crossing state can also be derived from the spiral train tracks of 1/3 around two magnetic flux tubes (represented by the bold green arcs that are connected at infinity) (Fig. 16 (b)). Two flipping operations on the crossing points in Fig. 16 (b) are performed by Majorana fermion operators ψ to map the spiral train track into minimum crossing state. Here the two open endings of the spiral track are connected by dashed lines that passes the border region of two fluxes

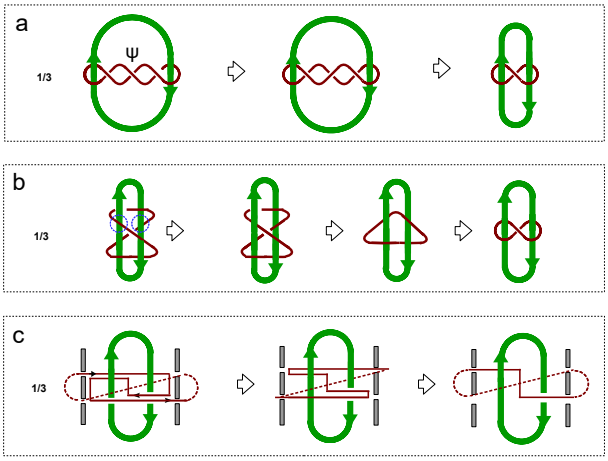

FIG. 16: (a) The initial configuration is a knot with three crossings. ψ is the Majorana fermion operator which flips the crossing state. The connected segments in the same plane topologically transform into a shorter segment. (b) The knot around flux dimer with respect to the train tracks for $e/3$ and its transformation under flipping operations. (c) The train track with respect to $e/3$ and its transformation under flipping operations.

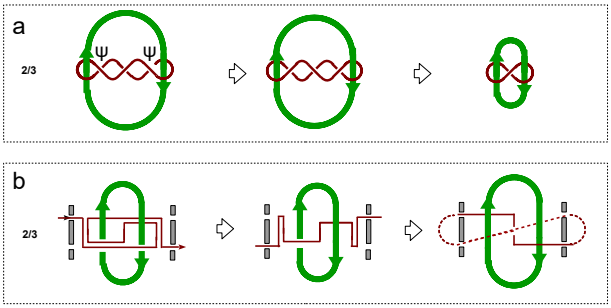

FIG. 17: (a) The initial knot for generating $2e/3$ is acted by two flipping operations on the first and the third crossings. (b) The transformation of train tracks under the two continuous flipping operations.

(Fig. 16 (b)). The track segment on the same side of the flux pair topologically transform into the minimum train track style, which is topologically equivalent to the single crossing knot in Fig. 16 (a). The projection of the spiral train track of Fig. 2 (b) into the bottom plane depicts the train track around the flux pair in Fig. 2 (c). The flipping operation on the middle crossing point in Fig. 16 (b) effectively brings the middle track segment in Fig. 16 (c) at the back of the flux pair to the front. The winding track segments on the same side of flux pair shrinks into the minimal track segment under topological transformation (Fig. 16(c)). When the source point and output point of the train track are connected by a dash line at infinity (Fig. 16(c)), the projected train track forms a minimal closed curve that is exactly topological equivalent to the single crossing state in Fig. 16 (a) and Fig. 16 (b). This topological operation protocol revealed a rigorous relationship between knot and train track.

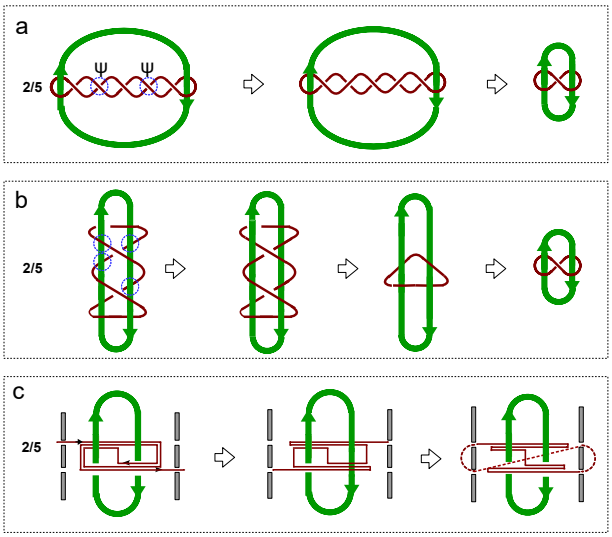

FIG. 18: (a) The knot with five crossings and its transformation process by flipping crossings demonstrates $2e/5$ anyon. (b) The corresponding knot around the flux dimer with respect to the train track of $2e/5$ and its transformation by flipping crossing. (c) The train tracks for the anyon with fractional charge of $2e/5$ and the topological transformation by flipping crossings.

The knot configuration of $2e/3$ is the mirror image of that of $e/3$. Based on the same initial knot lattice for $e/3$, two flipping operations on two crossings except the middle crossing brings the two segments at back to the front to fuse with middle segment into one (Fig. 17 (a)). When two flipping operations is performed on the train track of $2e/3$, the first flipping exchanges the position of the right outmost segment with the left one (Fig. 17 (b)). The second flipping operation brings the front (back) segment to the back (front) (Fig. 17 (b)). The resulted train track of $2e/3$ is exactly the spatial inversion of the track pattern of $e/3$ in Fig. 16 (c) .

The topological correspondence theory also holds for the knot lattice of $2e/5$. The train track of $2e/5$ exactly coincides with the corresponding knot lattice which initially has five crossings in Fig. 18 (a). Two flipping operations are performed on the second and the fourth crossing to connect the decreet segments, transforming it into the minimal crossing in Fig. 16 (a). When four flipping operations are performed on the spiral train track of $2e/5$ in Fig. 16 (b), it results in the same minimum track pattern with respect to the minimum crossing state. The flipping operation on the crossing is equivalent to exchanging the track segments on the projected train track in the bottom plane (Fig. 16 (c)). The two layers of train tracks in the back and that in the front of the flux dimer are exchanged twice by keeping the track continuous and connected. It finally maps into the same minimum crossing state and minimum rain track as above. Similarly, the knot of $3e/5$ is reduced to the mirror image of the minimal crossing knot of $2e/5$ after three flipping operations on the first, the third and the fourth crossing in Fig. 18 (a), so does the spiral track and the train track in the bottom plane.

The topological correspondence between the fractional charge in knot lattice and that of train track is a rigorous relation, which holds for the whole serial of fractional charges with odd denominator. For a general fractional charge $\nu = m/(2m+1)$, there are $2m+1$ crossings in the knot lattice, in which m crossings must be flipped to bring the knot lattice to the minimal crossing state. The total number of crossings in knot lattice $2m+1$ is proportional to the distance between two fluxes and inversely proportional to the strength of effective magnetic field. While for the spiral track around the two flux tubes, the magnetic field strength is inversely proportional to the total number of layers of train tracks around the flux pair $2m+1$. There are exactly $2m$ crossings to be flipped, or m pairs of track segments to be exchanged in the projected train tracks to reach the minimum train track state. Note that the train track must avoid self-crossing in the two dimensional projection plane. This mathematical constraint can be physically implemented by assigning a fermion on each track segment. The Laughlin wave function for N fermions with a filling factor $\nu = 1/(2m+1)$,

$$\psi(z_i) = \prod_{i<j}(z_i - z_j)^{2m+1} e^{-\sum_{i=1}^{N} \frac{|z_i|^2}{4l_B^2}}, \qquad (75)$$

admits a topological interpretation in this train track model. Each of the two ending points of the train track for $e/3$ in Fig. 16 (c) is attached by an electron. $(2m+1)$ pairs of track segments must be exchanged to convert the minimal crossing state of $+1$ in Fig. 16 (a) to that of -1 in Fig. 17 (a). Every exchanging operation contributes a -1 due to the antisymmetric character of two fermions, as summarized by the first term of Laughlins wave function $(z_i - z_j)^{2m+1}$. For example, the knot configuration for $e/3$ $(2e/3)$ in Fig. 16 (a) (Fig. 17 (a)) suggests that three exchanging operations must be performed to map the minimal knot of positive crossing to that of a negative crossing, this is described by $(z_i - z_j)^3$. In the train track pattern for $e/3$ $(2e/3)$ in Fig. 16 (c) (Fig. 17 (b)), each horizontal or vertical track segment is assigned with a fermion with its location labeled by z_i in Laughlin wavefunction. Therefore this topological correspondence theory provided a topological interpretation for Laughlin wave function.

2. *Mapping the knot lattice into fractional charge with even denominators in train track model*

The knot lattice of fractional charges with even denominator also has exact one-to-one correspondence with the train track generated by braiding two pairs of fluxes. The collective wave function of fractional charges with even denominator can also be constructed by the same topological transformation protocol above. For example, the typical train tracks with respect to $e/4$ and $3e/4$ are expanded by braiding two double-line tracks respectively.

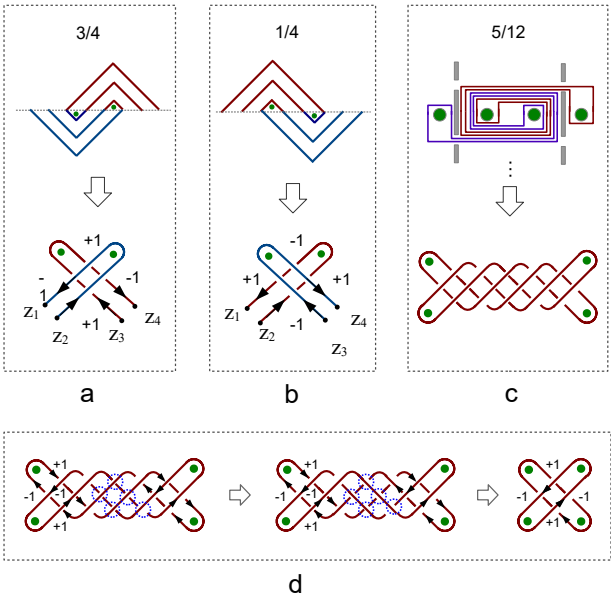

FIG. 19: (a) The train tracks for the fractional charge of $3e/4$ and its corresponding knot configuration. (b) The train track for $e/4$ and its corresponding knot. (c) The train track with fractional charge $Q = 5e/12$ and its corresponding knot pattern by braiding two current loops. (d) The explicit demonstration of flipping the five crossings (enclosed by the dashed blue circle) to bring the knot pattern back to the minimum crossing state.

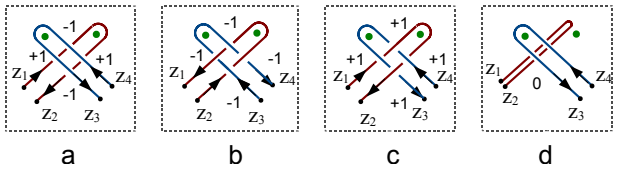

FIG. 20: The knot configuration with respect to the three terms in Pfaffian Eq. (77) of four crossings, (a) the first term, (b) the second term, and (c) the third term. (d) The fusion of the two segments, z_1 and z_2.

Each of the two knot patterns in Fig. 19(a) and (b) has four crossing sites. Each crossing site is characterized by a number that defines the chirality of crossing. Each of the four ending points of the knot pattern in Fig. 19(a) and (b) is assigned with an electron. Exchanging any pair of electrons at the crossing point maps a $+1$ to -1 (or vice versa). Stimulated by the collective wave function for the Moore-Read state in FQHE [42],

$$\psi_{MR} = Pf(\frac{1}{z_i - z_j}) \prod_{i<j} (z_i - z_j)^{2m}, \tag{76}$$

where $Pf(\frac{1}{z_i - z_j})$ is the Pfaffian, we constructed a collective wave function of the knot lattice for fractional charges with even denominator. Pfaffian is the square root of determinant, $Pf(M)^2 = \det(M)$. The reasonable Pfaffian equation for the knot configurations in Fig. 19(a) and (b) is summarized as following,

$$\begin{aligned} Pf(z_i - z_j) &= (z_1 - z_2)(z_3 - z_4) + (z_1 - z_3)(z_4 - z_2) \\ &+ (z_1 - z_4)(z_2 - z_3). \end{aligned} \tag{77}$$

The first term on the right hand side of Eq. (77) indicates the result of exchanging the track segments z_1 and z_2 (or z_3 and z_4) in Fig. 20 (a). The second term describes the knot configuration after exchanging z_1 and z_3 (or z_4 and z_2) (Fig. 20 (b)). The third knot configuration in Fig. 20 (c) depicts the exchanging of z_1 and z_4 (or z_2 and z_3). When the two track segments z_1 and z_2 (or z_3 and z_4) are on the same side of the flux, they fuse into one complete segment and contract continuously to zero when there is no flux tube or tracks to block their contraction (Fig. 20 (d)). The knot for other fractional charges with even denominator are constructed by further braiding operations on the minimum crossing configuration. For example, the knot pattern with respect to $Q = 5e/12$ is generated by braiding two loop currents three times, each braiding generates four more crossings accompanied by a mathematical constraint that none of the two loop currents is twisted (Fig. 19(c)). Five crossing sites (as labeled by the dashed circle) must be flipped to map the knot pattern back to the minimal crossing pattern (Fig. 19(d)). The collective wave function of the knot configuration with respect to $Q = 5e/12$ is expressed as

$$\psi(z_i) = Pf(z_i - z_j) e^{-\sum_{i=1}^{12} \frac{|z_i|^2}{4l_B^2}}. \tag{78}$$

The collective wave function for other filling fractions is constructed in a straight forward way following this topological transformation protocol. Therefore here we provided a new way of constructing collective wave function of strongly correlated electrons in two dimensions. This construction method also extends into three dimensional network of knot.

K. The irrational charges in train tracks around three fluxes

The train tracks around two fluxes generated the fractional charges that agrees with FQHE, and also predicted new serials of fractional charges. Therefore the two dimensional electron gas in strong magnetic field is effectively described by a gas of magnetic flux pairs surrounded by train tracks of electron. The number sequence of fractional charges around the flux pair approaches to $1/2$ when the total number of braiding operations goes to infinity. The half charge $1/2$ is not the only limit of fractional charge sequence. Irrational charges exist as the limit of the complex sequence of fractional charges produced by the train tracks around three magnetic fluxes (Fig. 21),

We first study an exemplar train track generated by braiding a winding path around three fluxes in Fig. 21 (a). The exchanging of the flux pair $[2, 3]$ twice in counterclockwise direction is denoted by the operator $\sigma^2_{(2,3);\circlearrowleft}$.

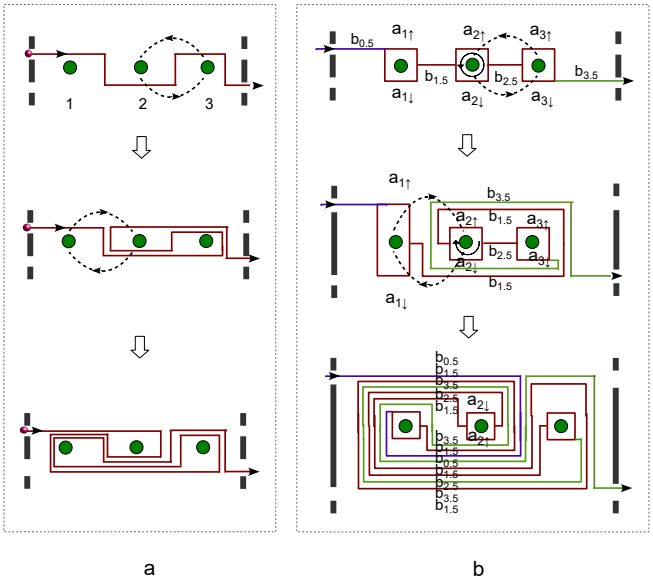

FIG. 21: (a) The stacked eclectic current configuration under a pair of braiding operations upon the magnetic flux trimer, i.e., $\sigma^2_{(1,2);\circlearrowleft}(s_2)\sigma^2_{(2,3);\circlearrowleft}(s_1)$. (b) The stacked electric currents under the braiding operations $\sigma_{(12);\circlearrowleft}(t_2)\sigma_{(23);\circlearrowleft}(t_1)$ with a general initial current configuration around the flux trimer.

Then the flux pair $[1,2]$ is exchanged twice in clockwise direction by $\sigma^2_{(1,2);\circlearrowleft}$. The combination of the two braiding operators,

$$\hat{B}_s = \sigma^2_{(1,2);\circlearrowleft}\sigma^2_{(2,3);\circlearrowleft}, \tag{79}$$

maps the initial train track into a new train track by keeping the order of three fluxes invariant simultaneously. The distribution of fractional charges along the train tracks around the three fluxes reads

$$\begin{aligned} Q_{1,\uparrow} &= \frac{a_{1,\uparrow}}{a_{1,\uparrow}+a_{1,\downarrow}} = \frac{3}{5}, \quad Q_{1,\downarrow} = \frac{a_{1,\downarrow}}{a_{1,\uparrow}+a_{1,\downarrow}} = \frac{2}{5}, \\ Q_{2,\uparrow} &= \frac{1}{5}, \quad Q_{2,\downarrow} = \frac{4}{5}, \quad Q_{3,\uparrow} = \frac{2}{3}, \quad Q_{3,\downarrow} = \frac{1}{3}. \end{aligned} \tag{80}$$

Repeated action of the braiding string operator $\hat{B}_s$ maps one fractional charge distribution into another distribution. The effective field strength is inversely proportional to the number of braiding operation of $\hat{B}_s$, which can be implemented by two effective magnetic fluxes oriented in antiparallel direction. The fractional charge sequence on the three fluxes would finally reach a stable distribution for an infinite number of braiding operations. However, the limit charge on the three fluxes are not half-charge any more.

In order to find the limit charge of fractional charge sequence on the three fluxes under the action of $\hat{B}_s$, the initial track distribution is labeled by a general value, as labeled by $a_{i,\uparrow}$ (or $a_{i,\downarrow}$) that counts the number of stacked currents above (or below) the ith magnetic flux, while $b_{i.5}$ counts the number of stacked bond current that bridges the flux pair $[i, i+1]$ (Fig. 21 (b)). Under the action of braiding string operator $\hat{B}_s$, the new stack number around a magnetic flux at time t_m is the linear combination of that at t_{m-1},

$$\begin{aligned} a_{1,\uparrow}(t_m) &= a_{1,\uparrow}(t_{m-1}) + b_{1.5}(t_{m-1}) + b_{2.5}(t_{m-1}) \\ &+ b_{0.5}(t_{m-1}) \\ a_{1,\downarrow}(t_m) &= a_{1,\downarrow}(t_{m-1}) + 2b_{1.5}(t_{m-1}) + b_{2.5}(t_{m-1}), \\ &+ b_{0.5}(t_{m-1}) + 2b_{3.5}(t_{m-1}) \\ a_{2,\uparrow}(t_m) &= a_{2,\downarrow}(t_{m-1}) + b_{1.5}(t_{m-1}) + b_{2.5}(t_{m-1}), \\ &+ b_{0.5}(t_{m-1}) + b_{3.5}(t_{m-1}) \\ a_{2,\downarrow}(t_m) &= a_{2,\uparrow}(t_{m-1}) + 3b_{1.5}(t_{m-1}) + b_{2.5}(t_{m-1}), \\ &+ b_{0.5}(t_{m-1}) + 3b_{3.5}(t_{m-1}) \\ a_{3,\uparrow}(t_m) &= a_{3,\uparrow}(t_{m-1}) + b_{1.5}(t_{m-1}) + b_{3.5}(t_{m-1}) \\ a_{3,\downarrow}(t_m) &= a_{3,\downarrow}(t_{m-1}) + b_{1.5}(t_{m-1}) + b_{3.5}(t_{m-1}). \end{aligned} \tag{81}$$

This iterative equation must combines with the equation for the current tracks that bridge two neighboring fluxes (Fig. 21 (b)),

$$\begin{aligned} b_{1.5}(t_m) &= 5b_{1.5}(t_{m-1}) + 2b_{2.5}(t_{m-1}) \\ &+ 2b_{0.5}(t_{m-1}) + 4b_{3.5}(t_{m-1}), \\ b_{2.5}(t_m) &= 2b_{1.5}(t_{m-1}) + b_{2.5}(t_{m-1}) + 2b_{3.5}(t_{m-1}), \\ b_{0.5}(t_m) &= b_{0.5}(t_{m-1}), \quad b_{3.5}(t_m) = b_{3.5}(t_{m-1}), \end{aligned} \tag{82}$$

where $b_{0.5}$ and $b_{3.5}$ are constant under arbitrary braiding and have no influence on the track redistribution. Therefore their value are set to zero for simplicity, i.e. $b_{0.5} = b_{3.5} = 0$. The iterative equations above transform into differential equations when the time step approaches to infinitesimal value. The stable solution for the track distribution can be derived by differential equation theory. The eigenvectors of the stable tracks distribution around the three fluxes are listed as following:

$$\begin{aligned} (a_{3,\uparrow}, b_{1.5}, b_{2.5}) &= (a_{3,\downarrow}, b_{1.5}, b_{2.5}) = (1/2, 1+\sqrt{2}, 1), \\ (a_{2,\uparrow}, a_{2,\downarrow}, b_{1.5}, b_{2.5}) &= (\frac{2+\sqrt{2}}{4}, \frac{2+3\sqrt{2}}{4}, 1+\sqrt{2}, 1), \\ (a_{1,\uparrow}, b_{1.5}, b_{2.5}) &= (1/\sqrt{2}, 1+\sqrt{2}, 1), \\ (a_{1,\downarrow}, b_{1.5}, b_{2.5}) &= (\frac{1+\sqrt{2}}{2}, 1+\sqrt{2}, 1). \end{aligned} \tag{83}$$

The trivial solutions $b_{1.5} = b_{2.5} = 0$ are omitted for simplicity. The fractional charge distribution around the three fluxes is derived from these eigenvectors,

$$\begin{aligned} Q_{1,\uparrow} &= \frac{2}{3+\sqrt{2}}, \quad Q_{1,\downarrow} = \frac{1+\sqrt{2}}{3+\sqrt{2}}, \\ Q_{2,\uparrow} &= \frac{2+\sqrt{2}}{4(1+\sqrt{2})}, \quad Q_{2,\downarrow} = \frac{2+3\sqrt{2}}{4(1+\sqrt{2})}, \\ Q_{3,\uparrow} &= Q_{3,\downarrow} = \frac{1}{2}, \end{aligned} \tag{84}$$

The fused bond tracks between flux No. 1 and No. 2 also carries irrational charges, $Q_{b1.5} = 1+\sqrt{2}$, which results

in irrational Hall resistance resistance between flux No. 1 and No. 2

$$R_{Hb_{1.5}} = R_0 \frac{1}{1+\sqrt{2}}. \tag{85}$$

The local Hall resistance around flux No. 1 is determined by $Q_{1,\downarrow} = Q_{1,\leftarrow} = \frac{1+\sqrt{2}}{3+\sqrt{2}}$,

$$R_{H1} = R_0 \frac{3+\sqrt{2}}{1+\sqrt{2}}. \tag{86}$$

These irrational Hall resistance only exist for train tracks generated by braiding three fluxes, which is beyond the current experimental observation of FQHE. This particular value of irrational Hall resistance is the output of the specific braiding string operator $\hat{B}_s$. A different combinatoric braiding sequence generates a different limit charge. As we proved, a braiding sequence can be implemented by a spatial distribution of magnetic flux tubes. The spatial scale of elementary magnetic flux quanta is below 10^{-10}, a precious manipulation of magnetic flux quanta is beyond current technology level but can pave a new way for future.

III. FRACTIONAL CHARGES IN ONE DIMENSIONAL LATTICE OF MAGNETIC FLUXES

The two dimensional electron gas in strong magnetic field is well approximated by a gas of free magnetic flux pairs which are surrounded by winding train tracks. When many flux pairs are confined in a limited space, the strong neighboring interaction between these flux pairs emerges as the dominant factor that drives the fractional charges distribution away from the conventional FQHE. Here we first study the one dimensional chain of flux pairs for simplicity. The one dimensional distribution of train track are first constructed by the topological surgery method with partial translation symmetry, and then constructed by general braiding operations without translation symmetry.

A. Fractional charges generated by topological surgery on one dimensional magnetic flux lattice

The topological surgery on the concentric loop tracks around one magnetic flux pair provided an exact correspondence between integral quantum Hall effect and FQHE. Here many flux pairs together with their concentric loop tracks are initially located on one dimensional lattice in Fig. 22-(0). The integral filling state $\nu = 2$ is represented by three layers of concentric loop tracks in Fig. 22-(0). A general integral filling state $\nu = m$ is represented by $m+1$ layers of concentric loop tracks. These concentric circles are first cut into two sets of

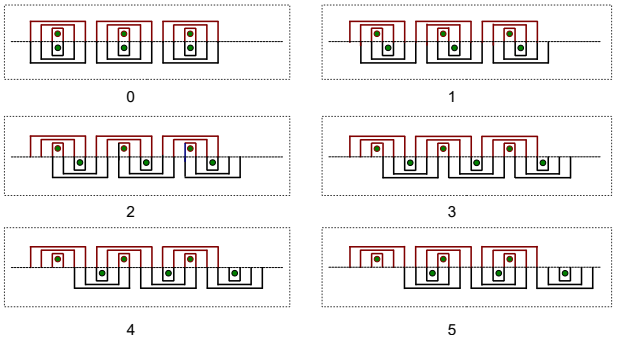

FIG. 22: (0) A chain of flux dimers oriented in the vertical direction, in which each flux dimer (the two green dots) is surrounded by three loop tracks. (1-5) The flux dimer is cut along their border line to generate two chains of semicircles around single flux. The upper semi-circles are collectively translated to the left hand side by p (p = 1,2,3,4,5) steps and reunite with the bottom chain, generated different train track patterns under different braiding operations.

concentric semicircles around single flux along the borderline between two fluxes. In Fig. 22, the set above (below) the cutting line is dyed blue (red). The cutting points are placed on one dimensional lattice with a lattice spacing of the perpendicular distance between the nearest neighboring loop tracks. Firstly, the concentric semicircles above the cutting line together with the flux they surround are translated to the right hand side by one step, and are docked with the semicircles below at their new locations of cutting points (Fig. 22-(1)). The isolated concentric loop tracks are united into one continuous train track for fractional charge $3e/5$, which periodically distributed along the one dimensional chain. This translational surgery operation is equivalent to braiding a simple track twice in clockwise direction periodically. Further more, two steps of translational surgery operation to the right hand side generates the one dimensional lattice of train tracks for fractional charge $3e/4$, which is equivalent to braiding the double-line tracks around two flux dimers in clockwise direction (Fig. 22-(2)). Three steps of translation generates three layers of independent open tracks winding through the one dimensional flux lattice (Fig. 22-(3)), indicating a conducting state of integral charges. Four steps of translation depicts the train track for fractional charge $e/4$, which matches the tracks generated by braiding the double track of two flux dimers in counterclockwise direction (Fig. 22-(4)). Five steps of translation generates the mirror pattern of train track after one-step translation (Fig. 22-(5)). Six steps of translation brings the train track pattern back to the initial concentric loop tracks with respect to integral filling state $\nu = 2$ in Fig. 22-(0). Each translation operation is equivalent to one effective magnetic field strength. The effective magnetic field oriented in negative direction reduces to zero step by step when the translation operation is performed from the 0th to the 3rd step. Then the effective magnetic field flips to positive direction and

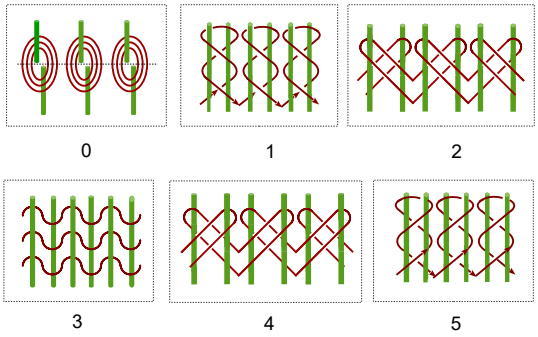

FIG. 23: The two dimensional knot lattice as an expansion of the one dimensional lattice of train tracks by p (p=1,2,3.4,5) steps of translation operations in Fig.22.

increase to generate the integral filling state $\nu = 2$. The topological surgery protocol under translation operation holds for the whole serial of fractional charges.

The one dimensional lattice of train tracks is the topological projection of two dimensional knot lattice. The initial train track of the integral filling state in Fig. 22-(0) is the projection of three layers of loop currents in Fig. 23-(0). The one dimensional lattice of train track for $2e/5$ is projected out by the two dimensional knot lattice in Fig. 23-(1), which is the mirror image of that for fractional charge $3e/5$ in Fig. 23-(5). The train tracks generated by braiding loop tracks around flux dimers is the projection of knot lattice of double tracks in Fig. 23-(2)(4). The three layers of monotonically propagating track in Fig. 23-(3) is exactly the three unknotted paths in two dimensional knot lattice. The weak interaction between the nearest neighboring flux pairs is preserved by the single connection track at the bottom of Fig. 23-(1)(5). While the double connection tracks at the bottom of Fig. 23-(2)(4) indicates a stronger coupling interaction between flux pairs. The loop tracks around isolated flux pairs are not connected in the knot lattice of integral filling state (Fig. 23-(0)), therefore fractionally charged states have strong topological correlation, which is not preserved in integral filling state.

The train tracks are the propagating paths of electron. Every propagating path is equivalent to a continuous connection of many directed line segments in Feynman diagram, which represents the generation and annihilation of a particle in space time. Therefore every semicircle arc that connects two cutting points can be interpreted as generating an electron at one cutting point and annihilating it at the other cutting point. Since every Feynman diagram is represented by a product string of quantum operators, each train track pattern in Fig. 22 can be summarized into a Hamiltonian. The Hamiltonian equation for the train tracks with an integral filling factor $\nu = n$ in Fig. 22 - (0) reads,

$$\begin{aligned} H_0 &= \sum_{r=1}^{\infty}\sum_{j=1}^{n+1} t\, c^{\dagger}_{r2(n+1)+(j+\frac{1}{2})} c_{r2(n+1)+(j-\frac{1}{2})} \\ &+ \sum_{r,j} t\, c^{\dagger}_{r2(n+1)+(j-\frac{1}{2})} c_{r2(n+1)+(j+\frac{1}{2})} e^{-i\phi 2\pi} \\ &+ h.c., \end{aligned} \tag{87}$$

where n is the integral filling factor. $h.c.$ represents Hermitian conjugation. t is the hopping rate. $j[< 2(n+1)]$ labels the location of cutting points between the nearest neighboring fluxes. The Hamiltonian H_0 is the initial state for translation operations. The translation operator $\hat{T}_p$ maps the location index of all cutting points p-steps forward to the right hand side,

$$\hat{T}_p c^{\dagger}_r = c^{\dagger}_{r+p}, \quad \hat{T}_p c_r = c_{r+p}, \quad \hat{T}_p \phi_r = \phi_{r+p}. \tag{88}$$

The translation operator $\hat{T}_p$ is first acted on the red semicircle tracks below the cutting line. One-step translation to the right hand side derives the Hamiltonian for one dimensional chain of $3e/5$ charges,

$$\begin{aligned} H_1 &= \hat{T}_1 H_0 \\ &= \sum_{r,j} t\, c^{\dagger}_{r2(n+1)+(j+\frac{1}{2})} c_{r2(n+1)+(j-\frac{1}{2})} \\ &+ \sum_{r,j} t\, c^{\dagger}_{r2(n+1)+(j+\frac{1}{2})} c_{r2(n+1)+(j+\frac{3}{2})} e^{-i\phi 2\pi \frac{1}{2(n+1)}} \\ &+ h.c.. \end{aligned} \tag{89}$$

This Hamiltonian also describes how Feynman diagrams are connected into train tracks. For the general case, p-step translation generates the Hamiltonian for other train tracks in Fig. 22, $H_p = \hat{T}_p H_0$,

$$\begin{aligned} H_p &= \sum_{r,j} t\, c^{\dagger}_{r2n+j+\frac{5}{2}} c_{r2n+j+\frac{3}{2}} \\ &+ \sum_{r,j} t\, c^{\dagger}_{r2n+j+\frac{3}{2})+p} c_{r2n+j+\frac{5}{2}+p} e^{-i\phi 2\pi \frac{p}{2(n+1)}} \\ &+ h.c.. \end{aligned} \tag{90}$$

The fractional magnetic flux reduces to an integral flux when $p = 2(n+1)$, which corresponds to integral Hall effect. This Hamiltonian has translation symmetry with respect to the position index of magnetic fluxes r. The Fourier transformation applies for the central index r instead of the track layer index j.

The Hamiltonian Eq. (90) describes the motion of electron in flux lattice before the stacked track layers fuse into one bundle. The track fusion process combines the internal index j into the phase factor of magnetic flux which becomes a fractional number, counting the partition of one flux into each track segment within the fused track bundle. As a result, the Hamiltonian for periodical train tracks can be mapped into the Harper Hamiltonian

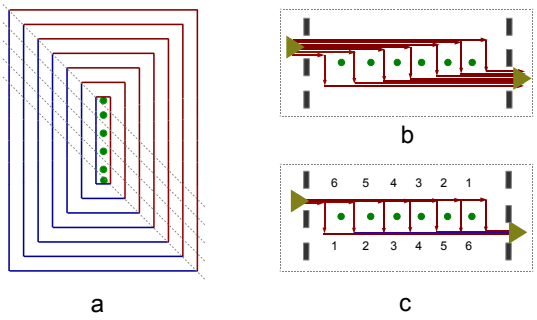

FIG. 24: (a) An unit cell of seven loop tracks around six magnetic fluxes. (b) The electron beam passes the six magnetic fluxes. (c) The local probability distribution around the six magnetic fluxes.

for one dimensional flux lattice [44],

$$H_{hp} = \sum_{r,j} t_x \; c^{\dagger}_{r+1,j} c_{r,j} + t_y \; c^{\dagger}_{r,j+1} c_{r,j} e^{-i2\pi\phi r} + h.c. \quad (91)$$

The rational number ϕ in Harper Hamiltonian is essentially the fractional filling factor ν of FQHE. A moving electron along these winding paths feels an integral flux before track fusion. The electron in the fused tracks flow in the same direction by splitting itself according to the local number of layers of stacked track segments around the flux. This physical phenomena is equivalent to cutting the integral flux into fractional flux and assign the fractional flux to each track segment, but keeping the electron as an integral charge. Therefore the Harper Hamiltonian could be derived from Hamiltonian Eq. (90).

The Harper Hamiltonian extends into the Hofstadter model [45] when the flux number ϕ is not a rational number. The energy spectrum showed a fractal structure [45]. As we showed in the correspondence theory between knot on torus and train track around flux pair, a rational filling factor leads to a closed path on torus and a closed train track around flux pair. While an irrational filling factor leads to an endless open track on torus and an open winding track generated by braiding operation over an arbitrary angle $\theta \neq n\pi, n = 1, 2, \cdots$. Therefore, the fractal structure in Hofstadter model is induced by the chaotic propagation path of electron and the open tracks generated by braiding operations over an irrational angle. The chaotic path results in the classical resistance of electron transportation, while the closed train tracks and knot paths result in the Hall resistance plateau in FQHE.

The translational surgery could also be performed on an one dimensional lattice of concentric electric loops around many fluxes to generate periodical fractional charge distribution. Fig. 24 (a) shows an unit cell of seven loop tracks around six magnetic fluxes for an one dimensional lattice of magnetic flux clusters. Five cutting lines (dashed lines in Fig. 24 (a)) divide the loop tracks into six groups of stacks. Each group of track stack

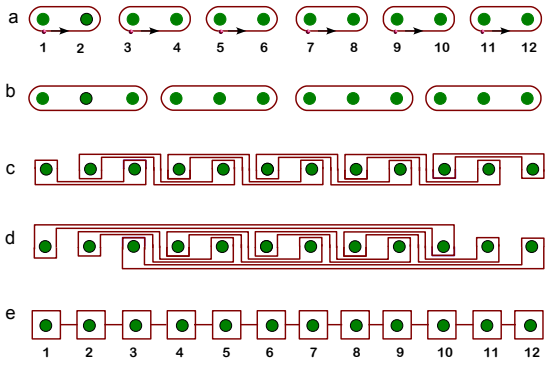

FIG. 25: (a) A chain of flux dimers, each of which is surrounded by an electric current loop (represented by the red circle). (b) The chain of flux trimers. Every electric loop current encloses three fluxes. (c) The stack electric currents around the lattice of magnetic fluxes generated by one counter-clockwise braiding over the nearest neighboring fluxes. (d) The train track generated by one more counterclockwise braiding between the first and the last flux. (e) A scheme representation of the most general current track distribution around the one dimensional flux lattice. Each edge is assigned with a weight factor that counts the number of layers of tracks that fused into the edge.

envelops one flux. Translating the each of six groups of track stack by one step downward along the cutting line generates seven independent paths passing the one dimensional lattice of six magnetic fluxes (Fig. 24 (b)). The track fusion results in six fractional charges $(6/7, 5/7, 4/7, 3/7, 2/7, 1/7)$ above the six fluxes (Fig. 24 (c)). These fractional charges periodically distributed along the one dimensional lattice of flux clusters.

B. Fractional charges generated by braiding one dimensional lattice of magnetic flux clusters

Besides the minimal loop current that winds around two nearest neighboring fluxes, a moving electron can also generate a larger loop current to enclose a flux cluster with more than two fluxes. When the total number of fluxes is fixed in the one dimensional lattice of flux cluster, the total electromagnetic energy is inversely proportional to size of flux cluster. This is because parallel currents attract each other and anti-parallel currents repel each other. The total energy of flux dimer lattice is the sum of six pairs of anti-parallel currents (Fig. 25 (a)),

$$H_{0,[2]} = \sum_{i=1}^{6} \frac{-\mu_0}{2\pi} l_b \ln(d) I_{i+1/2,j} I_{i+1/2,j+1}, \quad (92)$$

Here l_b is the lattice spacing between two neighboring fluxes. If the flux lattice is regrouped into triple clusters (Fig. 25 (b)), the total number of antiparallel current pairs grows up to eight, leading to a higher total energy

than that of dimer covering,

$$H_{0,[3]} = \sum_{i=1}^{8} \frac{-\mu_0}{2\pi} l_b \ln(d) I_{i+1/2,j} I_{i+1/2,j+1}. \quad (93)$$

Therefore the lattice of loop currents enclosing flux cluster of smaller size has lower energy.

Braiding two magnetic fluxes within a flux cluster does not change the topology of the loop current. In an one dimensional lattice of magnetic flux clusters (Fig. 25 (a)), synchronously braiding two fluxes that belong to the nearest neighboring clusters in clockwise direction produces the same train track (Fig. 25 (c)) as Fig. 22 - (4). As showed by the energy spectrum of antiparallel currents in Fig. 9, the unbraided loop current around flux dimer has the highest energy which is reduced by braiding the nearest neighboring clusters due to the generation of parallel currents. Therefore, braiding operation drives the system to a state with lower energy. The electrons on the bond prefer to gather around the track stack of an odd number of tracks (Fig. 25 c). Fig. 25 (c) shows the periodical distribution of fractional charges 3/4 and 1/4, that has a lower energy than the free dimer state,

$$H_1 = -\frac{\mu_0}{2\pi} l_b \sum_{r>l=1;i}^{4} (-1)^{r-l} \ln[(r-l)d](I_{i,l} I_{i,r}). \quad (94)$$

Braiding operation is an effective way of driving the one dimensional lattice of train tracks to ground state.

The electromagnetic energy derived from the Hamiltonian equation above is the eigen-energy of a train track configuration. The initial free dimer state is the highest excited state which has the maximal eigen-energy. The second highest excited state is generated by only one braiding upon only one pair of the nearest dimers loops. For a magnetic flux chain of N dimers, the second highest excited has $(N-1)$ fold degeneracy. The topological eigenstate shows only a pair of local fractional charged states, ($Q_{u,i} = 1/4$, $Q_{d,i} = 3/4$) and ($Q_{u,j} = 3/4$, $Q_{d,j} = 1/4$). While other unbraided dimer loops remains half-charged state. The third highest excited state are created by two continuous braiding operations over the same pair of dimer loops, which generates fractional charges, ($Q_{i,\uparrow} = 3/8$, $Q_{i,\downarrow} = 5/8$) or ($Q_{i,\downarrow} = 3/8$, $Q_{i,\uparrow} = 5/8$). In the case of infinite number of random braiding over the whole flux lattice, every flux is wrapped by a large number of current segments. The total number of upper currents almost equal to that of down currents around the flux. Correspondingly one electron splits into two equal half charges. In the end, all fractional charges converge to half charges, which is exactly the ground state of the lattice model of train tracks. Note that this half-charge state is a conducting half-charges state, which is completely different from initial free dimer state, where electrons are localized around the flux pair and showed an insulating state. The total electromagnetic energy of the current stacks in flux lattice finally reaches a fixed point as suggested by the energy spectrum of train tracks around single flux pair (Fig. 9). That fixed point is the energy of the ground state energy of this flux lattice system.

The braiding operation on two far separated fluxes induces long range charge fluctuation. A long range braiding operation can be equivalently implemented by a sequence of braiding operations on the nearest neighboring flux pairs. Each braiding operation covers the outmost layer of train track stack by a pair of anti-parallel currents, while an inverse braiding cancels one layer of anti-parallel currents. For example, braiding the first magnetic flux and the last magnetic flux generates a long range current bridge covering the whole chain (Fig. 25 (d)). This newly added current reset the charge splitting ratio around each magnetic flux core (Fig. 25 (d)). The upper fractional charge at the second magnetic flux is increased to $Q_{2,\uparrow} = 3/4$ and the down charge is reduced to $Q_{2,\downarrow} = 1/4$. While the fractional charge at the 3rd magnetic flux becomes ($Q_{3,\uparrow} = 5/6$, $Q_{3,\downarrow} = 1/6$). The flux covering the lattice sites from $i = 4$ to $i = 9$ are sandwiched in between two fractional charges ($Q_{i,\uparrow} = 3/8$, $Q_{i,\downarrow} = 5/8$) (Fig. 25 (d)). The denominator of these fractional charge is an even number which counts the number of currents on the bond between two neighboring fluxes. This exemplar braiding operation suggests long range braiding causes charge fluctuation in large spatial scale. The spatial range of topological correlation is proportional to the distance between the most far separated two fluxes in the braiding operator. Every long range braiding operator can be exactly express as the product of braiding operators over the nearest neighboring fluxes. In order to map the initial ordering of magnetic fluxes, $[1, 2, 3, ..., 12]$, to the final ordering $[12, 2, 3, ..., 1]$, we first bring the first flux to the last position, $[2, 3, ..., 12, 1]$, then bring the 12 flux to the first position, $[12, 2, 3, ..., 11, 1]$. This mapping can be realized by following mapping sequence,

$$\begin{aligned} B_{1,12} &= \sigma_{1,2}(t_1)\sigma_{2,3}(t_2)\cdots\sigma_{11,12}(t_{12})\sigma_{10,11}(t_{13}) \\ &\quad \sigma_{9,10}(t_{14})\sigma_{8,9}(t_{15})\cdots\sigma_{1,2}(t_{22}). \end{aligned} \quad (95)$$

σ_{ij} is the braiding operator on (ij) with σ_{ij}^{-1} as its inverse operator, and their product fuses into unity, $\sigma_{ij}\sigma_{ij}^{-1} = 1$. This mapping sequence generates the same topological pattern of current tracks as that under one straightforward operation between flux [1,12]. Note here the operation in the sequence above must be kept in the same direction (either clockwise or counterclockwise) as that of one step braiding $B_{1,12}$. Even though replacing one braid operator by its inverse operator also exchange the position of the nearest neighbors, it would map into a completely different topological pattern that mismatches the output of $B_{1,12}$.

Although different initial train tracks lead to different ultimate distribution of fractional charges after finite number of braiding operations, the limit charge distribution after infinite number of braiding operations could reach the same fixed point. The value of fixed point is determined by the sequence of braiding operations. For

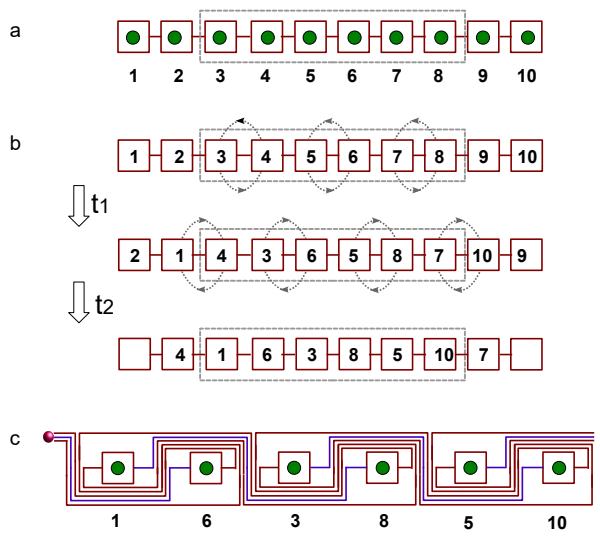

FIG. 26: (a) A general one dimensional lattice of train track distribution. (b) A collective braiding in counterclockwise direction is first performed (as labeled by t_1), followed by a collective clockwise braiding labeled by t_2. (c) The resultant train track pattern generated by the two collective braiding operations above.

the most general initial track distribution in Fig. 26 (a), which represents the fused train tracks in Fig. 25 (e) or Fig. 24 (c), we first perform the counterclockwise braiding operations on the nearest neighboring fluxes, and then translate the braiding operators to the left by one step to perform a clockwise braiding at the new locations in Fig. 26 (b). This operation depicts the train track pattern in Fig. 26 (c). Repeating this combinatoric braiding operation on the flux lattice infinite times drives the local charges to converge to the irrational charges in Eq. (84). While other combinations of braiding operations converge to different irrational charges. A closer observation on Fig. 26 (c) shows a periodical distribution of track stacks that can also be generated by the translational surgery method. Therefore, any periodical braiding operations on one dimensional flux lattice can be equivalently realized by translational surgery operations. The non-periodical braiding operations is more convenient for generating fractional charges in a lattice with impurity, which breaks the translational symmetry.

IV. FRACTIONAL CHARGES IN TWO DIMENSIONAL LATTICE OF MAGNETIC FLUXES

A. Fractional charges generated by translation of the two dimensional lattice of winding tracks

The train track pattern of fractional charges in two dimensional flux lattice can also be constructed by the topological surgery protocol under translation of magnetic fluxes. For example, The periodical distribution of

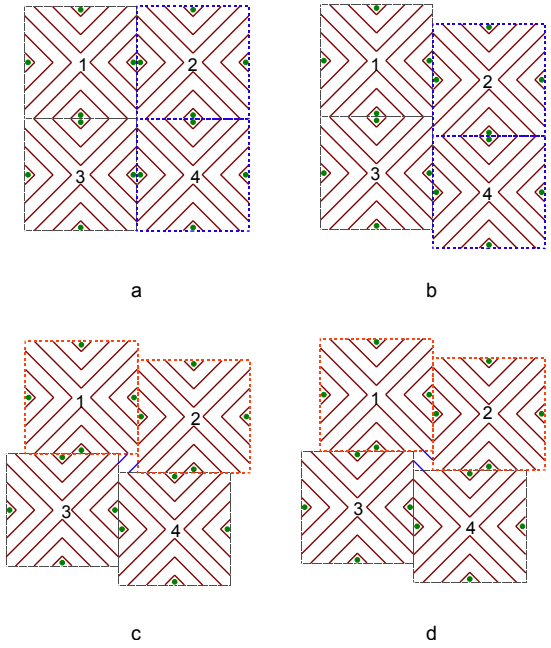

FIG. 27: (a) A square lattice of many flux pairs, each of them is surrounded by three layers of square curves. (b) The train track pattern under one step translation of unit cells No. 2 and No. 4 in the vertical direction. (c) The train track pattern under one step of translation of unit cells No. 1 and No. 2 to the right hand side. The two parallel blue lines bridge the unit cells (No. 1, No. 3) and (No. 2, No. 4) respectively. (d) The two parallel blue lines bridge the unit cells (No. 1, No. 2) and (No. 3, No. 4) respectively after the combined translation.

three layers of concentric squares around a pair of fluxes in two dimensions constructed the two dimensional lattice of integral filling state $\nu = 2$ in Fig. (27) (a). The unit cell contains four fluxes located on the middle point of its four edges (as labeled by the green disc in Fig. (27) (a)). Each flux within one unit cell combines with another flux in the nearest neighboring unit cell to form a flux pair, around which is three layers of concentric square. The three layers of concentric semi-squares intersect with the boundary of the unit cell, pinning down the docking sites for connecting tracks in another unit cell. Translating the column of two unit cells No. 2 and No.4 downward by one step and docking the tracks in their new locations one by one generates open strips of periodical winding tracks, separated by isolated concentric squares around flux pairs (Fig. (27) (b))). In order to break the flux pair oriented in vertical direction in Fig. 27) (b)), we group the unit cells No. 1 and No. 2 together and translate the whole row to the right hand side by one step. Most docking sites on the boundary naturally meet their next neighboring sites except the four sites on the corners (as showed by the empty square hole in the middle region where four unit cells meet in Fig. 27 (c)). There are only two possible ways to dock the four corner sites to avoid self-crossing of train tracks. One way is connecting the

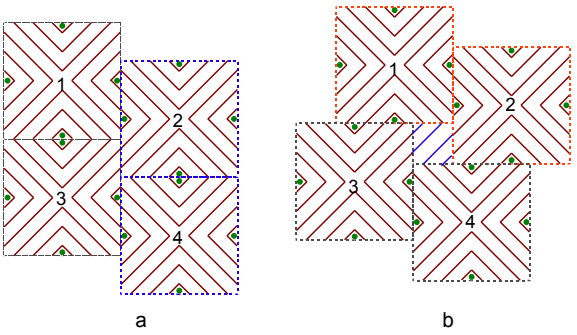

FIG. 28: (a) A new train track pattern is obtained by two-step translation on a column lattice of train tracks with three layers of squares around flux pair in Fig. 27 (a). (b) The train track pattern under two-step of translations on a row lattice of train tracks to the right hand side. There are four parallel blue lines bridging the unit cells (No. 1,No. 3) and (No. 2, No. 4) respectively, which can be replaced by another four parallel blue lines in perpendicular direction to bridge the unit cells (No. 1,No. 2) and (No. 3, No. 4).

unit cells (No. 1, No. 3) and (No. 2, No. 4) in Fig. 27 (c). The other way connects unit cells (No. 1, No. 2) and (No. 2, No. 3) in Fig. 27 (d). In the end, a periodical distribution of winding train tracks around the flux pairs is constructed over the whole two dimensional space. In the bulk region, there are five tracks passing through the border region between neighboring fluxes, interwind by the solo track between the nearest neighboring fluxes.

The translation by an odd number of steps generates a periodical distribution of open tracks around flux pairs. While the translation by even number of steps generates loop tracks that interwind each other with two fluxes enclosed inside. Taking the same initial track state as Fig. 27 (a), the column of two unit cells (No. 2 and No. 4 in Fig. 28) are combined together to translate downward by two steps, generating entangled loop track that encloses a pair of fluxes respectively (Fig. 28 (a)). Then the unit cells of No. 1 and No. 2 in Fig. 28 (a) together as one group is translated to the right by two steps. The two translation operations leaves a blank square around which the four corners of four unit cells meet. Each edge of the blank square in Fig. 28 (b) has two unconnected docking sites. Four parallel track segments are added to connect the eight docking sites under the self-crossing avoidance rule. The two neighboring unit cells (No. 1, No. 2) and (No. 3, No. 4) in Fig. 28 (b) that are aligned in the diagonal direction, or (No. 1, No. 3) and (No. 2, No. 4) in the off-diagonal direction are connected to construct winding tracks across the whole flux lattice.

Fractional charges transport in the network of fused train tracks generated by topological surgery. In order to read out the fractional charge from the network of train tracks, the nearest neighboring fluxes are connect by cross sectional bonds (represented by the blue bonds in Fig. 29 (a)) to construct a network of magnetic fluxes. The number of tracks that intersect the cross sectional

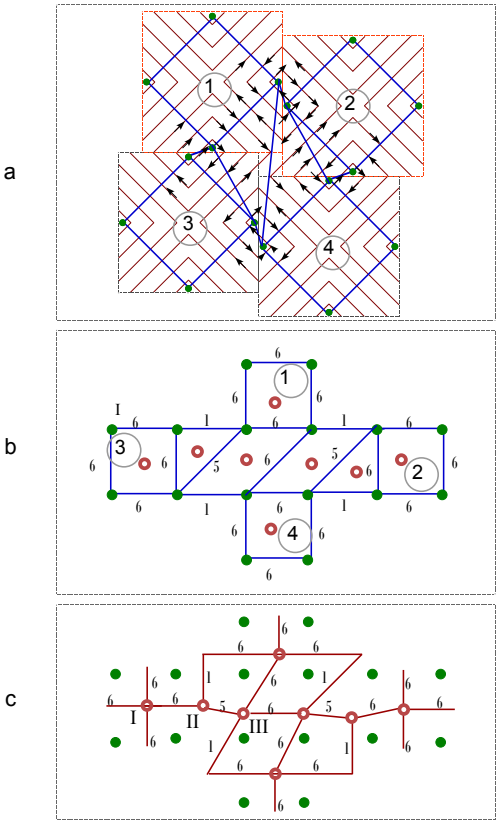

FIG. 29: (a) The blue lines depicts the network of cross sectional bonds that connects the nearest neighboring fluxes in the track lattice generated by one step of translation. (b) The network of the cross sectional bonds in (a) is reformed into a regular square lattice. (c) The dual network of track bundles around fluxes after topological path fusion. Each node (represented by the black annulus) is placed at the center of plaquette.

bond is labeled as its weight. The fluxes are relocated on a square lattice by keeping the topology of network invariant, depicting a brief network composed of square and triangle plaquette (Fig. 29 (b)). The center of each plaquette (represented by the red annulus in Fig. 29 (c)) is further represented by a node where fractional charges flows in and out to construct a dual network of source and sink point in Fig. 29 (c). The flow of fractional charges that connects the nearest neighboring source (or sink) nodes is perpendicular to the cross sectional bond and is labeled by its weight factor. Finally it yields the channel network for fractional charges after one step translation (Fig. 29 (c)). The channel network of fractional charge after and two-step translation can be derived following the same construction procedure as above.

The total charge that flows into a plaquette in Fig. 29 (a) exactly equals to that flows out of the plaquette, fulfilling the conservation law of electric charges. A current segment that is oriented into the center of the plaquette

contributes +1 on the weight factor, the opposite orientation contribute −1. The weight factor on a bond that connects two fluxes is the sum of the weight factors of all directed current segments that intersecting with this bond. We denote the weight factor of each bond as a_α, then the conservation of electric charge obeys the following equation,

$$\sum_\alpha a_{i,\alpha} = 0, \tag{96}$$

where i denotes the center of plaquette. This conservation law holds exactly for all train track patterns before the topological fusion. However the neighboring track segments become indistinguishable when the distance between the fluxes is reduced to De Brogelie wavelength. Then the track stacks within the plaquette fuse into a track bundle that branches to cross different bonds. In that case, the weight factor on each bound is counted by the total number of intersecting points on that bond without taking into account of the direction of the track flow. The weight factor after topological fusion is further normalized to fulfill the conservation of fractional charges,

$$Q_{i,\alpha} = \frac{2a_{i,\alpha}}{\sum_\beta |a_{i,\beta}|}, \tag{97}$$

where i labels the location of the sink point in the dual network in Fig. 29 (c). β indicates the direction of the bonds that is fixed to the ith node. α represents a specific track bundle. Fig. 29 (c) showed three different distributions of track bundles. For the first case, four identical track bundles meet at node type I in Fig. 29 (c). Each bundle has a weight factor of 6, indicating that two equal charges collide at the node and flow out of the plaquette along the other two track bundles. For the second case, three track bundles meet at node type II in Fig. 29 (c), one charge splits into two fractional charges, 1/6 and 5/6. For the third case, four track bundles meet at node type III in Fig. 29 (c). The four anisotropic weight factors, $(1, 5, 6, 6)$, are normalized as $(1/10, 5/10, 6/10, 6/10) = (1/10, 1/2, 3/5, 3/5)$. A fractional charge 3/5 spits into two fractional charges 1/10 and 1/2. Another fractional charge 3/10 flows in and out of the same track bundle to contribute the weight factor 3/5. The exemplar case above are generated by one-step translation. Two-step translation generates similar network track bundles as above. Topological fusion process erased the direction of current segments. Therefore a charge moves into the plaquette and bounces back without any loss is counted twice along the track bundle. Therefore a track bundle in the dual network could split itself to fulfill the conservation law of charges, $\sum_\alpha Q_{i,\alpha} = 0$. The fractional charge distribution strongly depend on construction rule of track bundle network. Only the nearest neighboring fluxes are connected in the case above. Connecting the next nearest neighboring fluxes introduce new track bundles that links to the same node in the dual network, which further split a elementary charge into more fragment.

The translation symmetry of topological surgery operation on two dimensional lattice of train tracks reveals a Hamiltonian for fractional charges in two dimensions. The Hamiltonian for train tracks undergoing a general p-step translation in two dimensions is expressed as $H_p^{[2d]} = \hat{T}_p H_0^{[2d]}$,

$$\begin{aligned} H_p^{[2d]} &= \sum_{x,y,j} t\ c^\dagger_{x2n+j+\frac{5}{2},y2n+j+\frac{5}{2}} \\ &\quad c_{x2n+j+\frac{5}{2},y2n+j+\frac{5}{2}} e^{i\phi r2(g+1),\uparrow} \\ &+ \sum_{x,y,j} t\ c^\dagger_{x2n+j+\frac{3}{2}+p_x,y2n+j+\frac{3}{2}+p_y} \\ &\quad c_{x2n+j+\frac{5}{2}+p_x,y2n+j+\frac{5}{2}+p_y} e^{-i2\pi\phi(\frac{p_x}{2(n+1)}+\frac{p_y}{2(n+1)})} \\ &+ h.c. \end{aligned} \tag{98}$$

This hamiltonian can be further simplified as the Hofstadter model in two dimensional lattice [45]. The fractal structure of energy spectrum of Hofstadter model reveals energy with respect to the knot path and chaotic path in two dimensional lattice of magnetic fluxes in real space. Every fractional charges corresponds to a train track pattern in two dimensional flux lattice.

B. The train track of fractional charges derived from the full vacuum states of two dimensional knot lattice

Another way of deriving train tracks in two dimensional flux lattice is constructing the full vacuum states of two dimensional knot lattice of electron paths [27]. A continuous self-avoiding path snaking through two dimensional lattice of magnetic fluxes represents a collective vacuum state of two dimensional knot lattice. In a local snapshot of square lattice of knots around a pair of fluxes in Fig. 30 (a), the flux locates at the vertex of square lattice surrounded by four crossing patterns of electric currents. Two crossing current segments is either an over-crossing or an under-crossing state. The vacuum state is represented by two uncrossing current segments. In the train track theory, a curve is forbidden to intersect with itself everywhere. While in the knot lattice model, this self-avoiding rule is naturally implemented by confining the block spin 1 of current crossing state to vacuum state, i.e., $S = 0$. The over-crossing (under-crossing) state corresponds to $S = 1$ ($S = -1$) [27]. A collective vacuum state of the knot lattice depicts a self-avoiding train track in two dimensional space, as showed by the exemplar pattern in Fig. 30 (b). Unlike the conventional spin 1, here the vacuum state of block spin 1 (i.e., $|S = 0\rangle = |O\rangle$) has two orthogonal internal states,

$$\begin{aligned} |O\rangle &= O_x|x\rangle + O_y|y\rangle, \quad \langle x|y\rangle = 0, \langle x|x\rangle = 1, \langle y|y\rangle = 1, \\ O_x &= \langle x|O\rangle, \ O_y = \langle y|O\rangle. \end{aligned} \tag{99}$$

Every vacuum state carries two turning arcs that bend the electric current into its perpendicular direction (Fig.

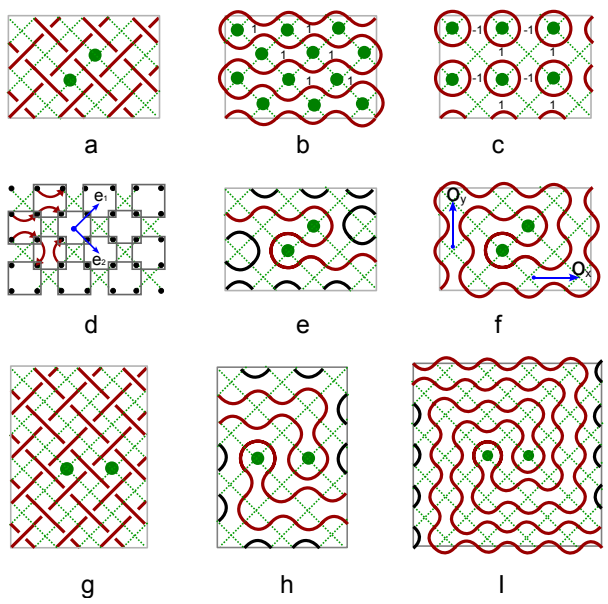

FIG. 30: (a) A square knot lattice pattern around two nearest neighboring magnetic fluxes that locate on the dual square lattice. The magnetic flux is represented by green disc. Bold red lines represent electron path. Dashed green lines draw the dual square lattice of magnetic fluxes.(b) The train track for the ferromagnetic phase of vacuum state. (c) The train track for the anti-ferromagnetic phase of vacuum state. (d) A general train track pattern of vacuum states is constructed in two dimensional lattice of vacuum states (showed as the square enveloped two vacuum arcs). (e) The train track of fractional charge 1/3 is designed on square lattice. (f) The train track of 2/5 is a vortex pattern on square lattice. (g) The knot lattice pattern around two next nearest neighboring magnetic fluxes. (h) The train track for fractional charge 1/4 is designed as two paths that wind around two fluxes respectively and avoid each other. (I) The train track for fractional charge 3/8.

30(b)). $O_x(O_y)$ denotes two turning arcs oriented in X-direction (Y-direction). These two turning arcs connect the current in one direction but disconnect that in its perpendicular direction. In the Hilbert space of vacuum states, the two vacuum components are equivalent to classical Ising spin, ($O_x = +1$, $O_y = -1$) or vice versa. Every train track in two dimensional lattice exactly corresponds to a spatial distribution of Ising spins. In the ferromagnetic phase, all vacuum arcs in the bulk are oriented in the same direction, those arcs perpendicular to that direction only exist on the edge to fulfill the conservation law of mass and charge (Fig. 30 (b)). In the anti-ferromagnetic phase, the nearest neighboring vacuum arc pairs are oriented into perpendicular directions, demonstrating a lattice of isolated current loops (Fig. 30 (c)). A general train track is constructed by translation and rotation operations on the unit cell of vacuum arc pairs, which is essentially a quadramer enveloping four lattice sites (as showed by the black square in Fig. 30 (d)).

The total energy of a general train track is the sum of the potential energy of interacting electric current pairs along the track. The orientation of the two current segments is either parallel or anti-parallel to each other. The potential energy in each unit cell is governed by the product of two current tensors,

$$\epsilon_r = u(I^{\alpha}_{r,a} I^{\bar{\alpha}}_{r,b}), \quad \alpha = 1; \bar{\alpha} = 2; \quad a, b = \leftarrow, \rightarrow, \uparrow, \downarrow . \quad (100)$$

where $u = -\frac{\mu_0 l_i}{2\pi} \ln[d]$ denotes the potential energy between two parallel electric currents. $\alpha(\bar{\alpha})$ denote the inner location of the two current segments. $a(b)$ denote the orientation of the current along the vacuum arc. r denotes the central location of the unit cell. The total energy of free quadramers is $H_1 = \sum_r \epsilon_r$, which admits an eigenstate with a random orientation of current segments within every unit cell. When we study the current flow from one unit cell to another unit cell, the conservation law of electric charge and mass confined the two docking currents that belongs to the two nearest neighboring unit cells respectively into the same direction. The coupling terms of two counter-propagating current segments should be eliminated. To exclude the coupling terms like

$$I^{\alpha}_{r,\leftarrow} I^{\beta}_{r+1,\rightarrow}, \; I^{\alpha}_{r,\rightarrow} I^{\beta}_{r+1,\leftarrow}, \; I^{\alpha}_{r,\uparrow} I^{\beta}_{r+1,\downarrow}, \; I^{\alpha}_{r,\downarrow} I^{\beta}_{r+1,\uparrow}, \quad (101)$$

the directed electric current is equivalently viewed as Feynmann diagram in quantum field theory and expressed by the hopping operator of fermions,

$$I^{\alpha}_{r,\rightarrow} = c_{ij,\alpha} c^{\dagger}_{i+1,j,\alpha}; \quad I^{\alpha}_{r,\uparrow} = c_{ij,\alpha} c^{\dagger}_{i,j+1,\alpha}. \quad (102)$$

Because the product of two identical fermion operators at the same lattice site is exactly zero, $c_{ij,\alpha} c_{ij,\alpha} = 0$, the counter-propagating currents meet at the same site naturally become zero. The fermion operator provides a natural repression of the Hamiltonian of coupled quadramers,

$$\begin{aligned} H_2 &= u \sum_{<r,r'>} \epsilon_r \epsilon_{r'} \\ &= I^{\alpha}_{r,a} I^{\bar{\alpha}}_{r,b} I^{\beta}_{r',a'} I^{\bar{\beta}}_{r',b'} \delta_{aa'} \delta_{bb'} \end{aligned} \quad (103)$$

where r indicates the center of plaquette. The eigenstate of Hamiltonian Eq. (103) corresponds to many continuously oriented winding paths. A topological correlation exists between the two current segments within an unit cell, even though they are the nearest neighboring current segments. This is because only continuously oriented current segments could form a well connected train track, the upper current propagates along a continuous path would finally turns back into its bottom partner arc within the same unit cell. Counter-propagating current segments could not survive in this continuous path.

The vortex path with double flux core can generates a serial of fractional charges after topological path fusion (as showed in Fig. 30 (e-I)). The magnetic fluxes are placed on the vertex of a square lattice. Every hopping current gains a phase factor when it turns around a flux. If we represent the two vacuum components (O_x and O_y)

by current operators, i.e., ($O_x = I_x I_x$ and $O_y = I_y I_y$), then $I_x = 1$ and $I_y = e^{i\pi/2} = i$. Whenever the vacuum state transforms from a X-state to a Y-state or vice versa, the vacuum arc gains a phase increment of $\pi/2$. Setting the flux as origin point and recording the sequence of vacuum state along the vortex path, it maps one of the two spiral arms of vortex path into a sequence of binary code. For example, the ferromagnetic phase in Fig. 30 (b) is represented by $(+1+1+1+1\cdots)$; the $(+1-1+1-1\cdots)$ denotes antiferromagnetic phase in Fig. 30 (c); $(+1-1+1+1)$ corresponds to Fig. 30 (e); $(+1-1+1+1-1-1)$ corresponds to Fig. 30 (f). Every flipping point from $+1$ to -1 is a kink excitation quantified by a vortex field,

$$V = \nabla \times \vec{O} = \partial_y O_x - \partial_x O_y. \tag{104}$$

The population number of these kinks is invariant during topological transformation and topological fusion since they are topological excitations. Since each magnetic flux exists as a forbidden tubular hole in space, a continuous path can only fuse with the current segments on the same side of the flux under topological transformation. Topological fusion induced a high degeneracy of fractional charge state, because topological transformation shortens or elongates the distance between current segments continuously to keep the topological character invariant but inevitably change the coupling potential energy between currents. The topological fusion of the red path in Fig. 30 (e) generates fractional charge 1/3. While fractional charge 2/5 is derived from Fig. 30 (f). If the two magnetic flux are placed on the next nearest neighboring sites in knot lattice of Fig. 30 (g), fractional charges with even denominator are generated after topological fusion. For instance, the winding track in Fig. 30 (h) and Fig. 30 (I) generates the fractional charge 1/4 and 3/8 respectively.

Picking up the closest current segments to the double flux core and stretching them upward to the third dimension maps a winding path of vacuum states into a knot lattice [27], which is constructed by the two elementary knots, the bosonic knot with currents avoiding the border region of two fluxes (Fig. 31 (a)) and the fermionic knot with two crossing currents penetrating through their border region (Fig. 31 (b)). Fixing one of the two identical fluxes that are enveloped in bosonic knot and flipping the other flux into opposite direction transforms the bosonic knot into a fermionic knot (Fig. 31 (b)). The two fundamental knots are the mother pattern for generating other fractionally charges. Even number of braiding operations generates the bosonic knot with half charge $\nu = e/2$ in Fig. 31 (c). Flipping an odd number of crossings in fermionic knot brings it back to the bosonic knot. A knot with odd number of crossings is a fermionic knot (Fig. 31 (b)(d)). Exchanging the locations of two fluxes in a fermionic knot maps the collective spin state $+1$ into to a negative spin state -1. For the knot with three crossings in Fig. 31 (d), it takes three braiding operations (or exchanging operations of the ending points) to

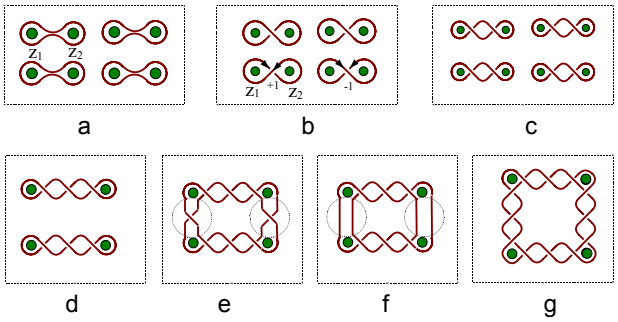

FIG. 31: (a) The square lattice of the minimum composite bosons of loop around flux dimer. (b) The knot lattice of the minimum composite fermion generated by one braiding operation. (c) The knot lattice of composite bosons generated by two braiding operations. (d) The knot lattice for free anyon with fractional $e/3$. (e) The knot lattice of coupled anyons with $e/3$ by a minimum composite fermion. (f) The knot lattice of coupled anyons with $e/3$ by the minimum composite boson. (g) The knot lattice of collectively coupled anyon of $e/3$.

map a $-1 = e^{i\pi}$ to $+1$. Therefore each braiding operator contributes a fractional phase $\pi/3$. Thus the knot carries a fractional charge $Q = e/3$ or $Q = 2e/3$. The statistical character of the knot current with odd number $(2m+1)$ of crossings matches the Laughlin wave function,

$$\psi(z_1, z_2) = (z_1 - z_2)^{2m+1} e^{-\frac{|z_1|^2+|z_2|^2}{4l_B^2}}, \tag{105}$$

where $z_i (i = 1, 2)$ labels the location of the electrons that is attached on the cutting ends of current tracks in Fig. 31. Exchanging two electrons is equivalent to flipping the orientation of one flux. For bosonic knot lattice with m crossings (Fig. 31 (c)), it takes $m/2$ (m is even) braiding operations to map the knot lattice to the elementary bosonic knot in Fig. 31 (a). Therefore different configurations of bosonic knot lattice carry the same half charge $Q = e/2$, revealing a high degeneracy of fractionally charged states with respect to different magnetic field strength which is proportional to the total number of crossings within the knot lattice. Under infinite number of braiding operations, the total number of crossings between two fluxes and the distance between two fluxes grows up to infinity. The effective magnetic field strength approaches to zero correspondingly. As a result, the fractional charges serial converges to the limit of half-charge state.

The knot lattice that binds a pair of fluxes can be viewed as composite boson or composite fermion. Weakly interacted composite particles offered an effective description for FQHE. To explore physics beyond FQHE, we construct strongly interacted composite particles from the dimer coverings of two dimensional flux lattice. A dimer covering pattern on square lattice can be implemented by either bosonic knot (Fig. 31 (a)) or fermionic knot (Fig. 31 (b)). The electromagnetic potential energy of a dimer covering is counted by electromagnetic poten-

tial Eq. (48). The total energy of of a dimer covering of $N_x \times N_y$ flux lattice by elementary bosonic knots in Fig. 31 (a) is counted as $E_{0,a} = N_x N_y E_0/2$, where E_0 is the electromagnetic potential of two antiparallel currents. Different dimer covering patterns share the same eigenenergy, indicating a Hilbert space of highly degenerated states. The degree of degeneracy is counted by Kasteleyn's counting method [46]. Here each flux at the ith site is viewed as a fermion represented by Grassmann variable η_i, the number of all possible dimer coverings Z is given by the Pfaffian of the matrix M, $Z = Pf[M]$, which is also the partition function of interacting Grassmann variables, $Z = \int [D\eta] \exp[\sum_{i<j} M_{ij}\eta_i\eta_j]$. For a $N_x \times N_y$ flux lattice, the degree of degeneracy of free dimer covering reads,

$$Z = \left[\prod_{k=1}^{N_y}\prod_{j=1}^{N_x}(2\cos[\frac{\pi j}{N_x+1}] + 2i\cos[\frac{\pi k}{N_y+1}])\right]^{1/2} \quad (106)$$

The degeneracy of free dimer state is reduced by introducing interacting tracks between two flux dimers. There are six vacuum states (or uncrossing states) around each flux dimer. Every vacuum state can be replaced by a positive crossing, a negative crossing or a dual vacuum state to bridge the neighboring flux dimers (Fig. 31 (e)(f)). Two mutually perpendicular currents carries zero electromagnetic energy, which is lower than the electromagnetic energy of two antiparallel currents in vacuum state. Therefore connecting the free flux dimers by crossing states reduces the total energy and drives the system to ground state. Fractional charges prefer existing on the ground state of a knot lattice with many crossing state. Fig. 31 (g) shows the knot lattice of many interacting anyons with fractional charge $Q = e/3$, where the nearest neighboring fluxes are connected by one dimensional knot lattice with three crossings. The distance between neighboring fluxes increases with respect to a decreasing magnetic field strength.

A knot lattice of strongly interacted composite bosons is constructed by connecting flux dimers with an even number of crossings. The total energy counts the electromagnetic energy of many fractional charges with an even denominator. We take a dimer covering of bosonic knots as the initial state (Fig. 32 (a)), fix the left flux within the dimer and braid the right flux with its vertical neighbor. It leads to a knot lattice of double currents with four crossings (Fig. 32 (b)). The collective wave function of these fractional charges with even denominator reads

$$\begin{aligned}\Psi_o &= \prod_{i=2le_x+2ne_y,} P_{fk;i}(z_i - z_{i\pm\vec{e}}),\\ &P_{fk;i}(z_i - z_{i\pm\vec{e}}) = (z_{i-e_x} - z_{i+e_x})(z_{i-e_y} - z_{i+e_y})\\ &+ (z_{i-e_x} - z_{i-e_y})(z_{i+e_y} - z_{i+e_x})\\ &+ (z_{i-e_x} - z_{i+e_y})(z_{i+e_x} - z_{i-e_y}). \quad (107)\end{aligned}$$

To introduce interaction between free composite bosons with four crossings, the vacuum state in the middle cell where four dimers meet (as enclosed by the dashed circle in Fig. 32 (b)) is replaced by crossing state of double currents. This generates a square lattice of block Ising spin $S = \pm 1$, in which each spin state is characterized by four crossings. The knot lattice pattern in Fig. 32 (c) represents the collective state of interacting anyon with fractional charge $Q = e/4$ or $Q = 3e/4$, governed by the Pfaffian equation,

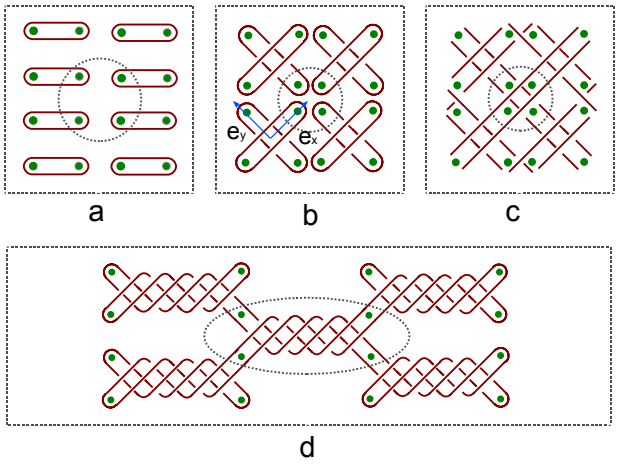

FIG. 32: (a) A homogeneous covering of square lattice by flux dimers surrounded by single loop current. (b) The knot lattice pattern after braiding the nearest neighboring flux dimers, formed a square lattice of isolated double crossings of two loop currents. (c) The isolated double crossings are coupled to one another by a double crossing of four open segments (enclosed in the dashed circle). (d) The knot lattice shows strongly coupled anyons with fractional charge $Q = 5e/12$.

$$\Psi_1 = \prod_{i=le_x+ne_y} P_{fk;i}(z_i - z_{i\pm e_x\pm e_y}), \quad (108)$$

Braiding each block spin in the knot lattice of $Q = e/4$ two more times generates the knot lattice of strongly correlated fractional charges $Q = 5e/12$ and $Q = 7e/12$ in Fig. 32 (d), which is represented by the corresponding wavefunction,

$$\Psi_m = \prod_{i=le_x+ne_y} P_{fk;i}(z_i - z_{i\pm e_x\pm e_y})^m, \quad (109)$$

where $m = 3$ counts the period of braiding operations over the current loop. The knot lattice of other serial of fractional charges with even denominator is derived by repeating the braiding operations above. The interaction between hybrid fractional charges is realized by replacing the coupling subunit (indicated by the crossing state within the dashed circle in Fig. 32 (d)) with a knot lattice of different fractional charges. The elementary knot pattern for constructing knot lattice is the intersection of open current segments. Because these current segments must be closed on the boundary to fulfill the conservation of charges, there always exist a serial of vacuum state of two uncrossing current segments aligned on the boundary to construct a collective knot.

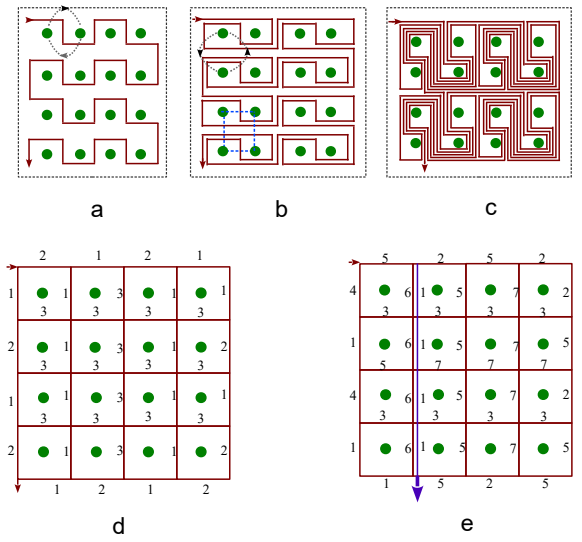

FIG. 33: (a) An electron passes through the two dimensional flux lattice by passing the border region between two nearest neighboring fluxes only once. (b) Periodical train track pattern is generated by a collective braiding over flux dimers in horizontal ordering. (c) Take the train track in (b) as initial state, another collective braiding on flux pairs in the vertical ordering is performed to generate a multilayered train tracks in two dimensional square lattice. (d) The number of layers of train track segments of Fig. (b) is labeled on each edge of the square lattice. (e) The weight distribution of train tracks in Fig. (c) is labeled on the edges of square lattice.

C. Fractional charges generated by periodically braiding electron path in two dimensional flux lattice

When an electron passes a two dimensional flux lattice to reach a fixed detector, all possible paths that connects the entrance point and detector point must be taken into account. Besides the traditional paths that propagate monotonically in one direction in path integral theory, the winding path of train tracks is generated by collective braiding of the electron path around flux pairs. An arbitrary path divides the two dimensional space into two separated domains. If there exists at least one flux in the opposite domain of other fluxes, the electron path can be continuously pushed around to wind through all fluxes under collective braiding operations. As a result, the probability density function of electron distributes the whole two dimensional flux lattice.

We first take the initial path as a single open path in two dimensional flux lattice that passes the border region between the nearest neighboring fluxes only once (Fig. 33 (a)). The entrance point is located at the left upper corner, and the detector is fixed on the left bottom corner (Fig. 33 (a)). The collective clockwise braiding operations on flux dimers oriented in horizontal direction transforms the initial single track into a periodical distribution of stacked tracks in two dimensions (Fig. 33 (b)). The track stacks fuse into track bundles around the four sides of each flux. The weight of each track bundle on one side is counted by the total number of layers of stacked track segments on that side. The weight distribution of the train track of Fig. 33 (b)in two dimensional flux lattice is labeled in Fig. 33 (d). When an elementary charge is input from the left upper corner (the red arrow in Fig. 33 (a)), it splits into two fractional charges, $2e/3$ that goes into the horizontal bond and $e/3$ flowing into the vertical bond (Fig. 33 (d)). The four electric currents that meet at a crossing node obey the Kirchhoff's conservation Law of charges, i.e., the sum of all currents flowing into one node equals to the sum of currents flowing out of that node. The fractional charges of $2e/3$ and $e/3$ alternatively distributed along the edges of the square lattice in Fig. 33 (d). In the bulk region, an integral charge e runs along the horizontal channels, but a vertical strip of fractional charge $e/3$ distributes alternatively in two dimensions (Fig. 33 (d)). This typical train track pattern revealed the key difference between edge and bulk as well as their exact correspondence.

Taking the train track lattice of Fig. 33 (b) as the initial pattern, a collective braiding operation over flux dimers oriented in vertical direction maps out a two dimensional lattice of heavy track stacks in Fig. 33 (c), which generates a serial of fractional charges distributed on the four edges of the square lattice. The fractional charge pair of $3e/4$ and $e/4$ distributes alternatively along the left edge in Fig. 33(e), with the gaps filled by the other fractional charge pair of $4e/5$ and $e/5$. The pair of $3e/5$ and $2e/5$ and the pair of $5e/7$ and $2e/7$ alternatively distributes along the right edge (Fig. 33 (e)). The fractional charge pair $4e/9$ and $5e/9$ only locate at the left upper corner (Fig. 33 (e)). The pair of $5e/7$ and $2e/7$ form convective flows on the upper edge. Integral charge runs in most channels of the bulk region except the channel that is connected to the output detector on the bottom edge (as represented by the arrow at the bottom of Fig. 33 (e)). The elementary charge splits into two $e/7$ and one $5e/7$ at the output detector node, in which one $e/7$ and one $5e/7$ still flows along the edge, only the fractional flow of $e/7$ from top to bottom is detected by detector, leading to the Hall resistance,

$$R_H = R_0 7/e. \tag{110}$$

This fractional Hall resistance is the output result of the special initial state in Fig. 33 (a) and the combinatorial braiding operation as Fig. 33 (a) shows. Therefore Hall resistance strongly dependence on the initial state and the spatial distribution of magnetic field strength.

The train track generated by braiding many periodical loop tracks in flux lattice leads to different fractional charge distribution on the edges from that in bulk. The four horizontal flux dimers that covers eight fluxes in Fig. 35 (a) compose the minimum unit of two dimensional lattice of loop tracks. We first braid the two middle fluxes in the same row in counterclockwise direction, then braid the two middle fluxes as two vertical flux dimers in counterclockwise direction, it generates the periodical train track pattern in Fig. (35) (c). The weight distribution

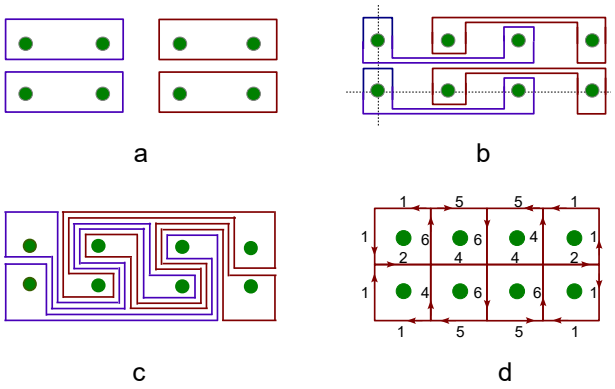

FIG. 34: (a) Four loop currents around four flux dimers oriented in horizontal direction. (b) The stacked train track after one counterclockwise braiding on the two middle fluxes in horizontal ordering. (c) The stacked train track after one more counterclockwise braiding on the two middle fluxes in vertical ordering. (d) The weight distribution of fused train tracks around fluxes is labeled on the edges of square lattice.

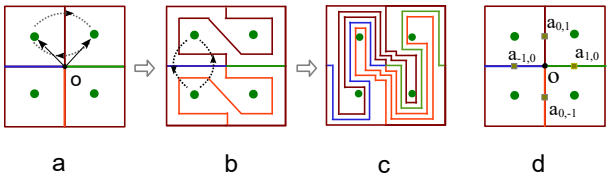

FIG. 35: (a) A general train track network around four fluxes is depicted with the four bonds meeting at the central node dyed in different colors. (b) The train track distribution after a clockwise braiding on the two flux dimer in horizontal ordering simultaneously. (c) Based on the track pattern of (b), another collective counterclockwise braiding is performed on two flux dimer in vertical ordering. (d) The weight distribution of stacked train tracks on the square network after track fusion. Each bond is assigned with a weight labeled by a_{ij}.

on the bonds around fluxes (Fig. (35) (d)) showed half charges on the left and right edge. The fractional charge pair $(1/6, 5/6)$ and $(4/5, 1/5)$ are distributed on the upper and bottom edge. The Kirchhoff's Law only holds for the bulk crossing nodes in Fig. (35) (d). The weights of fractional charges on certain edges violate Kirchhoff's Law due to the free charges that only run along edges instead of joining in the bulk. For example, only 3/5 of the edge current on the middle site of the upper edge in Fig. (35) (d) flows into the bulk track with a weight 6. 2/5 of the edge current passes this middle site to flow along another block of edge channel. Therefore, the edge current can be quantitatively isolated out of the bulk charges by applying Kirchhoff's Law for edges.

A general track distribution in two dimensional flux lattice which summarises both the open tracks and loop tracks is taken as initial track (Fig. 35 (a)), a clockwise braiding on the horizontal flux pair followed by a counterclockwise braiding on the vertical flux pair (Fig. 35 (a)(b)) generates an unit quadramer of stacked tracks for two dimensional lattice (Fig. 35 (c)). The weight of the four bonds in the bulk region evolves as braiding operations are performed by finite steps. The weight at the tth step is determined by the weight at the $(t-1)$th step,

$$\begin{aligned}
a_{[0,1]}(t) &= 3a_{[0,1]}(t-1) + 2a_{[0,-1]}(t-1) + a_{[-1,0]}(t-1) \\
&+ a_{[1,0]}(t-1), \\
a_{[0,-1]}(t) &= 2a_{[0,1]}(t-1) + 3a_{[0,-1]}(t-1) + a_{[-1,0]}(t-1) \\
&+ a_{[1,0]}(t-1), \\
a_{[-1,0]}(t) &= a_{[0,1]}(t-1) + a_{[0,-1]}(t-1) + a_{[-1,0]}(t-1), \\
a_{[1,0]}(t) &= a_{[0,1]}(t-1) + a_{[0,-1]}(t-1) + a_{[1,0]}(t-1),
\end{aligned} \tag{111}$$

Here t indicates the step of operation. The subscribe index of $a_{[i,j]}$ labels the location of the bond (Fig. 35 (d)). The weight on bonds determine the distribution of fractional charges on the bonds at a crossing node, which redistributes under braiding operations. The stable distribution of fractional charges is derived from the eigenvectors of the braiding operation matrix,

$$B = \begin{pmatrix} 3 & 2 & 1 & 1 \\ 2 & 3 & 1 & 1 \\ 1 & 1 & 1 & 0 \\ 1 & 1 & 0 & 1 \end{pmatrix}. \tag{112}$$

The weights on four bonds reach a stable distribution after infinite number of rounds of braiding operations,

$$a_{[0,1]} = a_{[0,-1]} = 1 + \sqrt{2}, \quad a_{[-1,0]} = 1, \quad a_{[1,0]} = 1. \tag{113}$$

The irrational charges and integral charges on the fur bonds still fulfil the conservation law of charges (Fig. 35 (h)), i.e., the Kirchhoff's Law of electric circuit.

The total electromagnetic energy of the two dimensional lattice of electric current stacks is the sum of the potential energy between every two vectorial currents. Unlike the parallel or antiparallel currents in one dimensional flux lattice, electric current stacks in two dimensional lattice are oriented into two perpendicular directions. The interaction between the vertical and horizontal currents is governed by the electromagnetic coupling equation,

$$H_{2D} = \sum_{i,j} -\frac{\mu_0 a^2}{4\pi} \ln(r_{ij}) I_i I_j [\mathbf{e}_j \times (\mathbf{e}_i \times \mathbf{e}_r)], \tag{114}$$

where $\mathbf{e}_i$ indicates the unit vector representing the orientation of electric current on the ith bond. $\mathbf{r}_{ij}$ is the relative position vector directed from the ith current to the jth current. $\mathbf{e}_r$ is the unit orientation vector of $\mathbf{r}_{ij}$. The eigenenergy strongly depends on the orientation of current bundle on each bond. Each current bundle is composed of parallel current segments after track fusion. For the the explicit charge distribution in Fig. 35 (d), the electric current strength is proportional to the weight of the bond. Note that the current stack on certain edge splits into edge current and bulk current. The bulk currents are arranged into convective flows, while the edge current runs monotonically in one direction. The bulk

current network transforms synchronously together with the edge current network under collective braiding operation which is implemented by applying magnetic field. The energy of edge current is counted by the interaction between edge currents and the bulk current stacks that obey the Kirchhoff's Law. Therefore the correspondence between bulk currents and edge currents is also summarized in the total electromagnetic energy. In the continuous limit, the edge fluxes surrounded by electric paths behaves like composite particles running along a closed loop chain, which is governed by the Calogero-Sutherland model from dimension reduction of composite fermion model in two dimensions [43]. This edge-bulk correspondence strongly depends on magnetic impurities, which introduced new fluxes into the flux lattice and more possible braiding strategy for generating fractional charges. The impurity played an important role in measuring fractional conductance in FQHE [1].

V. THE FRACTIONALLY CHARGED ANYON IN THREE DIMENSIONAL INTERLOCKING KNOT LATTICE OF MAGNETIC FLUX TUBES AND ELECTRIC CURRENT

A. The three dimensional interlocking knot lattice of magnetic fluxes and electric currents

The three dimensional array of parallel flux tubes represents exactly the magnetic field configuration in FQHE. The train tracks around the projection of these flux tubes in a two dimensional cross-sectional plane (Fig. 36 (a-b)) offered a rigorous topological picture of the trajectory of many propagating electrons confined in two dimensions. The thickness effect of the two dimensional electron gas is usually neglected in FQHE, because the magnetic field is constructed as homogeneous in experiment. As a result, the top layer and bottom layer of the 2D electron gas are braided simultaneously (Fig. 36 (b)). When the gradient of magnetic field strength is strong enough to make the electron in the top layer feels a different magnetic field strength from that in the bottom layer, it leads to different train tracks between the top layer and bottom layer, which can be equivalently map into each other by adding an opposite braiding operation on the two flux tubes themselves. In other words, the braided train track of electron around two parallel flux tubes can be topologically transform into an unbraided track of electron around the braided flux tubes after the same periods of opposite operations. We call this duality relation as topological duality between electric current and magnetic flux tubes. Fig. 36 (c) showed a typical example of this topological duality, in which the bottom layer is located at the strongest point of magnetic field strength, where a magnetic monopole is located at the center of a serial of concentric spheres. The endings of flux tubes are fixed to the bottom layer. The braided flux tubes map this case into a topologically equivalent train track

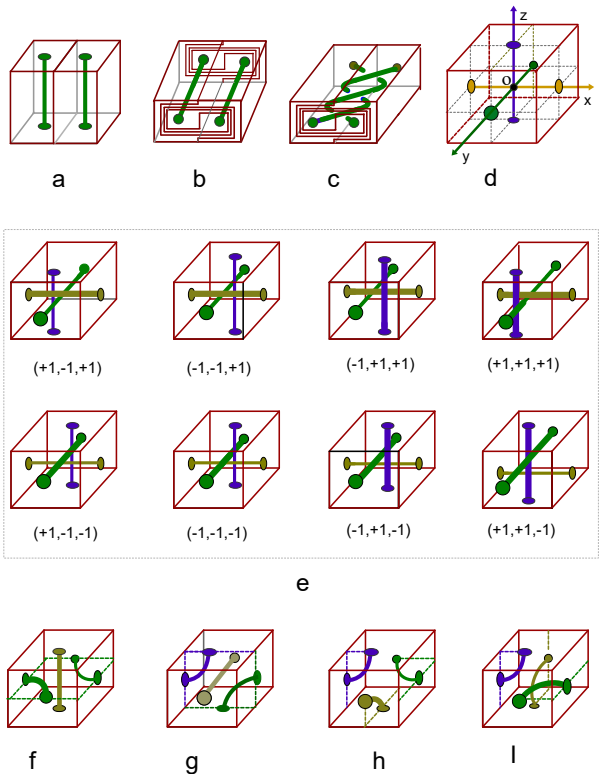

FIG. 36: (a) Flux tubes are surrounded by three dimensional network of electron paths denoted by the red edges of the cubic. (b) The electron paths in different layers perpendicular to the homogeneous magnetic fluxes are braided simultaneously. (c) The braided electron path and knotted magnetic flux tubes in an inhomogeneous magnetic field with one ending of the path fixed to a plaquette center. (d) The Cartesian coordinate system is label in an unit cubic of three dimensional lattice of magnetic fluxes. The magnetic fluxes in x-, y- and z-direction are represented by green, brown and blue axis correspondingly. (e) The eight spin states represented by three intersecting magnetic flux tubes. (f-I) The vacuum states represented by uncrossing magnetic flux tubes.

in homogeneous magnetic field as Fig. 36 (b). Therefore the train tracks of electron path in the top layer has an one-to-one correspondence with the knot structure of braided magnetic flux tubes in the bulk (showed by Fig. 36 (c)). The knot structure of the braided magnetic fluxes can be extracted from the fractional conductance of the train tracks in top layer. The braided magnetic flux tubes is not only a theoretical proposal. In fact, a helical magnetic field is found in the Sun's surface, illustrated by the eruption of coronal mass ejections [47].

The interlocking knot lattice of magnetic fluxes and electric currents is constructed on three dimensional cubic lattice. The Cartesian coordinate system for the cubic lattice is labeled in an unit cubic with its center locating at the origin point (Fig. 36 (d)). The edges of every unit cubic is implemented by electron path along which electron propagates, labeled by the red lines in Fig. 36 (d). There are three magnetic flux segments that winds

around in the unit cubic. Each magnetic flux segment within the unit cubic only connects two of the six face centers of the cubic lattice, which are also the ending points with other flux segments in the nearest neighboring cubic (Fig. 36 (d)). There are eight possible crossing states for the six straight flux segments that are parallel to the axis of coordinate (Fig. 36 (e)). Every straight flux segment connects two face centers that locate on the same axis face to face. These straight flux segments avoid intersecting with one another to construct a knot lattice. Similar to vacuum arc pair in two dimensional knot lattice, the four face centers in the same plane can be connected by two flux arcs that only bridge the nearest neighboring face centers. The last two face centers are connected by a straight flux segment in Fig. 36 (f)(g). There are three possible configurations for the uncrossing state with two vacuum arcs and one straight flux segment parallel to one of the three axels. The full vacuum state is consist of three flux arcs that connects three pairs of the nearest neighboring face centers. The two elementary full vacuum states are showed in Fig. 36 (h)(I), which can be mapped into other full vacuum states under the action of SO(3) group transformation.

The internal knot state in an unit cubic is characterized by block spin 1 vector in three dimensions. The three spatial components of block spin 1 in one direction is characterized by the projected locations of the two flux segments in the other two directions. For example, the flux segment parallel to Y-axis is determined by its projected locations on X-flux and Z-flux, labeled by $\hat{P}Y_x$ and $\hat{P}Y_z$ correspondingly, where $\hat{P}$ is the projection operator. The three components of spin 1 is defined as a normalized vector as following,

$$\begin{aligned} S_i &= \left(\frac{\hat{P}X_y - \hat{P}X_z}{|\hat{P}X_y - \hat{P}X_z|}, \frac{\hat{P}Y_z - \hat{P}Y_x}{|\hat{P}Y_z - \hat{P}Y_x|}, \frac{\hat{P}Z_x - \hat{P}Z_y}{|\hat{P}Z_x - \hat{P}Z_y|} \right) \\ &= (S_x, S_y, S_z), \end{aligned} \tag{115}$$

where i locates the center of the unit cubic. The normalized vector S_i is a three dimensional Ising spin, $S_\alpha = \pm 1$. The crossing knot patterns with respect to different values of Ising spin 1 are listed in Fig. 36 (e). The vacuum state is highly degenerated in the representation of spin 1, S = 0. In order to distinguish different vacuum states, each one of the six face centers is assigned by a unique label in Fig. 36 (d). The two face centers on the x-axis is labeled by $X_+ = (1, 0, 0)$ and $X_- = (-1, 0, 0)$, because one face center is on the positive side and the other face center is on the negative side, the labels for the other face centers on the other two axels is defined in the same way, $[Y_+ = (0, 1, 0); Y_- = (0, -1, 0)]$ and $[Z_+ = (0, 0, 1); Z_- = (0, 0, -1)]$. The corresponding spin vector of the vacuum states is characterized by a dimer covering of the six face centers. For example, a full vacuum state can be expressed by

$$O_i = (X_+ - Y_-,\ Y_+ - Z_-,\ Z_+ - X_-). \tag{116}$$

The vacuum state with two flux arcs in the same plane and one straight flux segment line perpendicular to this plane is expressed in a hybrid way. For example, the spin vector for the vacuum state in Fig. 36 (f) reads

$$O_i = (X_+ - Y_-,\ Y_+ - X_-,\ Z_+ - Z_-). \tag{117}$$

The spin vector Eq. (115) for $S_\alpha = \pm 1$ is equivalent to the expressions by the locations of face centers,

$$S_i = \left(\frac{X_+ - X_-}{|X_+ - X_-|}, \frac{Y_+ - Y_-}{|Y_+ - Y_-|}, \frac{Z_+ - Z_-}{|Z_+ - Z_-|} \right). \tag{118}$$

The spin vector for a general flux crossing state in unit cubic is defined by the same way as above. A combination of these elementary crossing configurations in three dimensional cubic lattice corresponds to a knot of magnetic fluxes. Therefore any knot in three dimensions can be represented by a collective state of many Ising spins in three dimensions.

The three dimensional knot lattice of electric current is constructed by replacing the intersecting nodes of the unit cubic with the same elementary crossing states as that of magnetic fluxes in Fig. 36. This dual knot lattice of electric currents interlocks with the knot lattice of magnetic fluxes, which can also be represented by a dual Ising spin vector. Braiding the knot lattice of magnetic fluxes (electric currents) generates the train tracks of electric current (magnetic fluxes) on the faces of unit cubic. Therefore, there exists a duality between electric fractional charges and magnetic fractional charges.

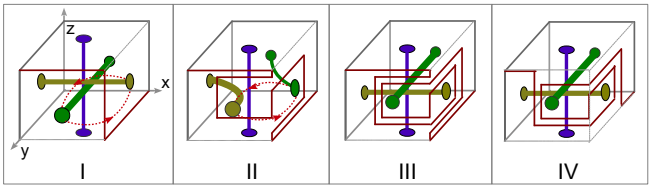

FIG. 37: I-IV, Three braiding operations on the two endings of x- and y-flux are performed to map the spin state $(+1, -1, +1)$ state into $(+1, -1, -1)$, leveling the green flux tube up above the yellow flux.

B. Fractional charges generated by train tracks in three dimensional knot lattice of magnetic fluxes and electric currents

The train tracks in three dimensional interlocking knot lattice is generated by braiding the nearest neighboring ending points of two flux segments to wind the electric current along the edges of an unit cubic. For an exemplar initial crossing state $S = (+1, -1, +1)$ in Fig. 37 (I), a counter-clockwise braiding on the two endings at X_+ and Y_+ bends the electric current from one face to its perpendicular neighboring face in Fig. 37 (II). The three flux segments turn into a hybrid vacuum state. One more counter-clockwise braiding leads to the train track in Fig. 37 (I-III), which breaks one elementary charge apart into

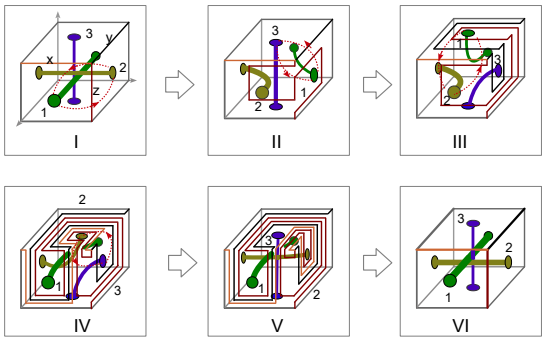

FIG. 38: I-VI, The braiding operations on the three nearest neighboring ending points by $\hat{B}_1$ maps the spin state $(+1,-1,+1)$ to $(-1,-1,-1)$.

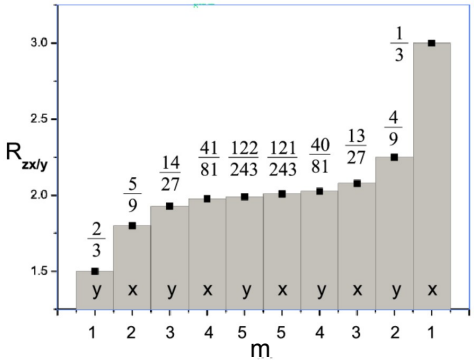

FIG. 39: The discrete distribution of fractional Hall resistance in the X- and Y- edge (R_{zx} and R_{zy}) in three dimensions is plotted against the number of braiding operations m.

a pair of fractional charges, $Q = e/3$ and $Q = e2/3$. The two counter-clockwise braiding exchanges the relative location of the two crossing fluxes oriented in X and Y axis and their projections to Z-axis correspondingly, flipping the initial spin state $S = (+1,-1,+1)$ to its mirror state $S = (+1,-1,-1)$ with respect to a reflection by the X-Y plane. Therefore the endings of the flux segments are anyons carrying a fractional phase $\exp[i\pi/2]$. The fractional charge $Q = e2/3$ first flows downward along the most left vertical edge in Fig. 37 (IV) and then turns to the right hand side along X-axis. Further more, $Q = e2/3$ splits into two fractional charges $Q = e/3$ on the middle edge along Z-axis in Fig. 37 (IV). One goes up along the Z-edges and the other one runs along Y-edge. For a general case, m periods of braiding operations generate a serial of fractional charges along the cubic edges, with a fractional charge $Q = e/m$ runs in the Z-edge between two flux ending points. These fractional charges result in fractional Hall resistance in three dimensional knot lattice, generally defined as following,

$$R_{\alpha\beta} = V_\alpha / v Q_\beta, \quad \alpha, \beta = x, y, z. \tag{119}$$

For the specific train track pattern in Fig. 37 (a) (IV), the fractional Hall conductance in three dimensions reads,

$$R_{zx} = R_0/(\frac{2e}{3}),\ R_{yz} = R_0/(\frac{2e}{3}),\ R_{zz} = R_0/(\frac{e}{3}). \tag{120}$$

Different braiding sequences leads to different serial of fractional Hall resistances. The braiding operation in two dimensional space is characterized by SO(2) group transformation. The braiding operations in three dimensions are typical non-Abelian operations which is originated from SO(3) group transformation. Braiding operations around different axels are not commutable.

Fig. 38 showed the train tracks generated by a string of counterclockwise braiding operations in three dimensional knot lattice,

$$\hat{B}_1 = \sigma_{(1,2);\circlearrowleft}\sigma_{(3,1);\circlearrowleft}\sigma_{(1,2);\circlearrowleft}\sigma_{(2,3);\circlearrowleft}. \tag{121}$$

The edges of the unit cubic in Fig. 38 is assigned with general weight factors, $(a_x(0), a_y(0), a_z(0))$, to search for the invariant limit charges after infinite number of braiding operations with arbitrary initial train tracks. Three nearest neighboring ending points are braided, as labeled by the green disk, yellow disk and blue disc at the center of three perpendicular faces in Fig. 38 (I). The border current between every two ending points are represented by the red, black and yellow edges of the cubic in Fig. 38 (I). The first counterclockwise braiding $\sigma_{(1,2);\circlearrowleft}$ exchanges the two ending points, No.1 and 2, mapping an initial spin state of $S = (+1,-1,+1)$ into a hybrid vacuum state, Fig. 38 (II). The second counterclockwise braiding $\sigma_{(3,1);\circlearrowleft}$ exchanges the two ending points, No. 1 and No. 3, driving the hybrid vacuum state to full vacuum state in Fig. 38 (III). The third counterclockwise braiding $\sigma_{(1,2);\circlearrowleft}$ brings the yellow vacuum arc and green vacuum arc into a crossing state in Fig. 38 (IV). The final counterclockwise braiding maps the hybrid vacuum state to a full crossing state $S = (-1,-1,-1)$ in Fig. 38 (V).

The initial weights of the electric train tracks along the three edges, $(a_x(0), a_y(0), a_z(0))$, represented by the yellow, red and black edges in Fig. 38, are assigned with a new weight distribution after track fusion, $(a_x(1), a_y(1), a_z(1))$ in Fig. 38. When the spin state $S = (+1,-1,+1)$ is mapped into $S = (-1,-1,-1)$ for m times by the string operator Eq. (121), the weight distribution obeys a difference equation,

$$\begin{aligned} a_z(m) &= a_x(m-1) + a_y(m-1) + 2a_z(m-1), \\ a_x(m) &= a_z(m-1) + a_y(m-1), \\ a_y(m) &= a_x(m-1) + a_z(m-1). \end{aligned} \tag{122}$$

The conservation equation, $a_x(m) + a_y(m) = a_z(m)$, holds at every step of braiding operation, showing an integral charge on the Z-edge and two fractional charges on X- and Y-edges,

$$Q_x(m) = \frac{a_x(m)}{a_z(m)},\ Q_y(m) = \frac{a_y(m)}{a_z(m)},\ Q_z(m) = 1. \tag{123}$$

The fractional charge distribution along the three edges

is given by the exact solution of the difference Eq. 122,

$$\begin{aligned} a_x(m) &= \frac{1}{4}[3^m-(-1)^m][a_y(0)+a_z(0)] \\ &+ \frac{1}{4}[3^m+3(-1)^m]a_x(0), \\ a_y(m) &= \frac{1}{4}[3^m-(-1)^n][a_x(0)+a_z(0)] \\ &+ \frac{1}{4}[3^m-3(-1)^m]a_y, \\ a_z(m) &= \frac{1}{4}[3^m-(-1)^m][a_x(0)+a_y(0)] \\ &+ \frac{1}{4}[3*3^m+(-1)^m]a_z(0). \end{aligned} \quad (124)$$

If the general initial charge distribution is assigned with the weight of single path, $a_x(0)=a_z(0)=1$ and $a_y(0)=0$, the two fractional charges at the mth steps reads,

$$Q_x(m)=\frac{3^m+(-1)^m}{2*3^m},\quad Q_y(m)=\frac{3^m-(-1)^m}{2*3^m}, \quad (125)$$

and the integral charge on Z-edge is $Q_z(m)=1$. The fractional charges on the X-edge and Y-edge converge to half-charge in the limit of infinite number of braiding operations,

$$Q_x(\infty)=Q_y(\infty)=\frac{1}{2}. \quad (126)$$

This limit charge is independent of initial charge distribution. The current on the X- and Y-edge comes from the splitting current of Z-edge. Fig. 39 shows that the three dimensional Hall resistance also shows a serial of plateaus but much less than that of two dimensional case. The fractional serial Eq. 125 is not the only fractional charge serial. A different fractional charge serial is induced by a different initial state. For instance, if the initial weight distribution is the eigenvector,

$$a_x(0)=1,\quad a_y(0)=1,\quad a_z(0)=2. \quad (127)$$

The weight distribution on the X- and Y-edge evolves according to the following equation,

$$a_x(m)=3^m,\quad a_y(m)=3^m,\quad a_z(m)=2*3^m. \quad (128)$$

This weight distribution constantly admits a half charge $Q=1/2$ on both X- and Y-edge despite of the number of braiding operations. In this case, the integral charge on Z-edge constantly split into two half charges on X-edge and Y-edge without causing any other fractions.

A different string of braiding operations from the counterclockwise braiding Eq. (121) leads to different fractional charge distributions. Here we only replace the last counterclockwise braiding operation in Eq. (121) with a clockwise braiding,

$$\hat{B}_2=\sigma_{(1,2);\circlearrowleft}\sigma_{(3,1);\circlearrowleft}\sigma_{(1,2);\circlearrowleft}\sigma_{(2,3);\circlearrowright}, \quad (129)$$

where the two ending points, No. 2 and No. 3, are exchanged in clockwise direction. Fig. 40 (VI) shows

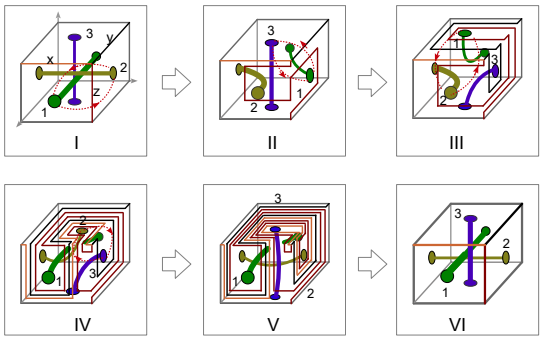

FIG. 40: I-VI, The braiding operations on the three nearest neighboring ending points by string operator $\hat{B}_2$ maps the spin state $(+1,-1,+1)$ to $(-1,+1,-1)$.

a different full crossing state $S=(-1,+1,-1)$ from that generated by $\hat{B}_1$. $S=(-1,+1,-1)$ is exactly the spatial inversion of the initial crossing configuration. When $\hat{B}_2$ maps $S=(+1,-1,+1)$ to $S=(-1,+1,-1)$ for m times, the weight distribution of the train track stack of electric current in Fig. 40 obeys the following evolution equation,

$$\begin{aligned} a_x(m) &= 2a_x(m-1)+a_y(m-1)+3a_z(m-1), \\ a_z(m) &= 2a_x(m-1)+2a_y(m-1)+3a_z(m-1), \\ a_y(m) &= a_x(m-1)+a_z(m-1). \end{aligned} \quad (130)$$

This difference equation is directly read out from the track distribution in Fig. 40 (V). The fractional charge serial generated by $\hat{B}_2$ also converges to stable values despite of different initial states,

$$\begin{aligned} \lim_{n\to\infty} Q_x(m) &= \lim_{m\to\infty}\frac{a_x(m)}{a_z(m)}=1, \\ \lim_{n\to\infty} Q_y(m) &= \lim_{m\to\infty}\frac{a_y(m)}{a_z(m)}=\frac{1}{3}. \end{aligned} \quad (131)$$

The X- and Z-edge carry an integral charge $Q_x(m)=Q_z(m)=1$. The fractional charge on Y-edge converges to $\frac{1}{3}$. The limit charge $\frac{1}{3}$ is completely different from that generated by $\hat{B}_1$. The limit charge is independent of initial state. Therefore it characterizes the special result of string operator action of $\hat{B}_i$.

The brief conservation equation for the weight distribution determined by $\hat{B}_1$, $a_x(m)+a_y(m)=a_z(m)$, failed for the recurrence equation governed by $\hat{B}_2$. For example, the same initial weight distribution $(a_x(0)=a_z(0)=1, a_y(0)=0)$ results in a different weight distribution here $(a_x(1)=5, a_y(1)=2, a_z(1)=5)$ which obviously violates the conservation equation. However, another initial state $(a_x(0)=0, a_y(0)=a_z(0)=1)$ leads to weight distribution of $(a_x(1)=4, a_y(1)=1, a_z(1)=5)$ after one step of operation by $\hat{B}_2$, fulfilling the conservation law, $a_x(1)+a_y(1)=a_z(1)$. But two periods of operation by $\hat{B}_2$ generates a weight distribution $(a_x(2)=24, a_y(2)=9, a_z(2)=26)$ which violates the conservation equation again. The oscillation behavior of

the weight distribution can be understood from the exact solution of the recurrence equation, which is derived by the Putzer algorithm. A matrix representation of this equation is expressed as $\vec{a}(m) = A\vec{a}(m-1)$, where A is the coefficient matrix,

$$A = \begin{pmatrix} 2 & 1 & 3 \\ 1 & 0 & 1 \\ 2 & 2 & 3 \end{pmatrix}. \tag{132}$$

The eigenvalue of this matrix is derived by the characteristic equation $det(A - \lambda' I) = 0$, which has an explicit form, $1+3\lambda'+5\lambda'^2-\lambda'^3 = 0$. The solutions of the characteristic equation are one real eigenvalue and two complex eigenvalues, approximated by their numerical values for simplicity,

$$\lambda_1 = \lambda e^{-i\theta}, \lambda_2 = \lambda e^{i\theta}, \lambda_3 = 5.57, \lambda = 0.42, \theta = 2.32. \tag{133}$$

The exact weight distribution on the three edges after m periods of braiding operations is given by $\vec{a}(m) = A^m\vec{a}(0)$, where A^m is determined by the three eigenvalues above,

$$\begin{aligned} A^m &= \lambda^m e^{-in\theta}\mathbb{I} + \lambda^m \frac{\sin(m\theta)}{\sin(\theta)}(A - \lambda e^{-i\theta}\mathbb{I}) \\ &+ \frac{\lambda_3^{m-1}}{\lambda}\sum_{j=0}^{m-1}(\frac{\lambda}{\lambda_3})^j \frac{\sin(j\theta)}{\sin(\theta)}(A - \lambda e^{i\theta}\mathbb{I})(A - \lambda e^{-i\theta}\mathbb{I})\mathbb{I}, \end{aligned} \tag{134}$$

where $\mathbb{I}$ is the identity matrix. Because the eigenvalue $\lambda = 0.42 < 1$, the amplitude of the first and the second term which are proportional to λ^n decays to zero when the number of braiding operation grows. The third term on the right hand side of Eq. (134) is the dominant term, showing an oscillating but converging weight distribution on the three edges. From the point view of physics, this oscillation behavior is caused by the edge current that does not join in the bulk. Fig. 40 is essentially a corner of the three dimensional cubic. A bulk node is attached by six edges that composed three pairs of perpendicular currents. The conservation equation of charges holds exactly at every bulk nodes except the surface nodes and corner nodes.

The two different fractional serials generated by two different string operators $\hat{B}_1$ and $\hat{B}_2$ above revealed the widespread existence of fractional charges in three dimensional knot lattice of magnetic fluxes. As shown in the two dimensional knot lattice of fluxes, different braiding operations are quantitatively equivalent to different distribution of effective magnetic field. A homogeneous magnetic field is only suitable for observing fractional charge in two dimensions. An intercrossing distribution of strong magnetic fluxes is the key setup for observing fractional charge in three dimensions, which is a big challenge but implementable on earth. Such a strong anisotropic magnetic field in nature exists on the surface of the Sun. More over, the temperature should be low enough to elongate the mean free path of electron to complete the winding operations of train track.

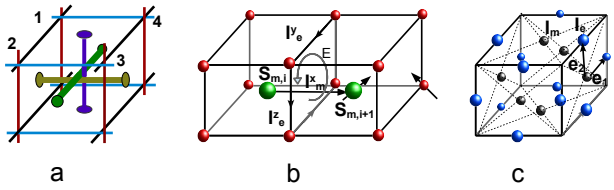

FIG. 41: (a) The three dimensional knot lattice of magnetic flux tubes(represented by the bold lines) interlocking with the knot lattice of electric currents(represented by the thin lines). (b) The crossing nodes of electric currents (represented by the red balls) construct a cubic lattice with the crossing node of magnetic fluxes(represented by big green balls) placed at the center of the square plaquette. (c) The dual face-centered cubic lattice of current segments with each current segment represented by its middle point (the small blue balls and gray balls indicate the electric currents and magnetic fluxes respectively).

C. The train tracks generated from the vacuum states of the three dimensional knot lattice of magnetic fluxes and electric currents

The winding train tracks emerge as the full vacuum state of two dimensional knot lattice of electric current. In three dimensional interlocking knot lattice of magnetic fluxes and electric currents, the winding train tracks also emerge as the full vacuum states of three dimensional knot lattice. Fig. 41 shows the three dimensional knot lattice of non-intersecting magnetic flux tubes that interlocks with a dual knot lattice of electric currents labeled by the non-intersecting edges of the unit cubic. Replacing the crossing nodes of electric currents by similar electric vacuum configurations to that of magnetic fluxes in Fig. 36 constructs the electric train tracks in three dimensional knot lattice of magnetic fluxes.

The crossing states of three perpendicular electric currents in Fig. 41 (a) is classified by the same Ising spins of crossing magnetic fluxes in Fig. 36. These electric crossing nodes (represented by the red dots in Fig. 41 (b) are located on the vertex of cubic lattice. The crossing nodes of magnetic fluxes are located at the center of every unit cubic (represented by the green dots in Fig. 41 (b). Every magnetic flux can be equivalently replaced by a magnetic current of a running magnetic monopole. According to electromagnetic field theory, a magnetic (electric) current generates a circling electric (magnetic) field around it. This mutual induction effect induced strong coupling interaction between the electric current segment and magnetic current segment in the three dimensional knot lattice. For example, the magnetic current I_m^x in Fig. 41 (b) induces a circular electric field E around the plaquette of electric currents, which accelerates (decel-

erates) the electric current segment if the circular field is in the same (opposite) direction as the electric segments. This coupling interaction is governed by the effective Hamiltonian,

$$H_1 = U \sum_{\mathbf{r}} \vec{I}_{m,\mathbf{r}} \cdot (\vec{I}_{e,\mathbf{r}+\mathbf{e}_1} \times \vec{I}_{e,\mathbf{r}+\mathbf{e}_2}), \tag{135}$$

where the magnetic current segments are located on the dual face-centered cubic lattice in Fig. 41 (c) (represented by black balls). The electric current segment is characterized by its middle point that is represented by the blue balls in Fig. 41 (c). This coupling terms is derived naturally from electromagnetic field theory but shares a similar form as Abelian Chern-Simons term, revealing the topological character of the three dimensional knot network of electromagnetic currents.

The coupling terms of electromagnetic current segments above does not capture the internal state of the crossing node. There exists a topological repulsive interaction between the two nearest neighboring nodes with the same crossing states, No. 1 and No. 2 in Fig. 41 (a). Because the vertical currents $I^z_{e,1}$ and $I^z_{e,2}$ (represented by the vertical red line) cannot fuse into each other without cutting the horizontal current $I^x_{e,1}$. In the opposite case that the two nearest neighboring nodes have opposite crossing states, such as $I^z_{e,3}$ and $I^z_{e,4}$ in Fig. 41 (a), the two vertical currents $I^z_{e,3}$ and $I^z_{e,4}$ can get closer enough to fuse into one current. We call this attractive interaction as topological attraction. The interaction between the nearest neighboring nodes is summarized into the following Hamiltonian,

$$H_2 = h \sum_{\langle \mathbf{ij} \rangle} \vec{S}_{\alpha,\mathbf{i}} \cdot \vec{S}_{\alpha,\mathbf{j}}, \tag{136}$$

here $\vec{S}_{\alpha,\mathbf{i}}, (\alpha = e, m)$ is the three dimensional Ising spin. The Hamiltonian Eq. (135) and Eq. (136) together form a complete Hamiltonian description for the three dimensional knot lattice of electromagnetic currents, $H = H_1 + H_2$. When the crossing electric currents at a node are mapped into non-intersecting vacuum arcs and assembly into a collective current pattern in three dimensional knot lattice of magnetic fluxes, a helical track around a tilted magnetic flux tube can be constructed self-consistently to visualize the FQHE in a tilted magnetic field [49]. If there is no other magnetic flux tubes blocked in between the nearest neighboring current segments, the electric current segments can fuse into one bundle under topological transformation, leading to fractional charges in three dimensional space. This three dimensional knot lattice model is a straightforward extension of the two dimensional knot lattice model [27], offered a new method for exploring the anyonic loops in three dimensional spin liquid [50].

VI. CONCLUSION

The topological path fusion theory sheds a light on the origin of the serial fractional charges similar to those in FQHE and beyond. Unlike the monotonic path in conventional path integral theory of quantum mechanics, if the folded path winds around many magnetic fluxes (more than two) in a nontrivial way, it could be equivalently mapped into train tracks in topology theory. Train tracks could be further viewed as topological projection of knot lattice. Since Abelian Chern-Simons field theory is a topological invariant of knot, it is equivalently a topological invariant of train tracks too. Physicist already made a successful construction for fractional Hall conductance with odd denominator in FQHE based on Abelian Chern-Simons field theory. It is natural to ask if knot lattice and train track could explain fractional Hall conductance or not.

The topological path fusion theory confirmed the effectiveness of knot lattice model and train track model for explaining fractionally charged anyons. The existed serial of fractional charges with odd denominator in FQHE is well explained by braiding the propagating path of an electron around magnetic flux pair, so does the serial of fractional charges with even denominator. The train track of single path around magnetic flux pair offered a new physical picture for Jain's composite fermion theory. The exact correspondence between integral and fractional quantum Hall resistance is also rigorously constructed by the topological surgery operations on train tracks. The topological mapping between train tracks and knot lattice revealed that the quantized Hall resistance is caused by electron running on regular knot path. The chaotic paths of electron result in the classical transportation phenomena, which is directly reflected by fractal structure of energy spectrum in Hofstadter model. More over, train tracks can also be constructed as the full vacuum state of knot lattice model, which further provides a systematic way of constructing collective wave function of anyon, such as the Laughlin wavefunction. This topological path fusion theory predicted irrational charges and fractionally charged anyon in three dimensions despite of the long-term belief that anyon cannot exist in three dimensions.

Even though this topological path fusion theory is developed in real space, similar winding paths also exist as energy flow in momentum space of boson-fermion pairing model [48]. Therefore it can be extended into momentum space of solid state physics. Fractional charges can be implemented in a multi-connected spatial domain without magnetic fluxes, such as a porous material with forbidden zones, fluid of light in optical cavity, and topological mixing of two quantum fluids. The rapid development of experimental technology for detecting anyon [51][52] provides a promising future to verify the predictions here, even though it is quite a challenge to construct such a strong magnetic field in laboratory. Further more, the topological path fusion theory also provides a possible

mechanism for generating factional masses of elementary particles, and sheds new light on 2+1 gravity theory and topological defect in liquid crystal [53]. It is quite promising to construct fractional charges or mass in physical system embedded in multi-connected spatial domain and explore new possibilities for topological quantum computation.

[1] H. L. Stormer, Rev. Mod. Phys. **71**, (1999) 875.
[2] R. B. Laughlin, Phys. Rev. Lett. **50**, (1983) 1395.
[3] J. K. Jain, Phys. Rev. Lett. **63**, (1989) 199.
[4] S. Michalakis, Nature. Rev. Phys. **2**, (2020) 392.
[5] G. Murthy, R. Shankar, Rev. Mod. Phys. **75**, (2003) 1101.
[6] M. Kapfer, P. Roulleau, M. Santin, I. Farrer, D. A. Ritchie, and D. C. Glattli, Science, **363**, (2019) 846.
[7] C. Nayak, S. H. Simon, A.Stern, M. Freedman and S. Das Sarma, Rev. Mod. Phys. **80**, (2008) 1083.
[8] B. Blok and X. G. Wen, Phys. Rev. B **42**, (1990) 8145.
[9] T. M. Rice, J. Magn. Magn. Mater., **310**, (2007) 454.
[10] W. P. Su, J. R. Schrieffer, A. J. Heeger, Phys. Rev. Lett. **42**, (1979) 1698.
[11] N. Traverso Ziani and F. Crépin and B. Trauzettel, Phys. Rev. Lett. **115**, (2015) 206402.
[12] C. Fleckenstein and N. Traverso Ziani and B. Trauzettel, Phys. Rev. B, **94**, (2016) 241406.
[13] X. F. Zhang and S. Eggert, Phys. Rev. Lett. **111**, (2013) 147201.
[14] R. Moessner and S. L. Sondhi, Phys. Rev. Lett. **105**, (2010) 166401.
[15] L. J. Lang, X. M. Cai, and S. Chen, Phys. Rev. Lett. **108**, (2012) 220401.
[16] J. He, S. P. Kou 2016 Chin. Phys. B **25**, (2016) 117310.
[17] Y. Aharonov, D. Bohm, Phys. Rev. **115**, (1959) 485.
[18] R. P. Feynman, Rev. Mod. Phys. **20**, (1959) 367.
[19] W. P. Thurston, Bull. Am. Math. Soc. **19**, (1988) 417.
[20] L. Mosher, Notices of the AMS, **50**, (2003) 354.
[21] E. Gouillart, J. L. Thiffeault, and M. D. Finn, Phys. Rev. E **73**, (2006) 036311.
[22] M. R. Allshouse, J. L. Thiffeault , Physica D **241**, (2012) 95.
[23] P. Boyland, M. Stremler, H. Aref, Physica D **175**, (2003) 69.
[24] J. L. Thiffeault, Phys. Rev. Lett. **94**, (2005) 084502.
[25] M. A. Stremler, S. D. Ross , P. Grover , and P. Kumar, Phys. Rev. Lett. **106**, (2011) 114101.
[26] F. Laimer, L. Kranabetter, L. Tiefenthaler, S. Albertini, F. Zappa, A. M. Ellis, M. Gatchell, and P. Scheier, Phys. Rev. Lett. **123**, (2019) 165301.
[27] T. Si, Chin. Phys. B, **28**, (2019) 040501.
[28] E. Witten, Commun. Math. Phys. **121**, (1989) 351.
[29] S. H. Strogatz, *Nonlinear Dynamics And Chaos: With Applications To Physics, Biology, Chemistry, And Engineering*, Westview Press, (2000).
[30] C. Yang and T. Lee, Phys. Rev. **87**, (1952) 404.
[31] A. Shapere and F. Wilczek, Nucl. Phys. B **320**, (1989) 669.
[32] S. Kivelson , D. H. Lee and S. C. Zhang, Phys. Rev. B **46**, (1992) 2223.
[33] Lütken C. A. and G. G. Ross, Phys. Rev. B **45**, (1992) 11837.
[34] C. A. Lütken and G. G. Ross, Phys. Rev. B **48**, (1993) 2500.
[35] C. A. Lütken, Journal of Physics A: Mathematical and General **26**, (1993) 811.
[36] C. Lütken, Nucl. Phys. B **396**, (1993) 670.
[37] B. P. Dolan, Journal of Physics A: Mathematical and General **32**, (1999) 243.
[38] B. P. Dolan, Phys. Rev. B **82**, (2010) 195319,
[39] B. P. Dolan, Journal of Physics A: Mathematical and Theoretical **44**, (2011) 175001.
[40] S. S. Murzin, S. I. Dorozhkin, D. K. Maude,and A. G. M. Jansen, Phys. Rev. B **72**, (2005) 195317.
[41] C. A. Lütken and G. G. Ross, Implications of experimental probes of the rg-flow in quantum hall systems, arXiv 0906.5551, (2009).
[42] G. W. Moore, N. Read, Nucl. Phys. B, **360**, (1991) 362.
[43] Y. Yu, Phys. Rev. B, **61**, (2000) 4465.
[44] P. G. Harper, Proc. Phys. Soc. London, Sect. A **68**, (1955) 874.
[45] D. R. Hofstadter, Phys. Rev. B **14**, (1976) 2239.
[46] P. W. Kasteleyn, Physica Amsterdam **27**, (1961) 1209.
[47] N. Seehafer, Electric current helicity in the solar atmosphere, Solar Phys., **125**, (1990) 219.
[48] T. Si, Phys. Lett. A, **383**, (2019) 126018.
[49] Y. Yu and S. J. Yang, Phys. Rev. B, **66**, (2002) 245318.
[50] T. Si and Y. Yu, Nucl. Phys. B, **803**, (2008) 428.
[51] H. Bartolomei, M. Kumar, R. Bisognin, A. Marguerite, J. M.Berroir, E. Bocquillon, B. Placais, A. Cavanna, Q. Dong, U. Gennser, Y. Jin, G. Feve, Science **368**, (2020) 173.
[52] J. Nakamura, S. Liang, G. C. Gardner and M. J. Manfra, arXiv:2006.14115, [cond-mat.mes-hall], (2020).
[53] A. L. Kholodenko, J. Geom. Phys. **33**, (2000) 23.